

# A topological theory for qLDPC: non-Clifford gates and magic state fountain on homological product codes with constant rate and beyond the $N^{1/3}$ distance barrier

Guanyu Zhu<sup>1</sup>

<sup>1</sup>*IBM Quantum, T.J. Watson Research Center, Yorktown Heights, NY 10598 USA*

We develop a unified theory for fault-tolerant quantum computation in quantum low-density parity-check (qLDPC) and topological codes. We show that there exist hidden simplicial complex structures encoding the topological data for all qLDPC and CSS codes obtained from product construction by generalizing the Freedman-Hastings code-to-manifold mapping. This is achieved by building manifolds corresponding to high-dimensional topological expanders from the Tanner graphs of the skeleton classical or quantum codes, which further form a product manifold and an associated thickened product code defined on its triangulation with only a constant qubit overhead. This suggests that qLDPC or more generally CSS codes obtained from product constructions are topological, and hence can admit cohomology operations such as cup products on their thickened counterparts, physically corresponding to higher symmetries in the underlying topological quantum field theory. When applying this mapping to a 3D hypergraph product code obtained from the product of 3 copies of good classical expander codes, we obtain the first non-Clifford logical CCZ gates via constant depth circuits on a code with constant stabilizer weight  $w = O(1)$ , constant rate  $K = \Theta(N)$ , and polynomial distance  $D = \Omega(N^{1/3})$ . When applied to logical CCZ on 3D homological product codes consisting of the product of a pair of good quantum and classical LDPC codes, we can further improve the distance to  $D = \Omega(\sqrt{N})$  exceeding the  $N^{1/3}$  distance barrier implied by the Bravyi-König bound for conventional topological codes with the aid of non-Euclidean geometries. Our work suggests that it is feasible to apply native logical non-Clifford gates on qLDPC codes or directly inject high-fidelity magic states as resources ('magic state fountain') without the distillation process. For the homological product construction, the fountain can inject  $\Theta(\sqrt{N})$  magic states in parallel in a single round.

## CONTENTS

I. Introduction	1	product codes with $\Omega(\sqrt{N})$ -distance	26
II. Non-Clifford logical gates on general simplicial complexes via cohomology operation	5	A. Constructing the thickened 3D homological product codes and logical non-Clifford gates	26
A. Logical Clifford gates for a 2D complex	5	B. Magic state fountain and logical gate structure	29
B. Logical non-Clifford gates for a 3D complex	8	C. Alternative construction of subspace codes	31
C. Generalization to $n$ -dimensional complex and higher gauge theory	8	D. Conjecture on the constant-depth equivalence between the skeleton and thickened qLDPC codes	32
III. Three-dimensional hypergraph product codes	9	VI. Discussion and outlook	32
IV. Non-Clifford logical gates on thickened 3D hypergraph-product codes	11	References	33
A. Building manifolds from classical codes	11		
B. Building 4-manifolds and the corresponding codes that admit triple cup products	13		
1. The modified construction	13		
2. Cycle and cocycle mapping	15		
C. Thickened 3D hypergraph-product code and its code parameter scaling	22		
D. Triple cup product and logical non-Clifford gates on the thickened 3D hypergraph product codes	25		
E. Magic rate and logical gate structure: counting the number of logical CCZ's from the number of triple intersection points	26		
V. Parallelizable non-Clifford logical gates and magic state fountain on constant-rate 3D homological			

## I. INTRODUCTION

With the recent advancement of quantum computing technology, we have entered the era of fault-tolerant quantum computing at the scale of  $O(10)$  to  $O(100)$  qubits [1]. A fundamental question towards further scaling up fault-tolerant quantum computation is how to minimize the space-time overhead.

In recent years, significant progress has been made on the theory of *quantum low-density parity check* (qLDPC) codes in terms low-overhead quantum information storage [1–12]. This includes the discovery of the *asymptotically good qLDPC codes* by Panteleev and Kalachev [6] achieving the optimal storage with constant space overhead and linear distance (see also [7]). Nevertheless, fault-tolerant quantum computation requires not only a

quantum memory, but also logical operations on top of that. A fundamental question is hence whether there exists an *asymptotically good quantum processor* which has constant space-time overhead in the computation with parallelizable logical gates and also linear distance, or some construction closely approaches that [13, 14].

Currently, there have been some ongoing efforts on the study of fault-tolerant logical gates on qLDPC codes [15–20]. The majority of them focus on performing logical measurements such as lattice-surgery-based protocols [15, 18–20] and homomorphic measurements [16, 17] to implement logical Clifford gates. Additional schemes of implementing non-Clifford gates such as the magic state distillation [21] are required to make the fault-tolerant computation universal. A brute-force approach would be to inject and distill the magic states with 2D surface codes and then SWAP them into the qLDPC code block. However, the state injection in this case cannot be parallelizable without increasing the space overhead, and one has not fully leveraged the power of qLDPC codes. Therefore, a parallelizable scheme for magic state injection in qLDPC codes is highly desirable.

The alternative to magic state distillation is to apply native transversal non-Clifford gates or directly inject high-fidelity magic states in qLDPC without distillation (*‘magic state fountain’*) [22], which can eliminate the costly space-time overhead of performing multiple rounds of distillation. A well-known scheme is to apply the transversal  $T$  gate on a 3D color code [23–28], or equivalently the transversal CCZ gate on three copies of 3D surface codes [26, 29]. However, such a scheme requires an additional  $O(d)$  space-time overhead compared to the 2D surface code. The code distance  $d$  in this case scales as  $d = O(N^{\frac{1}{3}})$  where  $N$  is the total number of qubits in a single code block, which scales worse than a 2D surface code  $d = O(\sqrt{N})$ . Detailed numerical comparisons have been made between these two approaches, and it was shown that the 3D color code only outperforms the surface-code magic state distillation at an error rate much lower than the threshold [30]. This fundamental  $N^{\frac{1}{3}}$ -distance barrier is implied by the Bravyi-Konig bound [31] stating that for an  $n$ -dimensional topological code defined on an  $n$ -dimensional Euclidean lattice, the logical gates have to lie within the  $n^{\text{th}}$  level of Clifford hierarchy. Therefore, it is so far a significant challenge to find native logical non-Clifford gates that exceeds the  $N^{\frac{1}{3}}$ -distance barrier. A crucial observation in this paper is that qLDPC codes essentially correspond to highly non-Euclidean geometry, and it is hence possible to go beyond the  $N^{\frac{1}{3}}$ -distance barrier, in particular, a non-Clifford logical gate is found for a family of qLDPC codes with distance  $D = \Omega(\sqrt{N})$ .

Another key insight in this work is that qLDPC code is not only efficient for quantum information storage, but also extremely efficient for producing and storing high-fidelity resource states such as magic states. For example, when using a specific family of constant-rate qLDPC codes with code parameters  $[[N, \Theta(N), \Omega(\sqrt{N})]]$

as a magic state fountain, one can inject  $\Theta(\sqrt{N})$  magic states in parallel in a single round with an effective distance  $D = \Omega(\sqrt{N})$ .

The first scheme of applying non-Clifford logical gate to a high-rate qLDPC code has been proposed recently in Ref. [22], where collective logical CCZ gates have been realized on homological qLDPC codes defined on 3-manifolds (the quasi-hyperbolic codes) with almost-constant rate (up to logarithmic reduction) and logarithmic distance. A further improvement by a logarithmic factor and achieving a constant encoding rate along with a logarithmic code distance by combining the quasi-hyperbolic codes with the quantum rainbow code has also been proposed in Ref. [32]. Moreover, It has been realized in Ref. [22] that a logical CCZ gate implemented by a constant-depth circuit in three identical copies of homological qLDPC codes can be understood as a *cohomology operation* corresponding to a 3-fold *cup product*. Same correspondence also exists for the transversal  $T$  gate in a 3D color code. Physically, this logical gate corresponds to the emergent higher symmetry [33–37] in a topological quantum field theory (TQFT): the  $\mathbb{Z}_2^3$  gauge theory, as has been studied in Refs. [37, 38]. Such a higher symmetry also corresponds to sweeping a gauged symmetry-protected topological (SPT) defect [37–42]. A recent work has further explored and classified logical gates in quantum codes via cohomology operations, which can go beyond the  $k$ -fold cup products corresponding to the color-code paradigm [43].

In algebraic topology, the cohomology operations such as cup products are defined on a *simplicial complex* structure [44] including the special case of a triangulated manifold. The homological qLDPC codes defined on a manifold naturally admit such cohomology operations as well as the TQFT description. On the other hand, a large class of qLDPC codes with desirable parameters are defined on a general chain complex that has a large expansion property, including the homological product of expander graphs [45, 46] or high-dimensional expanders [6, 47]. Nevertheless, a recent breakthrough by Freedman and Hastings [48] has unified these two different worlds: one relies on the systolic geometry of manifolds while the other focuses on the combinatorics of expanders. In particular, they show that any qLDPC code that is sparsely liftable can be mapped to a manifold with minimal dimension 11 which has *bounded local geometry* (the corresponding triangulation has bounded degree). This code-to-manifold mapping essentially erodes the distinction between general qLDPC (or even more generally CSS) codes and homological qLDPC codes defined on manifolds. In particular, the expansion properties and code parameters in the expander-based qLDPC codes are inherited by the homological codes defined on the manifold produced by the mapping. Nevertheless, this mapping is only applicable to a code defined on a 2D (3-term) chain complex. In order to apply non-Clifford gate which is at least in the third level of Clifford hierarchy, one needs to use a quantum code defined on a 3D (4-term) chain

complex.

In this paper, we further generalize the mapping in Ref. [48] to a mapping from a classical code to a manifold, which has also been suggested in Ref. [48]. The classical code is associated with a *Tanner graph*, which is a bipartite graph with two types of vertices corresponding to the bit and check variables respectively. It is also equivalent to a *hypergraph* where checks are placed on the vertices and bits on the hyperedges. Unfortunately, a general hypergraph is not a simplicial complex, and hence does not simply admit cohomology operation such as cup products. One could consider using a classical homological code defined on a graph where the bits are all placed on edges instead of hyperedges; however, it is proven that such classical codes cannot be good, i.e., having linear distance, since the corresponding graph will have 1-cycles with a logarithmic upper bound in size [49]. One way around this is to use the Sipser-Spielman construction [50] to place a local code on each vertex, which is mathematically equivalent to a sheaf [49]. However, defining cohomology operation on a sheaf is not straightforward and it can only be applied to specific classes of classical codes. Another way out which is more generally applicable is to go to a high-dimensional topological expander [47] associated with a higher-dimensional simplicial complex ( $\dim > 2$ ) [49]. Indeed it is possible to construct good classical codes on high-dimensional random simplicial complex, as shown in Ref. [51] (based on the random complex constructions in Refs. [52–55]), although these codes are not LDPC. Here, we instead consider building a higher-dimensional manifold (10-manifold) following the general spirit in Ref. [48], and obtain the simplicial complex from its triangulation. We start with the corresponding Tanner graph (or equivalently a hypergraph) of a classical LDPC code as the skeleton and then ‘thicken’ it into a manifold via handle construction. The manifold has a bounded local geometry due to the sparseness of the input Tanner graph equivalent to the LDPC condition, and hence admits a triangulation with bounded degree. This in turn gives rise to families of good classical LDPC codes on simplicial complexes that are high-dimensional topological expanders [47] without the need of local codes, which is interesting in its own right.

One can then use the manifolds built from classical or quantum codes as Legos to further construct a product manifold. For an input qLDPC code obtained from a product construction (i.e., via a homological product [46] or more generally balanced product [4]), one can use this method to build a thickened qLDPC code defined on the product of the manifolds built from either classical or quantum codes. This gives access to the mapping of higher-dimensional qLDPC codes that go beyond a 2D (3-term) chain complex to manifolds.

With the simplicial complex structure obtained from the manifold triangulation, we are now able to introduce cohomology operations including the triple cup products, which correspond to the emergent higher symmetries in

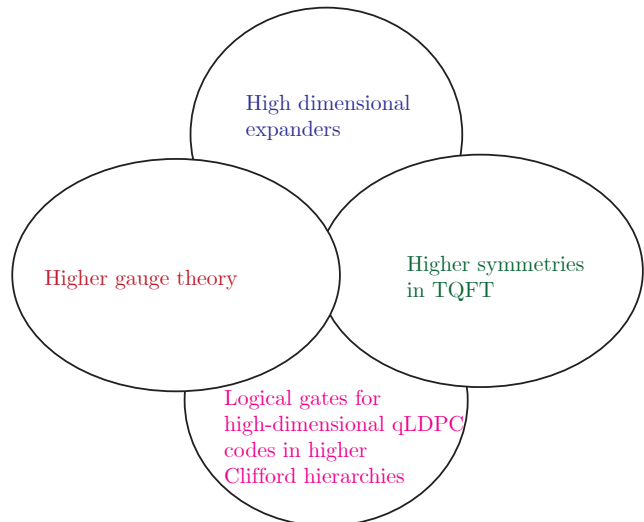


Figure 1. Several ‘higher structures’ across the area of physics, computer science and mathematics are connected through this work.

a higher gauge theory equivalent to a qLDPC code with qubits placed on higher-dimensional simplices (dimensions equal or higher than two). This gives rise to logical gates in higher Clifford hierarchies. Quite interestingly, we can see the deep connection between a few higher-dimensional structures across the area of physics, computer science and mathematics [47] through this work, as illustrated in Fig. 1.

One technical aspect is that the original construction in Ref. [48] considers high-dimensional manifolds (at least 11D) for the sake of killing spurious homologies, which is important from the perspective of systolic geometry and also necessary to avoid short distance in the corresponding subspace code. However, for the purpose of this paper, we can instead consider a subsystem-code encoding and treat the logical qubits with short logical operators as gauge qubits. In this way, we can use a manifold with much lower dimension (4D) obtained from the classical code to construct the qLDPC codes via product construction. Practically this can further reduce the average/maximal degree of the triangulations and hence the average/maximal stabilizer weight of the constructed codes.

In this work, we have obtained two types of qLDPC constructions. The skeleton of the first construction is based on a 3D hypergraph product code [45, 56] obtained from the homological product of three identical good classical expander codes. One further thickens each constituent classical code into a 4-manifold, and then obtain a thickened 3D hypergraph product code defined on the triangulation of a 12-manifold (qubits placed on 4-simplices) with constant stabilizer weight  $w = O(1)$ , constant encoding rate (linear dimension)  $K = \Theta(N)$ , polynomial subsystem-code distance  $D = \Omega(N^{\frac{1}{3}})$ , where

$K$  and  $N$  represent the number of logical and physical qubits respectively. Then a constant-depth circuit implementing the cohomology operation of a triple cup product between three identical copies of the thickened codes lead to a collective logical CCZ gate, consisting of  $\Theta(N)$  CCZ's which equal the total number of  $\mathbb{Z}_2$  triple intersection points, and addressing  $\Theta(N^{\frac{2}{3}})$  logical qubits. The partial addressing issue is resolved in the second construction.

We now consider the second construction, which is based on a 3D homological product code obtained from the product of a good classical expander code and a good quantum LDPC code. The classical and quantum codes are then mapped to the 4-manifold and 11-manifold respectively, which gives rise to the thickened homological product code defined on a 15-manifold with constant stabilizer weight  $w = O(1)$ , constant encoding rate  $K = \Theta(N)$ , and subsystem-code distance  $D = \Omega(\sqrt{N})$  which go beyond the  $N^{\frac{1}{3}}$ -distance barrier implied by the Bravyi-König bound for conventional topological codes defined on Euclidean lattices [31]. This is possible due to the fact that the good quantum LDPC code in Ref. [6] is constructed from a twisted product (or equivalently a balanced product code). The corresponding product manifold built out of this is highly non-Euclidean and the cycles can have much larger size than the case of a Cartesian product. This thickened code is a tensor product of three copies of non-identical qLDPC codes corresponding to different higher gauge theories where the qubits are placed on 6-simplices, 2-simplices and 7-simplices respectively. The triple-cup product cohomology operation between these three non-identical copies gives rise to a collective logical CCZ gates addressing all the  $K = \Theta(N)$  logical qubits and contain in total  $\Theta(N)$  CCZs.

For the homological product code construction, we further investigate the magic state fountain scheme first envisioned in Ref. [22], where we can directly inject  $\Theta(\sqrt{N})$  non-overlapping high-fidelity CCZ magic states with effective distance  $\Omega(\sqrt{N})$  into the qLDPC code in parallel in each single round. Both the injection rate and fidelity (effective distance) outperform those for the 3D topological color codes defined on a 3D cube with code parameters  $[[N, 3, \Theta(N^{1/3})]]$ , where one can only inject a single CCZ magic state with effective distance  $\Theta(N^{1/3})$  (see Sec. VB for more detailed comparison). We further show how to perform gate teleportation to implement logical CCZ gates using these magic states as resources. Although we have not reached the optimal  $\Theta(N)$  injection rate per round, we note that currently it is not the bottleneck for fault-tolerant computation on qLDPC codes, since so far there is no fully parallelizable logical measurement scheme that can implement  $\Theta(N)$  logical Clifford gates (generating the whole Clifford group) in a single logical cycle. A naive estimate, assuming non-overlapping logical Pauli measurements can be done in parallel, would lead to at most  $O(\sqrt{N})$  logical gates per logical cycle for a qLDPC code with  $O(\sqrt{N})$  distance, which just coincides with the injection rate of the magic

state fountain. Further improvement in the injection rate to  $\Theta(N)$  per round would require us to introduce more separable triple intersection structure into the manifold, likely via choosing more non-trivial maps during the handle attachment.

For the conceptual understanding rather than practical purpose, we can also obtain a subspace code construction instead of using subsystem-code encoding for the thickened homological product by killing all the spurious homology in the 11-manifold built from the quantum code following the recipe in Ref. [48]. This extra procedure can introduce extra space overhead and lead to a  $\text{polylog}(N)$  reduction of the encoding rate and distance according to the lower bound of the overhead in Ref. [48]. This hence gives rise to a subspace code with parameters  $K = \Omega(N)/\text{polylog}(N)$  and  $D = \Omega(\sqrt{N})/\text{polylog}(N)$ . The distance here directly corresponds to the  $i$ -systole (shortest length of all non-trivial  $i$ -cycles) of the manifold. Since this lower bound is due to the special proof technique used in Ref. [48], it is also possible to remove it in principle.

Finally, we make a conjecture about the constant-depth equivalence between the thickened qLDPC code and the skeleton qLDPC code with an additional constant factor of ancilla qubits. This will suggest that one can directly apply the logical gate via a constant-depth circuit on the skeleton qLDPC code with the additional ancilla qubits. This can avoid introducing the constant qubit overhead to the qLDPC code and can also potentially simplify stabilizer measurement and decoding.

The work is organized as follows. In Sec. II, we introduce the general theory of logical gates implemented via cohomology operations on a CSS code defined on a simplicial complex including the case of triangulation of a manifold. The theory uses an operator-valued cochain formalism, physically corresponding to a gauge field formalism, which has been previously introduced in Refs. [22, 37, 38]. In particular, we show the construction of triple cup products in a higher gauge theory equivalent to three non-identical copies of CSS codes, which will be used in constructing the non-Clifford logical gates in the two qLDPC codes introduced in this paper. The formalism also shows explicitly how to construct the constant-depth circuits composed of overlapping physical CCZ gates which in term give rise to the logical CCZ gates. In Sec. III, we introduce a 3D hypergraph product construction based on good random classical expander codes. In Sec. IV, we introduce the technique of building manifolds from the Tanner graph of the skeleton classical codes using handle construction, including the 10-manifold construction following the Freedman-Hastings construction in Ref. [48] and a modified lower-dimensional construction of 4-manifolds. We also show the details of the mapping between the cycles/cocycles in the skeleton classical code and the thickened cycles/cocycles in the corresponding manifold. These then pave the way for the construction of the thickened 3D hypergraph product code and derive the scaling of the encoding rate and code dis-

tance. We then show the existence of non-trivial triple cup product structure between three cocycles which geometrically corresponds to the triple intersection of their Poincaré dual cycles. This gives rise to the collective logical CCZ gates. We then count the number of triple intersection points to estimate the number of CCZ's. In Sec. V, we introduce the thickened 3D homological product code construction, including both the subsystem and subspace code versions. We then construct its logical CCZ gates via a triple cup product in the higher gauge theories. We further introduce the magic state fountain scheme and show how to inject magic states in parallel and consume these states for the gate teleportation protocol to implement parallelizable logical CCZ gates, as well as to derive its injection rate. We conclude our paper with the discussion and outlook of future directions and open problems.

*Note added*— During the preparation of this manuscript, we became aware of several other works on related topics [57–59]. The main difference is that the construction in the above papers needs to impose certain local combinatorial conditions for the underlying codes, while the construction of the present paper is fully topological and is applicable to arbitrary input classical or quantum codes. The construction in Ref. [57, 58] has further developed the idea of cup product and triple intersection points in Ref. [22] to the context of quantum sheaf codes. The specific construction of the algebraic codes in Ref. [57] leads to a stabilizer weight  $w = \text{polylog}(N)$  and has not yet satisfied the qLDPC condition. The encoding rate obtained in Ref. [57] for a logical CCZ gate is close to a constant, i.e.,  $K = \Theta(N^{1-\epsilon})$  and the distance is  $O(N^{\frac{1}{3}})/\text{polylog}(N)$ . In contrast, the present paper has achieved constant stabilizer weight  $w = O(1)$  and constant encoding rate  $K = \Theta(N)$ , and has also gone beyond the  $N^{\frac{1}{3}}$ -distance barrier and achieved an  $\Omega(\sqrt{N})$  distance. On the other hand, the scheme in Ref. [57] has also achieved the  $\gamma \rightarrow 0$  magic state distillation [60–62], which has not yet been achieved in the present paper.

## II. NON-CLIFFORD LOGICAL GATES ON GENERAL SIMPLICIAL COMPLEXES VIA COHOMOLOGY OPERATION

In this section, we first describe CSS codes defined on arbitrary simplicial complexes (including the triangulations on a manifold) in the language of  $\mathbb{Z}_2$  lattice gauge theory and then introduce the operator-valued cochain formalism (also called a gauge field formalism) to describe the cup product cohomology operations. We then show how to use the cohomology operation to perform a constant-depth circuit corresponding to logical non-Clifford gates.

### A. Logical Clifford gates for a 2D complex

We first consider a quantum CSS code defined on a 2D simplicial complex  $\mathcal{L}$ . The CSS code can be described by the following 2D (3-term) chain complex:

$$C_2 \xrightarrow{\partial_2 = \mathbf{H}_X^T} C_1 \xrightarrow{\partial_1 = \mathbf{H}_Z} C_0, \quad (1)$$

where  $\mathbf{H}_X$  and  $\mathbf{H}_Z$  are the parity check matrix for the  $X$ - and  $Z$ -checks respectively,  $C_i$  denotes the  $i^{\text{th}}$  chain group, and  $\partial_i$  denotes the  $i^{\text{th}}$  boundary map. The code space is defined by  $\mathcal{C} = \mathbb{C}_2^{|H_1(\mathcal{L}; \mathbb{Z}_2)|}$ , where  $H_1(\mathcal{L}; \mathbb{Z}_2) = \text{Ker}(\partial_1)/\text{Img}(\partial_2)$  is the 1st  $\mathbb{Z}_2$ -homology group.

A dual description of the same code is the following cochain complex:

$$C^2 \xleftarrow{d_1 = \mathbf{H}_X} C^1 \xleftarrow{d_0 = \mathbf{H}_Z^T} C^0, \quad (2)$$

where  $C^i$  and  $d_i$  denote the  $i^{\text{th}}$  cochain group and coboundary operator respectively. For simplicity, we sometimes suppress the index  $i$  and write the coboundary operator as  $d$ . In this dual description, the code space is defined by  $\mathcal{C} = \mathbb{C}_2^{|H^1(\mathcal{L}; \mathbb{Z}_2)|}$ , where  $H^1(\mathcal{L}; \mathbb{Z}_2) = \text{Ker}(d_1)/\text{Img}(d_0)$  is the 1st  $\mathbb{Z}_2$ -cohomology group.

We now introduce an *operator-valued cochain formalism* (also called a *gauge field formalism*) to describe the operators in the code, which originates from a (2+1)D topological quantum field theory (TQFT): the  $\mathbb{Z}_2$  lattice gauge theory. We define the operator valued 1-cochain  $a \in C^1(\mathcal{L}; \mathbb{Z}_2)$ , with its eigenvalues belonging to  $\{0, 1\}$ . The coefficient of each edge (1-cell)  $e$  in the 1-cochain corresponds to a Pauli- $Z$  operator as

$$(-1)^{a(e)} = Z(e) \in \{-1, 1\}. \quad (3)$$

Note that the Pauli operator has eigenvalues  $\pm 1$  instead. Physically,  $a$  corresponds to the 1-form  $\mathbb{Z}_2$  electric gauge field. Similarly, there also exists a 1-cochain  $b$  corresponding to the magnetic  $\mathbb{Z}_2$  gauge field, which is related to a Pauli- $X$  operator on each edge  $e$  as

$$(-1)^{b(e)} = X(e) \in \{-1, 1\}. \quad (4)$$

The coboundary operator, a lattice analog of the exterior derivative in the continuum case, acts on the  $\mathbb{Z}_2$ -valued 1-cochain as

$$(da)(f) = \sum_{e \subset f} a(e). \quad (5)$$

The  $Z$ -stabilizer of the CSS code located on face  $f$  can be expressed in terms of the operator-valued cochain as

$$S_f^Z = \prod_{e \subset f} Z(e) = (-1)^{\sum_{e \subset f} a(e)} = (-1)^{da(f)}, \quad (6)$$

which is also considered as a flux term in the gauge theory. The  $Z$ -stabilizer condition  $S_f^Z = 1$  becomes the

0-flux condition <sup>1</sup>

$$da(f) = 0. \quad (7)$$

The  $X$ -stabilizers on the vertex  $v$  can be expressed as

$$S_v^X = \prod_{e \supset v} X(e) = (-1)^{\sum_{e \supset v} b(e)}. \quad (8)$$

The  $X$ -stabilizer condition  $S_v^X = +1$  corresponds to Gauss's law (with zero charge) in the  $\mathbb{Z}_2$  gauge theory and can be expressed as <sup>2</sup>

$$\sum_{e \supset v} b(e) = 0. \quad (9)$$

Furthermore, the anticommutation relation between the Pauli- $X$  and  $-Z$  operator  $X_e Z_{e'} = (-1)^{\delta_{e,e'}} Z_e X_{e'}$  leads to the following anticommutation relation:

$$X_e (-1)^{f(a)} X_e = (-1)^{f(a+\bar{e})}, \quad (10)$$

where  $f$  is an arbitrary function of  $a$  and  $\bar{e}$  is the indicator 1-cochain that takes value 1 on edge  $e$  and 0 otherwise.

We now introduce cup products on a general  $n$ -dimensional simplicial complex  $\mathcal{L}$ . The vertices on the simplicial complex  $\mathcal{L}$  are assigned with a fixed global ordering. The cup product '∪' of a  $p$ -cochain  $\alpha^p$  and a  $q$ -cochain  $\beta^q$  gives rise to a  $(p+q)$ -cochain denoted by  $\alpha^p \cup \beta^q$ . One can explicitly define the cup product between  $\alpha^p$  and  $\beta^q$  evaluated on a  $(p+q)$ -simplex  $[v_0 v_1 \cdots v_{p+q}]$  as [44]

$$\begin{aligned} & (\alpha^p \cup \beta^q)([v_0 v_1 \cdots v_{p+q}]) \\ &= \alpha^p([v_0 v_1 \cdots v_p]) \beta^q([v_p v_{p+1} \cdots v_{p+q}]). \end{aligned} \quad (11)$$

Here, the arguments contain the labels of ordered vertices  $v_i$  with the ordering  $v_0 \prec v_1 \prec v_2, \dots \prec v_{p+q}$ . We illustrate the  $p=q=1$  case in Fig. 2(a). The cup product also induces a bilinear operation on cohomology:

$$\cup : H^p(\mathcal{L}) \times H^q(\mathcal{L}) \rightarrow H^{p+q}(\mathcal{L}). \quad (12)$$

We then introduce logical gates in two identical copies of CSS codes supported on a generic 2D simplicial complex  $\mathcal{L}$  via cohomological operation. One can consider the following unitary:

$$U = (-1)^{\int_{\Sigma_2} a \cup a'}, \quad (13)$$

where  $a$  and  $a'$  correspond to the electric gauge field on the two copies respectively, and  $\int_{\Sigma_2}$  is a discrete sum

over all the simplices in a non-trivial 2-cycle  $\Sigma_2$  of the simplicial complex  $\mathcal{L}$ . This sum can also be viewed as a cycle-cocycle pairing between  $\Sigma_2$  and  $a \cup a'$ , which is an inner product between the two vectors with  $\mathbb{Z}_2$  coefficients associated with the cycle and cocycle respectively. In the case that the simplicial complex  $\mathcal{L}$  forms the triangulation of a 2-manifold  $\mathcal{M}^2$ , we just take  $\Sigma_2 = \mathcal{M}^2$  since the only non-trivial 2-cycle is the entire manifold:

$$U = (-1)^{\int_{\mathcal{M}^2} a \cup a'}, \quad (14)$$

where  $\int_{\mathcal{M}^2}$  means summing over the simplices of the triangulation belonging to the manifold  $\mathcal{M}^2$ . Nevertheless, in the case of a general simplicial complex, the choice of  $\Sigma_2$  is not unique and this also leads to the opportunity for targeted logical gates acting on a subset of logical qubits, which will be studied in details in future works.

We note that physically  $U$  in Eq. (13) is nothing but the partition function (discrete path integral) of a (1+1)D  $\mathbb{Z}_2 \times \mathbb{Z}_2$  symmetry-protected topological phase (SPT) corresponding to the type-II cocycle [38].

The cup product evaluated on each 2-simplex  $[v_0, v_1, v_2]$  ( $v_i$  represents the three vertices in the simplex) can be computed as

$$(a \cup a')([v_0, v_1, v_2]) = a([v_0, v_1]) a'([v_1, v_2]), \quad (15)$$

as illustrated in Fig. 2(a). We can hence re-express the unitary  $U$  as

$$\begin{aligned} U &= (-1)^{\int_{[v_0 v_1 v_2] \in \Sigma_2} a([v_0, v_1]) a'([v_1, v_2])} \\ &= \prod_{[v_0 v_1 v_2] \in \Sigma_2} \text{CZ}([v_0 v_1], [v_1 v_2]), \end{aligned} \quad (16)$$

which shows that  $U$  is a constant-depth circuit composed of many CZ gates. For each 2-simplex, the CZ gate is between qubits supported on the edges  $[v_0 v_1]$  in the first copy of the quantum code and  $[v_1 v_2]$  on the second copy respectively. The CZ gate in each 2-simplex can overlap with the CZ gates in the neighboring 2-simplexes, which means  $U$  is not a strictly transversal gate but only a constant-depth circuit.

Now we need to check whether  $U$  is a logical gate, meaning its action should preserve the code space, i.e.,

$$U : \mathcal{C} \rightarrow \mathcal{C}. \quad (17)$$

An equivalent condition for the stabilizer code is that

$$P_{\mathcal{C}}[U, S]P_{\mathcal{C}} = 0, \quad (18)$$

meaning that  $U$  commutes with the stabilizer group  $\mathcal{S}$  when projected to the code space  $\mathcal{C}$ . Since  $U$  is a diagonal gate, it clearly commutes with all the  $Z$ -stabilizers. Now we only need to check the commutation relation for the  $X$ -stabilizers.

We consider an  $X$ -stabilizer  $S_{v;1}^X = \prod_{e \supset v} X^{(1)}(e)$  located at vertex  $v$  in the 1st copy of the quantum code.

<sup>1</sup>This can be considered as the lattice analog of the 0-flux condition in the continuum  $\vec{B} = \nabla \times \vec{a} = 0$ , where  $\vec{a}$  is the quantum vector potential.

<sup>2</sup>This is a lattice analog of Gauss's law in the continuous space  $Q = \int_{\Sigma} \vec{E} \cdot d\vec{S} = 0$  or equivalently  $\nabla \cdot \vec{E} = 0$ , where  $\vec{E}$  is the quantum electric field and corresponds to the cochain  $b$  in the lattice gauge theory.

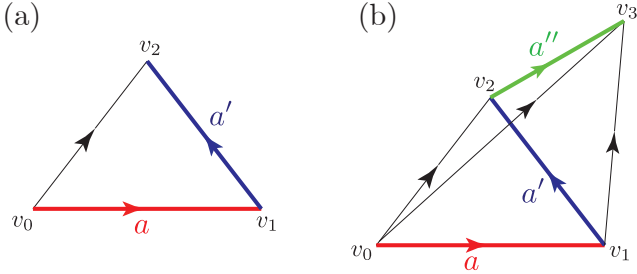


Figure 2. Cup product definition on simplicial complexes, where the arrows point from vertices with lower order to vertices with higher order. (a) Cup product of 1-cochains  $a \cup a'$  on 2D simplicial complex. One takes product of cocycle values on the red and blue edges respectively in each 2-simplex (triangle). (b) Cup product of 1-cochains  $a \cup a' \cup a''$  on a 3D simplicial complex. One takes the product of cocycle values on the red, blue, and green edges respectively in each 3-simplex (tetrahedron).

We then consider conjugating  $U$  with  $S_{v;1}^X$ :

$$\begin{aligned}
& S_{v;1}^X U S_{v;1}^X \\
&= \prod_{e \supset v} X^{(1)}(e) \left[ (-1)^{\int_{\Sigma_2} a \cup a'} \right] \prod_{e' \supset v} X^{(1)}(e') \\
&= (-1)^{\int_{\Sigma_2} (a + \sum_{e' \supset v} \bar{e}') \cup a'} \\
&= (-1)^{\int_{\Sigma_2} (a + d\bar{v}) \cup a'}, \tag{19}
\end{aligned}$$

where we have used Eq. (10) in the second equality. In the last line,  $d\bar{v} = \sum_{e' \supset v} \bar{e}'$  is the indicator 1-cochain taking value 1 on all the edges  $e'$  connected to the vertex  $v$  and 0 elsewhere, and  $\bar{v}$  is the indicator cochain that is 1 at  $v$  and 0 elsewhere.

We now require the following condition for  $U$  to be a logical gate:

$$P_C S_{v;1}^X U S_{v;1}^X P_C = U, \tag{20}$$

where  $P_C$  is the projector to the code space  $\mathcal{C}$ . This condition means  $U$  commutes with the stabilizer  $S_{v;1}^X$  in the code space, which is then equivalent to the following condition:

$$P_C (-1)^{\int_{\Sigma_2} (a + d\bar{v}) \cup a'} P_C = (-1)^{\int_{\Sigma_2} a \cup a'}. \tag{21}$$

The condition in Eq. (21) should be considered as the gauge-invariance condition in the code space, since  $a \rightarrow a + d\bar{v}$  is just a gauge transformation in the  $\mathbb{Z}_2$  gauge theory<sup>3</sup>.

<sup>3</sup>This is in analogy to the famous gauge transformation  $\vec{a} \rightarrow \vec{a} + \nabla\chi$  in Maxwell's theory or the corresponding gauge theory in the continuum, where  $\vec{a}$  is the quantum vector potential. The gauge invariance of the magnetic field  $B = \nabla \times \vec{a} = 0$  is satisfied due to the Stokes theorem:  $\nabla \times \nabla\chi = 0$

In order to show the gauge invariance, we need to use the Leibniz rule for the cup product [44]:

$$d\bar{v} \cup a' = d(\bar{v} \cup a') + \bar{v} \cup da'. \tag{22}$$

note that we have ignored the minus sign and replace it with the plus sign since these cochains are all  $\mathbb{Z}_2$ -valued (binary variables). We hence have

$$\begin{aligned}
P_C \int_{\Sigma_2} d\bar{v} \cup a' P_C &= P_C \left[ \int_{\Sigma_2} d(\bar{v} \cup a') + \int_{\Sigma_2} \bar{v} \cup da' \right] P_C \\
&= P_C \int_{\partial\Sigma_2} (\bar{v} \cup a') P_C + 0 = 0, \tag{23}
\end{aligned}$$

where we have used the Stokes theorem in the second equality and the fact that we are considering a non-trivial 2-cycle  $\Sigma_2$  without boundaries, namely  $\partial\Sigma_2 = 0$ , to show that the first term is zero. The second is zero due to the cocycle condition or physically the zero-flux condition in the code space, i.e.,  $da'(f) = 0$  on any face  $f$ , which corresponds to the stabilizer condition  $S_{f;2}^Z = \prod_{e \subset f} Z^{(2)}(e) = (-1)^{da'(f)} = 1$  according to Eq. (6). We have hence proved Eq. (20) and (21) and that  $U$  is indeed gauge-invariant in the code space and hence a logical gate.

Mathematically, the gauge invariance condition is associated with the topological invariance of  $U$  with respect to arbitrary deformation of the cocycles by coboundaries, which can hence also be called the *coboundary invariance*.

Now we show what type of logical gate this unitary  $U$  corresponds to. Since the cochain  $a$  and  $a'$  in Eq. (13) becomes cocycles in the code space due to the zero-flux condition  $da = da' = 0$ , we can re-express them using the 1-cocycle basis  $\{\alpha^1\}$  and  $\{\beta^1\}$  for both copies of codes:

$$a = \sum_{\alpha^1} \hat{n}_\alpha \alpha^1, \quad a' = \sum_{\beta^1} \hat{m}_\beta \beta^1, \tag{24}$$

where the quantum variable  $\hat{n}_\alpha$  and  $\hat{m}_\beta$  with eigenvalues  $\{0, 1\}$  are the winding numbers for cocycles  $\alpha^1$  and  $\beta^1$  respectively. We can hence re-express  $U$  as

$$\begin{aligned}
U &= \prod_{\alpha^1, \beta^1} (-1)^{\int_{\Sigma_2} (\hat{n}_\alpha \alpha^1) \cup (\hat{m}_\beta \beta^1)} = \prod_{\alpha^1, \beta^1} [(-1)^{\hat{n}_\alpha \hat{m}_\beta}]^{\int_{\Sigma_2} \alpha^1 \cup \beta^1} \\
&= \prod_{\alpha^1, \beta^1} \overline{\text{CZ}}[(\alpha^1; 1), (\beta^1; 2)]^{\int_{\Sigma_2} \alpha^1 \cup \beta^1}, \tag{25}
\end{aligned}$$

where the third equality has used the relation  $(-1)^{\hat{n}\hat{m}} = \overline{\text{CZ}}$ . Here,  $(\alpha^1; 1)$  and  $(\beta^1; 2)$  are the labels of the logical qubit using the cocycle basis and the copy number. The logical CZ gate between logical qubits  $(\alpha^1; 1)$  and  $(\beta^1; 2)$  is only non-trivial (not logical identity) if and only if  $\int_{\Sigma_2} \alpha^1 \cup \beta^1$  evaluates non-trivially.

In the case that  $\mathcal{L}$  is the triangulation of a 2-manifold  $\mathcal{M}^2$ , we can just take  $\Sigma_2 = \mathcal{M}^2$ . The cup product sum now has a geometric interpretation as the  $\mathbb{Z}_2$  intersection number of their Poincaré dual cycles:

$$\int_{\mathcal{M}^2} \alpha^1 \cup \beta^1 = |\alpha_1^* \cap \beta_1^*|. \tag{26}$$

## B. Logical non-Clifford gates for a 3D complex

For a 3D simplicial complex  $\mathcal{L}$ , we still put qubits on the edge (1-cell),  $Z$ -check on the face (2-cell), and  $X$ -check on the vertex (0-cell), which corresponds to the following chain complex:

$$C_3 \xrightarrow{\partial_3} C_2 \xrightarrow{\partial_2=\mathbf{H}_X^T} C_1 \xrightarrow{\partial_1=\mathbf{H}_Z} C_0. \quad (27)$$

We still use 1-cochain  $a$  and  $b$  as the gauge field which corresponds to the Pauli  $Z$  and  $X$  operators respectively as in Eqs. (3) and (4).

We can now defined the desired unitary via cup products as

$$U = (-1)^{\int_{\Sigma_3} a \cup a' \cup a''}, \quad (28)$$

In the above expression,  $a$ ,  $a'$  and  $a''$  represent 1-cochains supported on each of the three copies of CSS codes respectively.

In the case of simplicial 3-complex, the cup-product on each 3-simplex  $[v_0, v_1, v_2, v_3]$  can be evaluated as

$$(a \cup a' \cup a'')([v_0, v_1, v_2, v_3]) = a([v_0, v_1])a'([v_1, v_2])a''([v_2, v_3]), \quad (29)$$

as illustrated in Fig. 2(b). We can hence re-express the unitary  $U$  as

$$\begin{aligned} U &= (-1)^{\int_{[v_0, v_1, v_2, v_3] \in \Sigma_3} a([v_0, v_1])a'([v_1, v_2])a''([v_2, v_3])} \\ &= \prod_{[v_0, v_1, v_2, v_3] \in \Sigma_3} \text{CCZ}([v_0, v_1], [v_1, v_2], [v_2, v_3]), \end{aligned} \quad (30)$$

which explicitly shows the corresponding constant-depth circuit composed of many CCZ gates coupling the qubits in three copies of CSS codes. Similar to 2D case, one can also verify that  $U$  preserves the code space  $\mathcal{C}$  and is hence a logical gate.

We note that physically  $U$  in Eq. (31) is nothing but the partition function (discrete path integral) of a (2+1)D  $\mathbb{Z}_2 \times \mathbb{Z}_2 \times \mathbb{Z}_2$  SPT corresponding to the type-III cocycle [38].

To understand what logical gate  $U$  corresponds to, we can re-express  $U$  with the 1-cocycle basis  $\{\alpha^1\}$ ,  $\{\beta^1\}$  and  $\{\gamma^1\}$  as

$$\begin{aligned} U &= \prod_{\alpha^1, \beta^1, \gamma^1} (-1)^{\int_{\Sigma_3} (\hat{n}_\alpha \alpha^1) \cup (\hat{m}_\beta \beta^1) \cup (\hat{l}_\gamma \gamma^1)} \\ &= \prod_{\alpha^1, \beta^1, \gamma^1} \left[ (-1)^{\hat{n}_\alpha \hat{m}_\beta \hat{l}_\gamma} \int_{\Sigma_3} \alpha^1 \cup \beta^1 \cup \gamma^1 \right] \\ &= \prod_{\alpha^1, \beta^1, \gamma^1} \overline{\text{CCZ}}[(\alpha^1; 1), (\beta^1; 2), (\gamma^1; 3)]^{\int_{\Sigma_3} \alpha^1 \cup \beta^1 \cup \gamma^1}. \end{aligned} \quad (31)$$

The logical CCZ gate between logical qubits  $(\alpha^1; 1)$ ,  $(\beta^1; 2)$  and  $(\gamma^1; 3)$  is only non-trivial (not logical identity) if and only if  $\int_{\Sigma_3} \alpha^1 \cup \beta^1 \cup \gamma^1$  evaluates non-trivially.

In the case that  $\mathcal{L}$  is the triangulation of a 3-manifold  $\mathcal{M}^3$ , we can just take  $\Sigma_3 = \mathcal{M}^3$ . The triple cup product sum now corresponds to the  $\mathbb{Z}_2$  triple intersection number of the Poincaré dual 2-cycles:

$$\int_{\mathcal{M}^3} \alpha^1 \cup \beta^1 \cup \gamma^1 = |\alpha_2^* \cap \beta_2^* \cap \gamma_2^*|. \quad (32)$$

## C. Generalization to $n$ -dimensional complex and higher gauge theory

We can generalize the above results to  $n$  copies of identical CSS codes supported on an  $n$ -dimensional simplicial complex  $\mathcal{L}$  with qubits placed on the 1-simplices (edges). The corresponding 1-form gauge fields  $a_{(i)}$  are operator-valued 1-cochains in the  $i^{\text{th}}$  copy of code ( $i = 1, \dots, n$ ). The constant-depth unitary circuit implementing the logical gate is hence:

$$U = (-1)^{\int_{\Sigma_n} a_{(1)} \cup a_{(2)} \cup \dots \cup a_{(n)}}, \quad (33)$$

where  $\Sigma_n \in H_n(\mathcal{L}; \mathbb{Z}_2)$  is an arbitrary  $n$ -cycle of  $\mathcal{L}$ . In the case that the simplicial complex  $\mathcal{L}$  forms the triangulation of a manifold  $\mathcal{M}^n$ , we can just take  $\Sigma_n = \mathcal{M}^n$ . One can verify that  $U$  preserves the code space  $\mathcal{C}$  in a similar way to the case of lower dimensions.

Now we start deriving the corresponding logical gate of the constant depth circuit  $U$ . In the code space  $\mathcal{C}$ , all the gauge fields are cocycles satisfying  $da_{(i)} = 0$ . We can hence re-express them using the 1-cocycle basis  $\{\alpha_{(i)}^1\}$  of the cohomology group  $H^1(\mathcal{L}^n; \mathbb{Z}_2)$  for the  $i^{\text{th}}$  copy of codes:

$$a_{(i)} = \sum_{\alpha_{(i)}^1} \hat{m}_{\alpha, i} \alpha_{(i)}^1, \quad (34)$$

where the quantum variable  $\hat{m}_{\alpha, i}$  with eigenvalues  $\{0, 1\}$  are the winding numbers. The constant-depth circuit  $U$  can hence be re-expressed as

$$\begin{aligned} U &= (-1)^{\sum_{\{\alpha_{(i)}^1\}} \int_{\Sigma_n} (\hat{m}_{\alpha, 1} \alpha_{(1)}^1) \cup (\hat{m}_{\alpha, 2} \alpha_{(2)}^1) \cup \dots \cup (\hat{m}_{\alpha, n} \alpha_{(n)}^1)} \\ &= \prod_{\{\alpha_{(i)}^1\}} [(-1)^{\hat{m}_{\alpha, 1} \hat{m}_{\alpha, 2} \dots \hat{m}_{\alpha, n}} \int_{\Sigma_n} \alpha_{(1)}^1 \cup \alpha_{(2)}^1 \cup \dots \cup \alpha_{(n)}^1] \\ &= \prod_{\{\alpha_{(i)}^1\}} \overline{C^{n-1}Z}[\alpha_{(1)}^1, \alpha_{(2)}^1, \dots, \alpha_{(n)}^1]^{\int_{\Sigma_n} \alpha_{(1)}^1 \cup \alpha_{(2)}^1 \cup \dots \cup \alpha_{(n)}^1}, \end{aligned} \quad (35)$$

where we have used the relation  $(-1)^{\hat{m}_1 \hat{m}_2 \dots \hat{m}_n} = \overline{C^{n-1}Z}$ . Here,  $\alpha_{(i)}^1$  serve as the more compact labels of the logical qubits using the cocycle basis and the copy number  $i$ . This logical  $C^{n-1}Z$  gate is only non-trivial (not logical identity) if and only if the exponent  $\int_{\Sigma_n} \alpha_{(1)}^1 \cup \alpha_{(2)}^1 \cup \dots \cup \alpha_{(n)}^1$  evaluates non-trivially. In the



case that the  $n$ D simplicial complex  $\mathcal{L}$  is the triangulation of a manifold  $\mathcal{M}^n$ , we can just take  $\Sigma_n = \mathcal{M}^n$ . The cup product sum in the exponent now corresponds to an  $n$ -fold  $\mathbb{Z}_2$  intersection number of the Poincaré dual  $(n-1)$ -cycles  $\alpha_{n-1;(i)}^*$ :

$$\int_{\mathcal{M}^n} \alpha_{(1)}^1 \cup \alpha_{(2)}^1 \cup \dots \cup \alpha_{(n)}^1 = |\alpha_{n-1;(1)}^* \cap \alpha_{n-1;(2)}^* \dots \cap \alpha_{n-1;(n)}^*|. \quad (36)$$

So far we have been focused on the case of 1-form gauge theories, which correspond to the CSS codes with qubits placed on the 1-simplices (edges) of the simplicial complex  $\mathcal{L}$ , i.e., associated with the 1-chain group  $C_1$ . More generally, we also consider higher gauge theories, also called  $q$ -form gauge theories, which corresponds to the CSS codes with qubits placed on the  $q$ -simplices of an  $n$ D simplicial complex  $\mathcal{L}$ , i.e., associated with the  $q$ -chain group  $C_q$ . The  $X$ -stabilizers and  $Z$  stabilizers are placed on the  $(q-1)$ -simplices and  $(q+1)$ -simplices respectively. The corresponding chain complex is as follows:

$$C_n \rightarrow \dots \rightarrow C_{q+1} \xrightarrow[\text{Z-stabilizer}]{\partial_{q+1}=\mathbf{H}_Z^T} C_q \xrightarrow[\text{qubit}]{\partial_q=\mathbf{H}_X} C_{q-1} \rightarrow \dots \quad (37)$$

We then introduce the  $q$ -form electric gauge fields ( $1 \leq q \leq n$ ) as operator-valued  $q$ -cochains  $a^q \in H^q(\mathcal{L}; \mathbb{Z}_2)$ .

Now we investigate the corresponding cohomology operation. As an example, we consider the triple cup product operation that will give rise to logical non-Clifford gate. Since it is a  $q$ -form gauge theory, one can define  $q-2$  types of CSS codes on the simplicial complex  $\mathcal{L}$  or manifold. We consider the triple cup product operation on three copies of CSS codes (not necessarily identical copies) with qubits putting on the  $q_1$ -,  $q_2$ - and  $q_3$ -simplices respectively satisfying  $q_1 + q_2 + q_3 = n$ , with the associated electric gauge fields being  $a^{q_1}$ ,  $a^{q_2}$  and  $a^{q_3}$  respectively. The corresponding constant-depth circuit can be expressed as

$$U = (-1)^{\int_{\Sigma_n} a^{q_1} \cup a^{q_2} \cup a^{q_3}}, \quad (38)$$

which can be evaluated according to the general definition of cup products in Eq. (11). We can re-express the circuit  $U$  using the cohomology basis  $\{\alpha^{q_1}\}$ ,  $\{\beta^{q_2}\}$ , and  $\{\gamma^{q_3}\}$  to derive the corresponding logical gate:

$$\begin{aligned} U &= \prod_{\alpha^{q_1}, \beta^{q_2}, \gamma^{q_3}} (-1)^{\int_{\Sigma_n} (\hat{n}_\alpha \alpha^{q_1}) \cup (\hat{m}_\beta \beta^{q_2}) \cup (\hat{l}_\gamma \gamma^{q_3})} \\ &= \prod_{\alpha^{q_1}, \beta^{q_2}, \gamma^{q_3}} \left[ (-1)^{\hat{n}_\alpha \hat{m}_\beta \hat{l}_\gamma} \int_{\Sigma_n} \alpha^{q_1} \cup \beta^{q_2} \cup \gamma^{q_3} \right] \\ &= \prod_{\alpha^{q_1}, \beta^{q_2}, \gamma^{q_3}} \overline{\text{CCZ}}[(\alpha^{q_1}; 1), (\beta^{q_2}; 2), (\gamma^{q_3}; 3)] \int_{\Sigma_n} \alpha^{q_1} \cup \beta^{q_2} \cup \gamma^{q_3}. \end{aligned} \quad (39)$$

In the case that the  $n$ D simplicial complex  $\mathcal{L}$  is the triangulation of a manifold  $\mathcal{M}^n$ , we can just take  $\Sigma_n = \mathcal{M}^n$ .

The cup product sum in the exponent now corresponds to an  $n$ -fold  $\mathbb{Z}_2$  intersection number of the Poincaré dual cycles:

$$\int_{\mathcal{M}^n} \alpha^{q_1} \cup \beta^{q_2} \cup \gamma^{q_3} = |\alpha_{n-q_1}^* \cap \beta_{n-q_2}^* \cap \gamma_{n-q_3}^*|. \quad (40)$$

We can easily generalize the triple cup product sum above to a  $k$ -fold cup product sum.

All our qLPDC code constructions in this paper utilize the cohomology operations in such higher gauge theories to implement logical non-Clifford gates.

### III. THREE-DIMENSIONAL HYPERGRAPH PRODUCT CODES

In order to achieve a quantum code with constant rate and power-law distance which supports logical non-Clifford gates, we construct a 3D hypergraph product code [45, 56] obtained from the homological product [46] of three good identical classical codes.

The good 1-cycle code  $\mathcal{C}$  with parameters  $[n, k, d]$  corresponds to the following chain complex  $\mathcal{L}$ :

$$C_1 \xrightarrow{\partial_1=\mathbf{H}} C_0, \quad (41)$$

where  $\mathbf{H}$  is the parity check matrix of the classical code. The bit and check variables are associated with  $C_1$  and  $C_0$  respectively. The length of the code (the number of bits) is denoted by  $n = \dim(V)$ , where  $V$  is the vector space spanned by all possible bit configurations represented by  $n$ -dimensional binary vectors. The code space is the subspace  $\mathcal{C} = \text{Ker } \mathbf{H} = \text{Ker } \partial_1 = H_1(\mathcal{L}; \mathbb{Z}_2) \subset V$ , where  $H_1$  represents the 1st  $\mathbb{Z}_2$ -homology group. The code length (number of bits) is  $n$ . We have the dimension of the classical code equaling to the 1st  $\mathbb{Z}_2$ -Betti number  $k = \dim(\text{Ker}(\mathbf{H})) = \dim(H_1(\mathcal{L}; \mathbb{Z}_2)) = b_1$ . For good classical code, the dimension is linear, i.e.,  $k = b_1 = \Theta(n)$ , while the distance equals the combinatorial  $\mathbb{Z}_2$  1-systole is also linear, i.e.,

$$d = \text{sys}_1(\mathcal{L}; \mathbb{Z}_2) = \Omega(n). \quad (42)$$

We now recall the definition of a combinatorial  $\mathbb{Z}_2$   $i$ -systole  $\text{sys}_i(\mathcal{L}; \mathbb{Z}_2)$  on the simplicial complex  $\mathcal{L}$  as

$$\text{sys}_i(\mathcal{L}) = \min\{|c_i| : c_i \in H_i(\mathcal{L}; \mathbb{Z}_2)\} \quad (43)$$

where  $|c_i|$  is the number of  $i$ -simplices on which the  $i$ -cycle  $c_i$  is non-zero.<sup>4</sup>

We also consider the transposed 0-cocycle code  $\mathcal{C}^T = \text{Ker}(\mathbf{H}^T) = \text{Ker}(\delta^0) = \text{Ker}(H^0)$  with the parameters

<sup>4</sup>Throughout this paper, the systole we discuss corresponds to the combinatorial systole including the manifold cases appeared later, where we consider the combinatorial systoles on the triangulation  $\mathcal{L}$  of the manifold.

$[n^T, k^T, d^T]$ , which is described by the following chain complex

$$C_1 \xleftarrow{\delta_0=H^T} C_0. \quad (44)$$

The distance of the transposed code  $\mathcal{C}^T$  equals the combinatorial  $\mathbb{Z}_2$  0-cosystole:

$$d^T = \text{sys}^0(\mathcal{L}; \mathbb{Z}_2). \quad (45)$$

Here, we recall the definition of the  $i$ -cosystole as:

$$\text{sys}^i(\mathcal{L}) = \min\{|c^i| : c^i \in H^i(\mathcal{L}; \mathbb{Z}_2)\}. \quad (46)$$

Now to optimize the performance of the logical CCZ gates, we want to make the transposed code  $\mathcal{C}^T$  also a good code. In order to achieve that, we start with a parity check matrix  $H$  of a good  $[n, k, d]$  classical code with full rank. Such a code can be obtained from random construction of good LDPC code. We then construct a new parity check matrix  $\bar{H} = H^T H$  and the associated code  $\bar{\mathcal{C}}$  with the symmetric property that  $\bar{H} = \bar{H}^T = H^T H$ . Therefore, we have the corresponding code length  $\bar{n} = \bar{n}^T = n$  due to the matrix multiplication rule and  $\bar{k} = \bar{k}^T$ . We can then obtain the following useful lemma:

**Lemma 1.** *For a classical code  $\bar{\mathcal{C}}$  with the parity check matrix  $\bar{H} = H^T H$ , where  $H$  is the parity check matrix of a good  $[n, k, d]$  classical LDPC code with full rank, we have  $\bar{\mathcal{C}} = \bar{\mathcal{C}}^T = \text{Ker}(\bar{H}) = \text{Ker}(\bar{H}^T) = \text{Ker}(H)$ . Moreover, the code  $\bar{\mathcal{C}}$  and its transposed code  $\bar{\mathcal{C}}^T$  are also good classical LDPC codes with linear dimension ( $\bar{k} = \Theta(n)$ ) and linear distance ( $\bar{d} = \Omega(n)$ ).*

*Proof.* Since  $H$  has full rank, meaning there is no redundant checks (the rank now equals the number of rows which is the number of checks), we hence have the following identity through the rank-nullity theorem:

$$\begin{aligned} \text{rank}(H) &= \dim(\text{Im}(H)) = \dim(V) - \dim(\text{Ker}(H)) \\ &= n - k = n^T, \end{aligned} \quad (47)$$

where  $n^T = \dim(V^T)$  is the number of checks in  $\mathcal{C}$  equaling the number of bits in the transposed code  $\mathcal{C}^T$  and  $V^T$  the vector space associated with the check variables in  $\mathcal{C}$  or equivalently the bit variables in  $\mathcal{C}^T$ . We hence have

$$\begin{aligned} \text{rank}(H^T) &= \text{rank}(H) = \dim(V) - \dim(\text{Ker}(H)) \\ &= n^T - k^T = n^T, \end{aligned} \quad (48)$$

where  $k^T$  is the dimension of the transposed code and we have  $k^T = 0$ . This leads to  $\text{Ker}(H^T) = 0$ . We thus have

$$\text{Ker}(H^T H) = \text{Ker}(H), \quad (49)$$

which leads to

$$\text{Ker}(\bar{H}) = \text{Ker}(\bar{H}^T) = \text{Ker}(H). \quad (50)$$

This means both the 1-cycle code  $\bar{\mathcal{C}} = \text{Ker}(\bar{H}) = H_1$  and the transposed 0-cocycle code  $\bar{\mathcal{C}}^T = \text{Ker}(\bar{H}^T) = H^0$

corresponds to the same good classical code with both linear dimension and linear distance. In particular, we now have a linear scaling for both the 0<sup>th</sup> and 1<sup>st</sup> Betti numbers corresponding to the dimensions of the of  $\bar{\mathcal{C}}$  and  $\bar{\mathcal{C}}^T$  respectively:

$$\begin{aligned} \bar{k} &= b_1 = \text{rank}(H_1(\mathcal{L}; \mathbb{Z}_2)) = \Theta(n), \\ \bar{k}^T &= b_0 = \text{rank}(H_0(\mathcal{L}; \mathbb{Z}_2)) = \text{rank}(H^0(\mathcal{L}; \mathbb{Z}_2)) = \Theta(n), \end{aligned} \quad (51)$$

where we have used the isomorphism between the  $i^{\text{th}}$   $\mathbb{Z}_2$  homology and cohomology groups  $H_i(\mathcal{L}; \mathbb{Z}_2) \cong H^i(\mathcal{L}; \mathbb{Z}_2)$  due to the universal coefficient theorem [44]. Since  $\bar{\mathcal{C}} = \bar{\mathcal{C}}^T = \mathcal{C}$ , we have

$$\bar{d} = \bar{d}^T = d = \Omega(n). \quad (52)$$

Although the code space of  $\bar{\mathcal{C}}$  and  $\mathcal{C}$  is identical, their corresponding tanner graph is still different. Nevertheless, since both  $H^T$  and  $H$  are sparse matrices ( $\mathcal{C}$  is a classical LDPC code), their multiplication  $H^T H = \bar{H}$  is also a sparse matrix which means the code  $\bar{\mathcal{C}} = \bar{\mathcal{C}}^T$  is also an LDPC code.  $\square$

We note that here we focus on the case that the good classical code  $\mathcal{C} = \text{Ker}(H)$  with a full-rank parity check matrix is obtained from a random bipartite expander graph. One can have the same construction using the Sipser-Spielman code [50], while the proof for the properties of  $\bar{H} = H^T H$  will be a bit different. We will leave this discussion for future works or updated version of this paper.

We now take a homological product of three identical copies of code  $\bar{\mathcal{C}} = \text{Ker}(\bar{H}) = \text{Ker}(H^T H)$  to form a 3D hypergraph product code with parameters  $[N, K, D]$ , where  $N = 3n^3$ . The total chain complex of the 3D hypergraph product code has the product form  $\tilde{X} = X \otimes X' \otimes X''$  and corresponds to the chain complex

$$\tilde{C}_3 \xrightarrow{\partial_3} \tilde{C}_2 \xrightarrow{\partial_2=H_X^T} \tilde{C}_1 \xrightarrow{\partial_1=H_Z} \tilde{C}_0. \quad (53)$$

where  $\tilde{C}_i$  denotes the  $i$ -chain group of the total complex  $\tilde{X}$ . In particular, we have the following relations to the chain groups of the three classical codes:

$$\begin{aligned} \tilde{C}_0 &= C_0 \otimes C'_0 \otimes C''_0, \\ \tilde{C}_1 &= C_1 \otimes C'_0 \otimes C''_0 + C_0 \otimes C'_1 \otimes C''_0 + C_0 \otimes C'_0 \otimes C''_1, \\ \tilde{C}_2 &= (C_1 \otimes C'_1 \otimes C''_0) \oplus (C_0 \otimes C'_1 \otimes C''_1) \oplus (C_1 \otimes C'_0 \otimes C''_1) \\ &\quad \oplus (C_2 \otimes C'_0 \otimes C''_0) \oplus (C_0 \otimes C'_2 \otimes C''_0) \oplus (C_0 \otimes C'_0 \otimes C''_2), \\ \tilde{C}_3 &= C_1 \otimes C_1 \otimes C_1, \end{aligned} \quad (54)$$

which tell us how to compose the vertices, edges, faces, and cubes with vertices and edges in the input classical code. For the new code, we can use the Künneth theorem to get the corresponding 1st homology and cohomology,

i.e.,

$$\begin{aligned}\tilde{H}_1 &= (H_1 \otimes H'_0 \otimes H''_0) \oplus (H_0 \otimes H'_1 \otimes H''_0) \\ &\quad \oplus (H_0 \otimes H'_0 \otimes H''_1) \\ \tilde{H}^1 &= (H^1 \otimes H'^0 \otimes H''^0) \oplus (H^0 \otimes H'^1 \otimes H''^0) \\ &\quad \oplus (H^0 \otimes H'^0 \otimes H''^1).\end{aligned}\quad (55)$$

One can quickly verify that the dimension, which equals the first Betti number, is still linear:

$$\begin{aligned}K = \tilde{b}_1 &= b_1 \cdot b'_0 \cdot b''_0 + b_0 \cdot b'_1 \cdot b''_0 + b_0 \cdot b'_0 \cdot b''_1 \\ &= \Theta(n) \cdot \Theta(n) \cdot \Theta(n) = \Theta(N),\end{aligned}\quad (56)$$

where  $K$  and  $N$  represent the total number of logical and physical qubits respectively. The  $Z$ -distance is the combinatorial 1-systole

$$D_Z = \text{sys}_1(\tilde{\mathcal{L}}; \mathbb{Z}_2) = \Omega(n) = \Omega(N^{1/3}), \quad (57)$$

and the  $X$ -distance is the combinatorial 1-cosystole

$$D_X = \text{sys}^1(\tilde{\mathcal{L}}; \mathbb{Z}_2) = \Omega(n^2) = \Omega(N^{2/3}), \quad (58)$$

where we have used the Künneth theorem in Eq. (54). The overall distance is hence

$$D = \min(D_Z, D_X) = \Omega(N^{1/3}). \quad (59)$$

#### IV. NON-CLIFFORD LOGICAL GATES ON THICKENED 3D HYPERGRAPH-PRODUCT CODES

##### A. Building manifolds from classical codes

We generalize the code-to-manifold mapping in Ref. [48] from the case of quantum codes to the case of classical codes. The manifolds built from the classical or quantum codes will then serve as the Legos of the product construction of the thickened qLDPC codes.

Roughly speaking, the construction of the manifold can be considered via a ‘*plumber’s view*’ as thickening the tanner graph of a skeleton classical code along extra-dimensions with the thickness being only  $O(1)$  as illustrated by Fig. 3, which hence only leads to a constant overhead of the thickened classical code defined on the manifold.

A general classical expander code corresponds to a 2-term  $\mathbb{Z}_2$ -chain complex in Eq. (41) can be defined on a bipartite Tanner graph or equivalently a hypergraph. When viewed as a Tanner graph  $G_T = (V_B, V_C, E)$ , the bits and checks are represented by the two types of vertices  $V_B$  and  $V_C$  represented by circles and squares respectively, while the edge  $E$  connecting them encodes the boundary map, as illustrated in Fig. 3(a,c,e). When viewed as a hypergraph  $G_h = (V, E_h)$ , the checks are on the vertices  $V$  while the bits are associated with a hyper-edge  $E_h$  composed by the edges connecting to a circle.

In order to construct a manifold from this classical code, we first need to lift the  $\mathbb{Z}_2$ -chain complex to a  $\mathbb{Z}$ -chain complex. For classical code, one can just use a ‘naive’ lift, which maps 0 mod 2 to  $0 \in \mathbb{Z}$  and 1 mod 2 to  $1 \in \mathbb{Z}$  and obtain the following lifted chain complex:

$$\hat{C}_1 \xrightarrow{\hat{\partial} = \hat{H}} \hat{C}_0, \quad (60)$$

where  $\hat{\partial}$  and  $\hat{H}$  are the lifted boundary map and parity check matrices with  $\mathbb{Z}$  coefficients respectively obtained from the  $\mathbb{Z}_2$  parity check matrix  $\bar{H} = H^T H$  as discussed in Sec. III.

As has been observed in Ref. [48], one cannot directly obtain the manifold and the underlying simplicial complex structure from the above lifted chain complex. The issue is that on a manifold or more generally a simplicial complex, and edge (1-cell) is always adjacent to two vertices (0-cells). This is not true for a general two-term chain complex corresponding to a hypergraph where a hyperedge can be adjacent to more than two vertices. In order to resolve this issue, we need to promote the bits from 1-cells (edges) to higher-dimensional cells. An obvious choice is to promote the bits to 2-cells (faces), but that may introduce spurious homologies as pointed out in Ref. [48], which may lead to an  $O(1)$  distance. Instead, we need to go to higher dimensions and put bits on 4-cells, and checks on 3-cells, which will leads to a good separation between the dimension of the logical cycles/cocycles having large systoles with the spurious cycles/cocycles with  $O(1)$  systoles. We construct the following cellular chain complex  $\mathcal{L}$  corresponding to the handle decomposition of a 10-dimensional manifold  $\mathcal{M}^{10}$ :

$$\begin{array}{ccccccc} C_{10} & \rightarrow & \cdots & \rightarrow & C_5 & \rightarrow & C_4 \xrightarrow{\hat{\partial} \sim \bar{H}} C_3 \rightarrow C_2 \rightarrow \cdots, \\ & & & & & & \text{bit} \quad \quad \text{check} \end{array} \quad (61)$$

where the boundary map  $\partial_4$  instructing how the 4-cells are attached to the 3-cells can be obtained from the information in the lifted parity check matrix  $\hat{\partial} = \bar{H} = H^T H$  (omit the hat for simplicity). This means the portion of the above cellular chain complex  $C_4 \xrightarrow{\hat{\partial} \sim \bar{H}} C_3$  is isomorphic to the lifted chain complex Eq. (60) obtained from the classical code. Here, the chain group  $C_i$  is only non-trivial for  $i = 3, 4, 6, 7$ , and we can re-express the above cellular chain complex as

$$\cdots \rightarrow 0 \rightarrow C_7 \xrightarrow{\hat{\partial}^T \sim \bar{H}^T} C_6 \rightarrow 0 \rightarrow C_4 \xrightarrow{\hat{\partial} \sim \bar{H}} C_3 \rightarrow 0 \rightarrow \cdots. \quad (62)$$

Note that there is a symmetry between  $C_4$  and  $C_6$ , and between  $C_3$  and  $C_7$ , which is a reflection of Poincaré duality of a manifold. We can further write down the dual

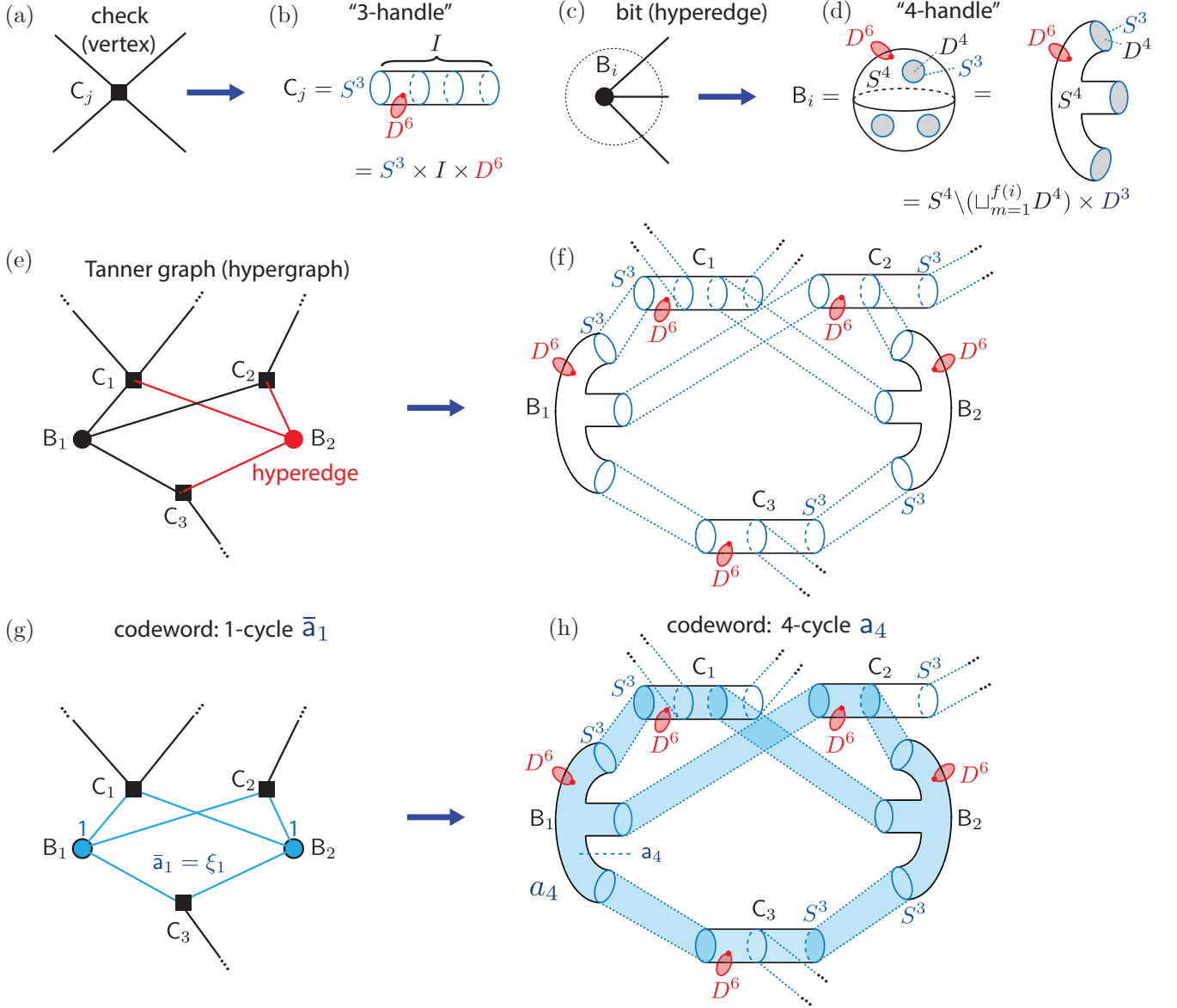


Figure 3. A plumber's view of classical codes. (a) A check  $C_j$  on the vertex (square). (b) The check  $C_j$  is mapped to a “3-handle”  $C_j = S^3 \times I \times D^6$ . (c) A bit  $B_i$  on a hyperedge composed of multiple edges connected to a single circle. (d) The bit  $B_i$  is mapped to a “4-handle” corresponding to a 4-sphere  $S^4$  with multiple 4-disks  $D^4$  being removed and then thickened by  $D^6$ . It has multiple legs which can be connected to the neighboring “3-handles”. (e) A bipartite Tanner graph with two types of vertices corresponding to checks (squares) and bits (circles) respectively. Equivalently one can consider it as a hypergraph where the checks are placed on the vertices (square) and the bits placed on the hyperedge (red). (f) The Tanner graph is thickened to a handlebody where the “4-handles” are attached to the adjacent “3-handles” according to the boundary map in the skeleton Tanner graph and via gluing them along the attaching region  $S^3 \times D^6$  of the “4-handles”. (g) A codeword of the classical code  $\bar{C}$  is a 1-cycle  $\bar{a}_1$  supported on a subset of hyperedges (blue). (h) The codeword is thickened to a 4-cycle  $a_4$  (blue) in the 10-manifold.

cellular chain complex  $\mathcal{L}^*$ :

$$\cdots \leftarrow 0 \leftarrow C_3^* \xleftarrow{\hat{\partial} \sim \bar{H}} C_4^* \leftarrow 0 \leftarrow C_6^* \xleftarrow{\hat{\partial}^T \sim \bar{H}^T} C_7^* \leftarrow 0 \leftarrow \cdots \quad (63)$$

We can see that  $\hat{\partial} = \bar{H}$  instructs the attachment between

the dual 4-cells in  $C_4^*$  and the dual 3-cells in  $C_3^*$ , which are the dual of 6-cells and 7-cells respectively.

We now introduce the handle construction of the smooth 10-manifold  $\mathcal{M}^{10}$ . We first follow the type of handle construction procedure in Ref. [48], and will need to modify it later to further lower the dimension.

A 10D  $k$ -handle is a 10-manifold  $h_k = D^k \times D^{10-k}$

along with its attaching region  $\partial D^k \times D^{10-k} = S^{k-1} \times D^{10-k}$ , where  $D^k$  and  $S^{k-1}$  represents a  $k$ -dimensional ball and a  $(k-1)$ -dimensional sphere respectively. Roughly speaking, a  $k$ -handle can be considered as a thickened  $k$ -cell. Handlebodies are unions of a sequence of handles where each handle is attached (glued) along its attaching region to the previous union of handles. We build the handlebodies start with 0-handles, which are 10-balls  $h_0 = 0 \times D^{10} = D^{10}$  with no attaching region. One then step by step attaches handles of increasing indices  $k$  to the previously constructed handlebodies until attaching the 10-handles  $h_{10} = D^{10} \times 0 = D^{10}$  which has the empty co-attaching region  $D^k \times \partial D^{10-k}$  to close the 10-manifold.

Following Ref. [48], we first build a 4-handlebody  $H$ , which corresponds to a 10-manifold with boundary that is the union of  $k$ -handles of indices  $k = 0, 1, 2 \dots, 4$ . This can be viewed as the right part of the cellular chain complex in Eq. (62) starting from  $C_4$ . We then take another identical copy of the 4-handlebody  $H$ , which can be viewed as the left part of the dual cellular chain complex Eq. (63) according to Poincaré duality. We hence obtain the closed manifold  $\mathcal{M}^{10} = \mathcal{D}H$  as the double of  $H$  by gluing the two copies of  $H$  along their boundary  $\partial H$  with an identity map  $id_{\partial H}$ , i.e.,  $\mathcal{D}H = H \cup_{id_{\partial H}} H$ . Due to Poincaré duality, in the second copy the  $k$ -handles becomes the  $(10-k)$  handles such that we obtain the full cellular chain complex in Eq. (63).

We first assign a 0-handle  $h_0 = 0 \times D^{10} = D^{10}$  to each check in the classical code, and then attach a 3-handle  $h_3 = D^3 \times D^7$  to the boundary of each 0-handle  $h_0$ . The attaching region of  $h_3$  is  $\partial D^3 \times D^7 = S^2 \times D^7$ , and the attaching map in this case is

$$S^2 \times D^7 \hookrightarrow \partial D^{10} = S^9. \quad (64)$$

We hence get a  $(0, 3)$ -handlebody  $\sqcup_{j=1}^{n^T} (S^3 \times D^7)_j \equiv \sqcup_{j=1}^{n^T} C_j$ , where  $\sqcup$  represents a disjoint union,  $C_j$  represents the “3-handles” corresponding to the  $j^{\text{th}}$  bit, and  $n^T$  is the number of checks. The quote on “4-handles” means they are handlebodies themselves containing handles of lower indices following the convention in Ref. [48]. We also call  $C_j$  the check “handle”, which can also be rewritten as  $C_j = (S^3 \times I \times D^6)_j$  as illustrated in Fig. 3(a, b). Note that when choosing the symmetric parity check matrix  $\mathbb{H} = \mathbf{H}^T \mathbf{H}$ , we have  $n^T = n$  equal to the number of bits.

We then attach “4-handles”  $B_i$  to each “3-handles”  $C_j$ , where  $B_i$  refers to the “4-handles” corresponding to the  $i^{\text{th}}$  bit (also call them bit “handles”). The attachment is determined by the lifted boundary map  $\hat{\partial}$  from the classical code as

$$\hat{\partial} B_i = \sum_{j \in I_i} C_j, \quad (65)$$

where  $I_i$  indexes all the  $C_j$  incident to  $B_i$ . Note that all the coefficient on the right of the above equation is +1 since we have chosen the naive lift that maps all 1

mod 2 to  $1 \in \mathbb{Z}$ . This data is also encoded in the Tanner graph or equivalently the hypergraph of the skeleton classical code as illustrated in the correspondence between Fig. 3(e) and (f). As shown in Fig. 3(c,d), each “4-handle” has the form  $B_i = N_i^4 \times D^6$  where the  $D^4$  in the standard 4-handle is replaced by a punctured 4-sphere  $N^4 = S^4 \setminus \sqcup_{m=1}^{f(i)} D_m^4$ , where  $f(i) = |I_i|$  represents the number of check “handles”  $C_j$  that the  $i^{\text{th}}$  bit “handle” is incident to given by the lifted boundary map  $\hat{\partial}$ . The attaching region of a “4-handle”  $B_i$  is  $\sqcup_{m=1}^{f(i)} (\partial D^4 \times D^6)_{i,m} = \sqcup_{m=1}^{f(i)} (S^3 \times D^6)_{i,m}$ , similar to the case of the standard 4-handle. We then glue the attaching region of the “4-handles” to the boundary of the “3-handles”  $\partial C_j = (S^3 \times \partial D^7)_j = (S^3 \times S^6)_j$  [see Fig. 3(f)]. The corresponding attaching map from  $B_i$  to the adjacent  $C_j$  is hence:

$$(S^3 \times D^6)_{i,m} \hookrightarrow (S^3 \times S^6)_j, \quad (66)$$

with the attaching rule specified by Eq. (65). We hence have built the desired 4-handlebody  $H$  from the classical code. After taking the double of  $H$ , we obtain the closed 10-manifold  $\mathcal{M}^{10} = \mathcal{D}H$  as mentioned above.

Now we show how the logical information is mapped from the skeleton classical code to the thickened code on the manifold  $\mathcal{M}^{10}$ . A codeword of the skeleton classical code corresponds to the 1-cycle  $\bar{a}_1 = \xi_1$  on the hypergraph  $G_h$ , and is illustrated in Fig. 3(g), where the highlighted hyperedges are the support of the codeword. Now the 1-cycle  $\xi_1$  forms the skeleton of the codeword in the manifold code corresponding to the 4-cycle  $a_4$ , as illustrated in Fig. 3(g,h).

## B. Building 4-manifolds and the corresponding codes that admit triple cup products

### 1. The modified construction

In order to lower the dimensions of the constructed manifold for practical purpose, we will now modify the manifold construction in Ref. [48] to a 4-manifold  $\mathcal{M}^4$  where the bits are now placed on 2-cells. From the perspective of systolic geometry, the lowering of the manifold dimension can lead to spurious cycles/cocycles with  $O(1)$  size which makes the systole only  $O(1)$ , as has been discussed in Ref. [48]. However, as will be elaborated later, one can use a subsystem code idea that chooses proper cycle/cocycle basis to encode the logical information, such that the distance in the subsystem code is still large.

The modified construction still follows the handle construction as discussed in Sec. IV A. We choose the “1-handles” corresponding to the checks as

$$C_j = (S^1 \times D^3)_j = (S^1 \times I \times D^2)_j, \quad (67)$$

as shown in Fig. 4(a,b). Similarly, we choose the “2-handles” corresponding to the bits as the thickened punc-

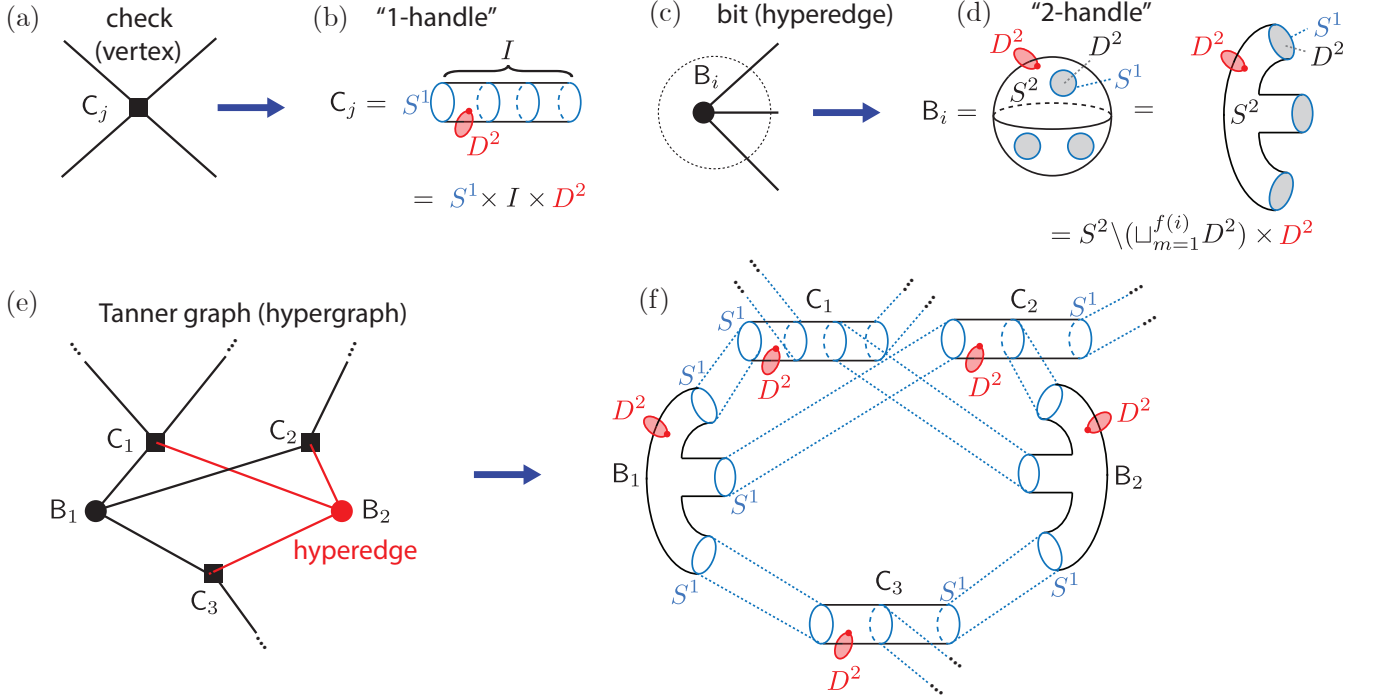


Figure 4. (a,b) The check  $C_j$  is mapped to a “1-handle”  $C_j = S^1 \times I \times D^2$ . (c,d) The bit  $B_i$  is mapped to a “2-handle” corresponding to a 2-sphere  $S^2$  with multiple 2-disks  $D^2$  being removed and then further thickened by  $D^2$ . (e) A Tanner graph or equivalently a hypergraph. (f) The Tanner graph is thickened to a handlebody where the “2-handles” are attached to the adjacent “1-handles” according to the boundary map in the skeleton Tanner graph and via gluing them along the attaching region  $S^1 \times D^2$  of the “2-handles”.

tured 2-spheres

$$B_i = \left( S^2 \setminus (\cup_{m=1}^{f(i)} D^2) \times D^2 \right)_i, \quad (68)$$

as illustrated in Fig. 4(c,d). Similar to the 10-manifold construction above, we attach the handle according to the lifted boundary map  $\hat{\partial}$  and Eq. (65), which is also encoded in the Tanner graph in Fig. 4(c). The attaching map from the “2-handles”  $B_i$  to the “1-handles”  $C_j$  corresponds to disjoint embedding of the attaching regions:

$$(S^1 \times D^2)_{i,m} \hookrightarrow \partial(S^1 \times D^3)_j = (S^1 \times S^2)_j, \quad (69)$$

as illustrated abstractly in Fig. 4(f) and concretely in Fig. 5. The  $C_j$ -“handle”, which has dimension 4, is illustrated in Fig. 4(a) with a 1D projection, can also be shown with a 2D and 3D projection respectively as in Fig. 5(b,c). In the 2D projection in (b), the cylinder  $S^1 \times I$  is displaced along the  $D^2$  direction, where the shaded region represents the boundary of the  $C_j$ -“handle”:  $\partial C_j = S^1 \times \partial D^3 = S^1 \times S^2$ . In the 3D projection in (c), the cylinder is displaced along two  $D^1$  directions, which gives rise to a thickened cube, i.e., cube  $D^3$  times a circle  $S^1$  in the extra dimension. Now the boundary of this cube is  $\partial D^3 = S^2$ , which gives rise to the boundary of the  $C_j$ -“handle”  $S^1 \times S^2$ . We then visualize the attaching map in Eq. (69) abstractly illustrated in Fig. 5(d) with the concrete 2D projection in Fig. 5(e),

where the  $B_1$ ,  $B_2$  and  $B_3$  “handles” are attached (glued) to the boundary of the  $C_1$ -handle. The attaching regions  $S^1 \times D^2$  are highlighted in red. A more concrete illustration is shown via the 3D projection in Fig. 5(f), where one can clearly see that the  $B_i$ -“handles” are attached to the boundary of the thickened cube  $S^1 \times D^3$  (as a thickened 2-sphere  $S^1 \times S^2$ ) with the attaching regions  $S^1 \times D^2$  being highlighted.

So far, we have built the desired 2-handlebody  $H$  from the classical code, which is essentially a thickened Tanner graph. We then take the double of  $H$  to obtain the closed 4-manifold  $\mathcal{M}^4 = \mathcal{D}H$  similar to the previous construction of the 10-manifold. Consider a tubular segment  $S^1 \times I \times D^2$  (i.e., a tubular neighborhood of  $S^1 \times I$ ) either inside the  $C_j$ - or the  $B_i$ -handles, the double produces

$$(S^1 \times I \times D^2) \cup_{id_{S^1 \times I \times S^1}} (S^1 \times I \times D^2) = S^1 \times I \times S^2 \quad (70)$$

since two disks glued along their common  $S^1$  boundary form a sphere, i.e.,  $D^2 \cup_{id_{\partial D^2 = S^1}} D^2 = S^2$ , as shown in Fig. 6(a). More concrete illustration with 3D projection is shown in Fig. 6(b), where each square region (orange)  $D^2$  has a boundary  $S^1$  which is identified to the  $S^1$  boundary in the other identical copy. At the junction where multiple  $B_i$ -“handles” are attached to a single  $C_j$ -“handles” as illustrated abstractly in Fig. 6(c) and more concretely with the 3D projection in Fig. 6(d), the only additional care that needs to be taken is on the left and

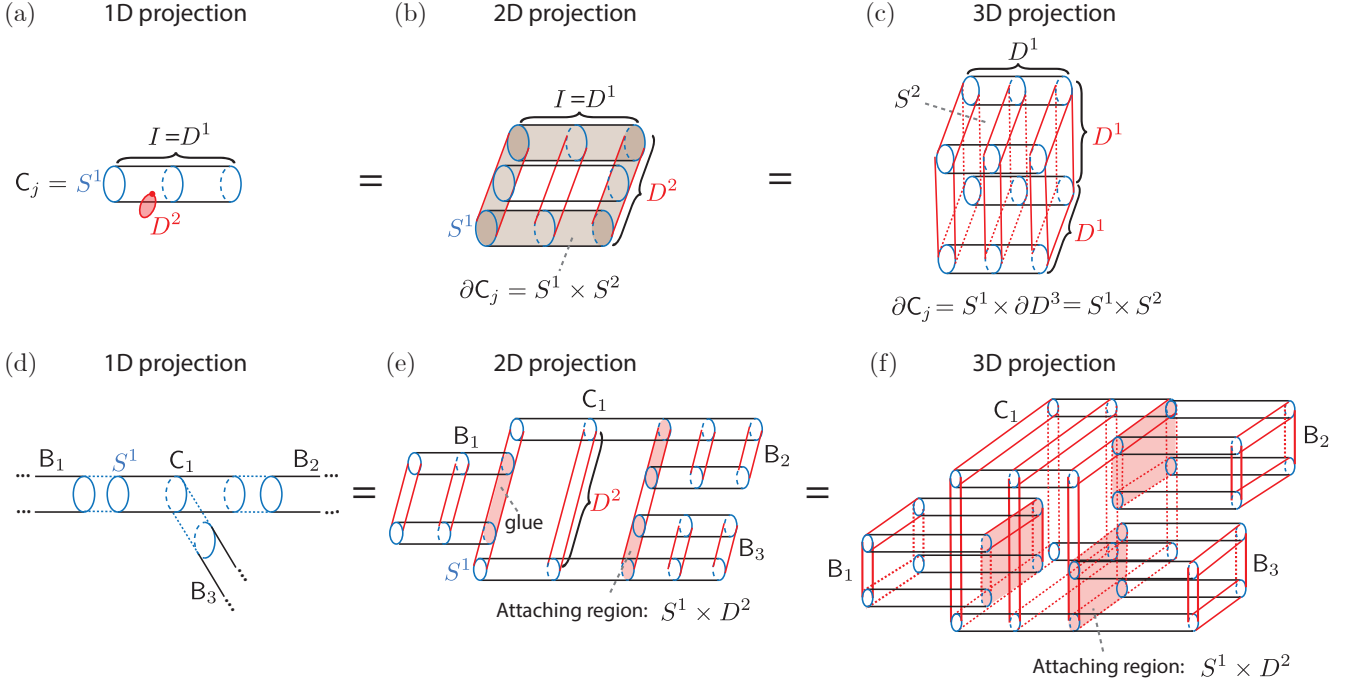


Figure 5. (a) The “1-handle”  $C_j$  represented in the 1D projection, where both  $D^2$  and  $S^1$  should be viewed as along extra dimensions. (b) 2D projection:  $S^1$  can be displaced along  $I = D^1$  or  $D^2$ . (c) 3D projection:  $S^1$  can be displaced along  $D^1$  in three different directions. One can view the “1-handle” as a 3D cube thickened along  $S^1$  in the extra dimension. The boundary of the cube is a 2-sphere  $S^2$ , while the boundary of the “1-handle” is a 2-sphere thickened along  $S^1$ , i.e.,  $S^1 \times S^2$ . (d) Illustration of three “2-handles”  $B_1, B_2$  and  $B_3$  attached to a “1-handle”  $C_1$  in the 1D projection. (e) 2D projection: the attaching regions  $S^1 \times D^2$  (highlighted) of three “2-handles” are glued to the boundary of the “1-handle”. (f) 3D projection: one can visualize the attaching region (highlighted) as a thickened 2-disk:  $S^1 \times D^2$ .

right boundaries of the  $C_j$ -“handle” where we attach the  $B_i$  “handles”. Note that the regions (green) outside the attaching regions (red), i.e.,  $(S^1 \times D^2) \setminus \sqcup_m (S^1 \times D^2)_m$  are boundaries in the 2-handlebody  $H$ , which are hence identified with the same regions in the identical copy as shown in Fig. 6(d). The rest of the regions are all tubular segments  $S^1 \times I \times D^2$  which can be identified using the rules in Fig. 6(a,b) as described above.

We now reach the following lemma:

**Lemma 2.** *The  $r$ -dimensional manifold  $\mathcal{M}^r$  ( $r \geq 4$ ) built from handle construction with the input of Tanner graph  $G_T$  of a classical LDPC code  $\tilde{\mathcal{C}}$  with  $n$  bits satisfies the following properties:*

1.  $\mathcal{M}^r$  has a bounded local geometry, i.e., each vertex in its triangulation is adjacent to  $O(1)$  simplices.
2.  $\mathcal{M}^r$  contains  $\Theta(n)$  total number of  $k$ -simplices ( $0 \leq k \leq D$ ), i.e.,  $\dim(C_k) = \Theta(n)$ , where  $C_k$  represents the  $k^{\text{th}}$  chain group.

The proof of the above lemma is contained in the proof of Theorem 1.2.1 in Ref. [48] which considers the more general case of mapping a quantum LDPC code to a manifold with bounded geometry. Some subtlety of this proof is discussed in footnote 5. The essence of the proof is the following:

Since the Tanner graph of a classical LDPC code has bounded degree, each  $B_i$ -“handle” will only be attached to  $O(1)$   $C_j$ -“handles”. Hence each simplex will only be attached to constant number of simplices and the maximal vertex degree is hence only  $O(1)$ . Since each “handles” is a constant-size manifold with boundary that can be triangulated with constant number of simplices, the total number of simplicies is proportional to the number of “handles”, which is in turn proportional to the number of bits and checks, i.e.,  $\Theta(n)$ . Note that the total number of checks is also  $\Theta(n)$  since the rate is constant for good classical LDPC codes.

## 2. Cycle and cocycle mapping

There is a following mapping between the basis cycles/cocycles in the skeleton classical code and those in the thickened simplicial LDPC code defined on the triangulation  $\mathcal{L}$  of the 4-manifold  $\mathcal{M}^4$ :

$$\bar{a}_1 \rightarrow a_2, \quad \bar{b}_0 \rightarrow b_1, \quad \bar{a}^1 \rightarrow a^2, \quad \bar{b}^0 \rightarrow b^1, \quad (71)$$

which belong to the cycle/cocycle basis  $\{a_2\}, \{b_1\}, \{a^2\}$  and  $\{b^1\}$ . Due to the introduction of Poincaré duality  $H_k(\mathcal{L}; \mathbb{Z}_2) \cong H^{4-k}(\mathcal{L}^*; \mathbb{Z}_2)$  from the double of the 4-

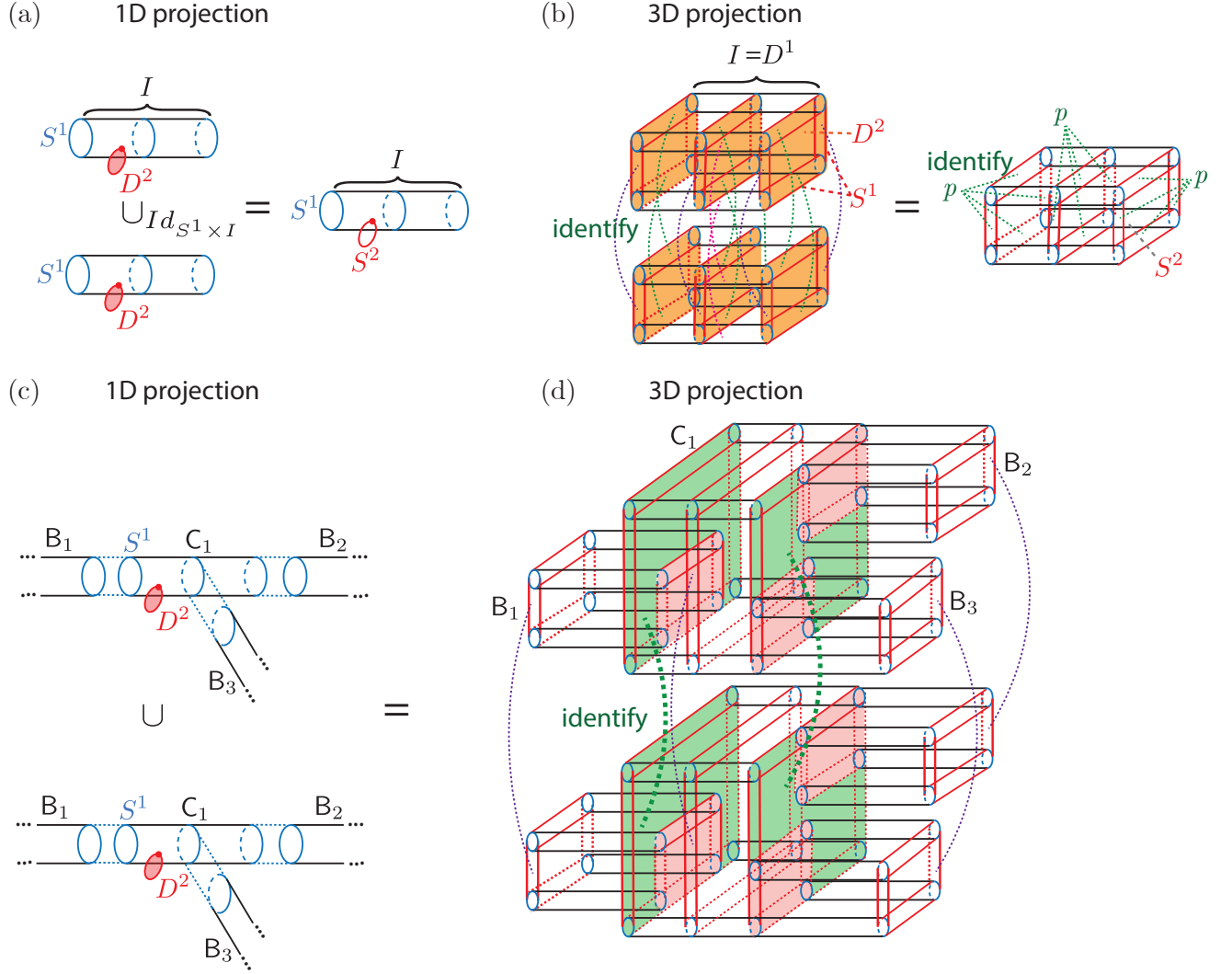


Figure 6. (a) Illustration of the double of a tubular segment  $S^1 \times I \times D^2$  in the 1D projection. Two  $D^2$ 's are glued along their common  $S^1$  boundary and form an  $S^2$ . The double hence becomes  $S^1 \times I \times S^2$ . (b) Illustration of the double of a tubular segment in the 3D projection. Note that the vertical 2-disks  $D^2$  in the two copies are highlighted and glued in pair along the common  $S^1$  boundary. This becomes equivalent to a single copy where the boundary of each 2-disk  $D^2$  are identified to a single point and hence becomes  $S^2$ . (c) Illustration of the double of two junction regions where three “2-handles” are attached to a “1-handle”. (d) Visualizing the junction region in the 3D projection: the 2-disks  $D^2$  including the attaching regions (highlighted in red) in the two copies are identified in the same way as the tubular segment in (b). The boundary regions of the 1-handle  $C_j$  outside the attaching regions (highlighted in green) in each copy are identified with each other like a wormhole.

handlebody, the above cycles and cocycles all have their Poincaré dual cocycles and cycles on the dual triangulation  $\mathcal{L}^*$ :

$$a_2 \sim a^{*2}, \quad b_1 \sim b^{*3}, \quad a^2 \sim a_2^*, \quad b^1 \sim b_3^*. \quad (72)$$

These new cycle/cocycle classes in the dual triangulation  $\mathcal{L}^*$  also have corresponding classes in the original triangulation  $\mathcal{L}$  due to the isomorphism  $H_k(\mathcal{L}; \mathbb{Z}_2) \cong H_k(\mathcal{L}^*; \mathbb{Z}_2) \cong H_k(\mathcal{M}^4; \mathbb{Z}_2)$  and  $H^k(\mathcal{L}; \mathbb{Z}_2) \cong H^k(\mathcal{L}^*; \mathbb{Z}_2) \cong H^k(\mathcal{M}^4; \mathbb{Z}_2)$ , which have essentially the same support in the continuous picture of the manifold  $\mathcal{M}$ . For simplicity, we also use the

same set of notations to represent these corresponding cycles/cocycles in the original triangulation  $\mathcal{L}$ , i.e.,  $a^{*2}, b^{*3}, a_2^*$  and  $b_3^*$ .

Besides the Poincaré duality isomorphism, since we are considering  $\mathbb{Z}_2$  homology, there is an additional isomorphism between the  $k^{\text{th}}$   $\mathbb{Z}_2$ -homology and cohomology in the same triangulation  $\mathcal{L}$ , i.e.,  $H_k(\mathcal{L}; \mathbb{Z}_2) \cong H^k(\mathcal{L}; \mathbb{Z}_2)$  due to the universal coefficient theorem [44]. One can consider the  $k^{\text{th}}$  homology group  $H_k$  and  $k^{\text{th}}$  cohomology group  $H^k$  as  $\mathbb{Z}_2$  vector spaces. The above isomorphism corresponds to the following pairing (inner product) of the basis vector ( $k$ -cycle  $c_k$ ) and the dual basis vector



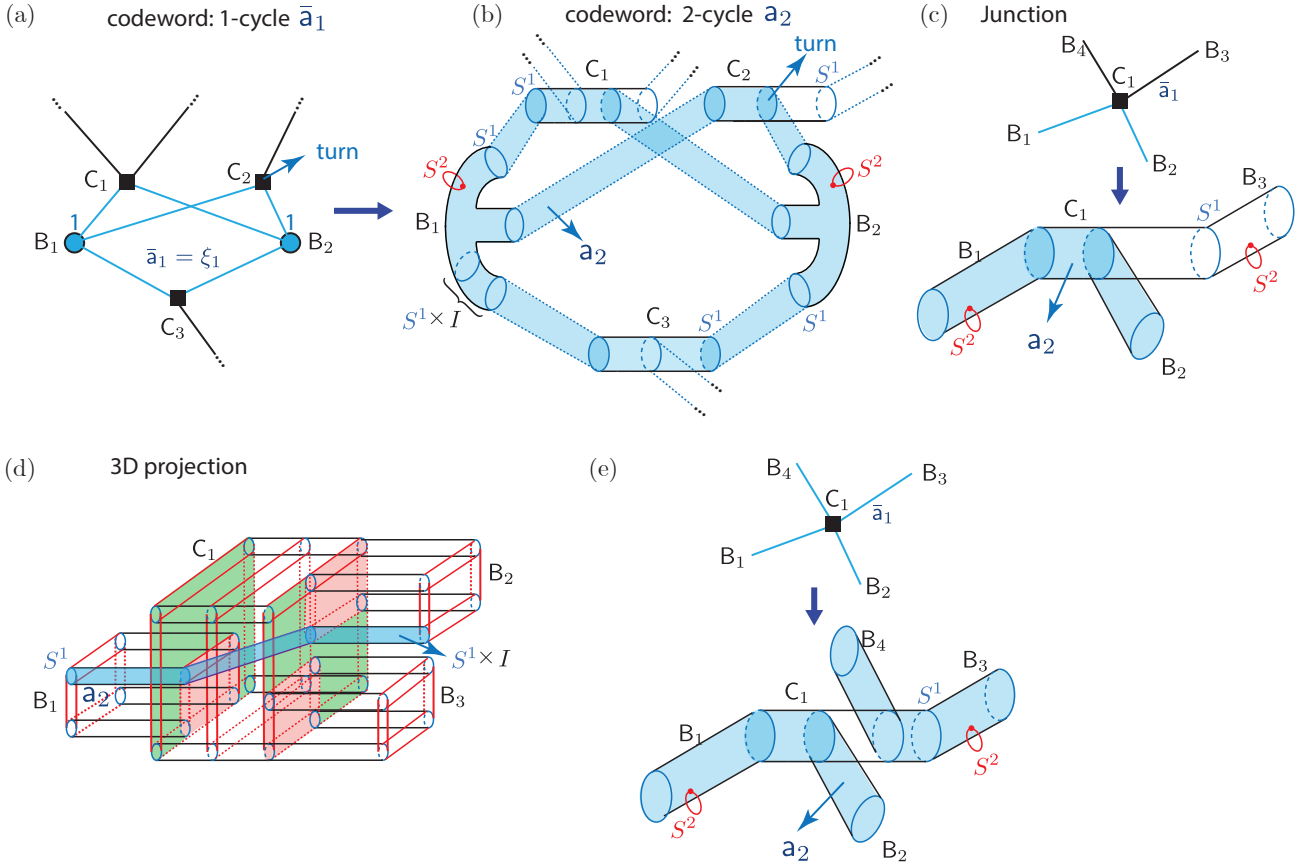


Figure 7. (a) The codeword as a 1-cycle  $\bar{a}_1$  in the skeleton hypergraph. The 1-cycle can turn at the check (square vertex). (b) Visualization of the 4-manifold, where each tubular segment is thickened along  $S^2$ . The codeword is thickened into a 2-cycle  $a_2$  in the manifold. (c) The thickened 2-cycle codeword can turn at the junction where multiple “2-handles” are attached to a single “1-handle”. (d) Geometric understanding of the turning of 4-cycle in the 3D projection. The 2-cycle can be viewed as the worldsheet (trajectory) of  $S^1$ . The  $S^1$  can be transported along the extra dimensions. (e) The codeword in the skeleton hypergraph always occupies even number of hyperedges (bits) connected to a vertex (check). When there are more than two hyperedges being occupied in the skeleton hypergraph, one can always resolve the corresponding thickened 2-cycles in the manifolds via the equivalence relation in homology.

( $k$ -cocycle  $c'^k$ ):

$$\int_{\mathcal{M}^4} (c_k)(c'^k) \equiv \int_{c_k} c'^k = |c_k \cap c'^k| = \delta_{c,c'}, \quad (73)$$

where in the second expression we sum the  $\mathbb{Z}_2$ -coefficients of the cocycle  $c'^k$  over the cycle  $c_k$  and is equivalent to the number of overlap  $k$ -simplices between the support of the cycle-cocycle pair. We call the cycle and cocycle with the same label  $c$ , i.e.,  $c_k$  and  $c^k$  (and hence overlapping on single  $k$ -simplex) a conjugate pair, since later they will be used to compose the logical- $Z$  and logical- $X$  operators respectively (which are conjugate variables) in the product construction. In our example, we have the following conjugate pairs:  $a_2 \leftrightarrow a^2$  and  $b_1 \leftrightarrow b^1$ .

Now combining the above isomorphism with Poincaré duality, we have

$$H_k(\mathcal{L}; \mathbb{Z}_2) \cong H^{4-k}(\mathcal{L}^*; \mathbb{Z}_2) \cong H_{4-k}(\mathcal{L}^*; \mathbb{Z}_2) \cong H_{4-k}(\mathcal{L}; \mathbb{Z}_2). \quad (74)$$

This leads to a pair of dual cycles on  $\mathcal{L}$ :  $c_k$  and  $c_{4-k}^*$ , which has a non-trivial  $\mathbb{Z}_2$  intersection with each other, namely

$$|c_k \cap c_{4-k}^*| = 1. \quad (75)$$

More generally, for any pair of basis cycles, one has

$$|c_k \cap c_{4-k}^*| = \delta_{c,c'}, \quad (76)$$

which is equivalent to the overlapping relation of the conjugated cycle-cocycle pair in Eq. (73). Note that the above intersection condition can be re-written as the cup product sum of their Poincaré dual cocycles:

$$\int_{\mathcal{M}^4} c^{4-k} \cup c'^k = \delta_{c,c'}, \quad (77)$$

which is related to the isomorphism  $H^k(\mathcal{L}^*; \mathbb{Z}_2) \cong H^{4-k}(\mathcal{L}^*; \mathbb{Z}_2)$ .

In the following, we analyze the properties of each type of cycles or cocycles as well as their Poincaré duals.

### 1. 2-cycles:

We first investigate the codeword of the classical code  $\bar{\mathcal{C}}$  associated to 1-cycle  $\bar{\mathbf{a}}_1$ , which is mapped to the 2-cycle  $\mathbf{a}_2$  in the triangulation  $\mathcal{L}$  of the manifold  $\mathcal{M}^4$ , as illustrated in Fig. 7(a,b). The 1-cycle  $\bar{\mathbf{a}}_1 = \xi_1$  can be considered as a sub-hypergraph of the hypergraph  $G_H$ , which forms the skeleton of the 2-cycle  $\mathbf{a}_2$  in the thickened code. More concretely, this means the thickened 2-cycle  $\mathbf{a}_2$  is the boundary of the tubular neighborhood of  $\xi_1$ , which has the form

$$\mathbf{a}_2|_\tau = \xi_1|_\tau \times \partial D^2 = \xi_1|_\tau \times S^1 = S^1 \times I \quad (78)$$

in a local tubular segment  $\tau = S^1 \times I \times S^2$ , where  $\mathbf{a}_2|_\tau$  and  $\xi_1|_\tau = I$  denotes the segment of  $\mathbf{a}_2$  and  $\xi_1$  supported within  $\tau$ . Since each  $\mathbf{B}_i$  “4-handle” corresponds to a single hyperedge in the hypergraph, the 2-cycle needs to completely experience the entire  $\mathbf{B}_i$  “2-handle” it goes through, as shown in Fig. 7(b). We emphasize that although  $\bar{\mathbf{a}}_1 = \xi_1$  is a non-geometric 1-cycle defined on a hypergraph which is not a simplicial complex, the thickened 2-cycle  $\mathbf{a}_2$  is a geometric cycle defined on a simplicial complex. We have hence turned the classical code into a geometric object by shifting to higher dimensions.

Another property of the 1-cycle codeword of the classical code is that it can *turn* at the check vertex  $\mathbf{C}_j$ , meaning that the cycle can occupy only a portion of the hyperedges connected to the check vertex, as illustrated in Fig. 7(a). Therefore, the thickened 2-cycle codeword should also be able to turn at a  $\mathbf{C}_j$ -“handle”, as illustrated in Fig. 7(b, c). The turning location corresponds to the junction where more than two  $\mathbf{C}_j$ -“handles” are attached to a  $\mathbf{B}_i$ -“handle”. The turning is more concretely illustrated with the 3D projection in Fig. 7(d), where the 2-cycle  $\mathbf{a}_2$  can occupy a tubular region  $S^1 \times I$  in this segment which goes directly to one of the other  $\mathbf{B}_i$ -“handles”.

Now for the 2-cycle  $\mathbf{a}_2$  in our construction, it can only occupy even number of attached  $\mathbf{B}_i$ -“handles” at each junction to satisfy the cycle condition  $\partial_2 \mathbf{a}_2 = 0$ . When there are more than two  $\mathbf{B}_i$ -“handles” being occupied, one can resolve the 2-cycle by pairing up the occupied  $\mathbf{B}_i$ -“handles” in an arbitrary way, as illustrated in Fig. 7(e).

### 2. 1-cocycles:

We then consider the codeword of the transposed classical code  $\bar{\mathcal{C}}^T$  associated with the 0-cocycle  $\bar{\mathbf{b}}^0$ , which is mapped to the 1-cocycle  $\mathbf{b}^1$  in the thickened code defined on the triangulation  $\mathcal{L}$  of the manifold  $\mathcal{M}^4$ , as illustrated in Fig. 8.

The 0-cocycle  $\bar{\mathbf{b}}^0$  occupies vertices  $v$  (orange squares) on the hypergraph  $G_h$ . In the dual hy-

pergraph  $G_h^*$  where the vertex and hyperedge is interchanged,  $\bar{\mathbf{b}}^0$  corresponds to a dual 1-cycle  $\eta_1^* \in H_1(G_h^*; \mathbb{Z}_2)$  occupying the dual hyperedges  $e_h^*$ , as illustrated by orange lines in Fig. 8(a).

An important property is that the 0-cocycle  $\bar{\mathbf{b}}^0$  can turn at a bit  $\mathbf{B}_i$  (circle), as illustrated in Fig. 8(b). In the dual hypergraph picture, the dual 1-cycle  $\eta_1^*$  turns at the dual vertex  $\mathbf{B}_i$ . Note that in order for  $\bar{\mathbf{b}}^0$  to be a valid codeword of  $\bar{\mathcal{C}}^T$  or equivalently a valid 0-cocycle, at each bit  $\mathbf{B}_i$ , there has to be even number of adjacent checks being occupied by  $\bar{\mathbf{b}}^0$  [see Fig. 8(a,b)] in order to satisfy the parity constraint in  $\bar{\mathcal{C}}^T$  or equivalently the zero coboundary condition at the corresponding hyperedge  $e_{h,i}$ , i.e.,  $d\bar{\mathbf{b}}^0(e_{h,i})=0$ . In the dual hypergraph picture, this means a single dual vertex (circle) has to be adjacent to even number of occupied dual hyperedges.

Another important property is that the 0-cocycle  $\bar{\mathbf{b}}^0$  (codeword of  $\bar{\mathcal{C}}^T$ ) has to split into all directions at each check  $\mathbf{C}_j$  to satisfy the even-parity condition at the neighboring  $\mathbf{B}_i$ , which plays the role of a parity check in the transposed code  $\bar{\mathcal{C}}^T$ . This is also equivalent to satisfying the 0-coboundary condition at the corresponding hyperedge  $e_{h,i}$ , i.e.,  $d\bar{\mathbf{b}}^0(e_{h,i})=0$ . Note that this is consistent with the dual hypergraph description, since in  $G_h^*$ , the check  $\mathbf{C}_j$  plays the role of a dual hyperedge  $e_{h,j}^*$ . Therefore, all legs of this dual hyperedge has to be occupied by the dual 1-cycle  $\eta_1^*$ .

We then investigate the corresponding 1-cocycle in the thickened code. It is more convenient to describe these 1-cocycles geometrically with their Poincaré dual cycles on the dual triangulation  $\mathcal{L}^*$ . An example of a 2D cellular (square) complex  $\mathcal{L}$  (black) and its dual complex  $\mathcal{L}^*$  (green) is illustrated in Fig. 8(c).

As shown in Fig. 8(d), the dual 1-cycle  $\eta_1^*$  in the skeleton classical code forms the skeleton of the 1-cocycle  $\mathbf{b}^1$  and its dual 3-cycle  $\mathbf{b}_3^*$ , which are the boundary of the tubular neighborhood of  $\eta_1^*$  (i.e., locally as  $\eta_1^*|_\tau \times D^3$ ). In any tubular segment  $\tau = S^1 \times I \times S^2$ , the 1-cocycle and its dual 3-cycle is supported on the thickened cycle:

$$\mathbf{b}^1|_\tau \sim \mathbf{b}_3^*|_\tau = \eta_1^*|_\tau \times S^2 = I \times S^2, \quad (79)$$

as illustrated in Fig. 8(d). On the  $\mathbf{B}_i$  with multiple legs, there can be crossing of  $\eta_1^*$  as has been shown in Fig. 8(a). Since there has to be an even number of branches being occupied, we can always resolve  $\eta_1^*$  using the homology equivalence relation. As illustrated in Fig. 8(d), one can either connect the top to the left and the bottom to the right (solid line), or instead the top to the right and the bottom to the left (dashed line). The thickened cocycle  $\mathbf{b}^1$  and its dual cycle  $\mathbf{b}_3^*$  can be reconnected the same way.

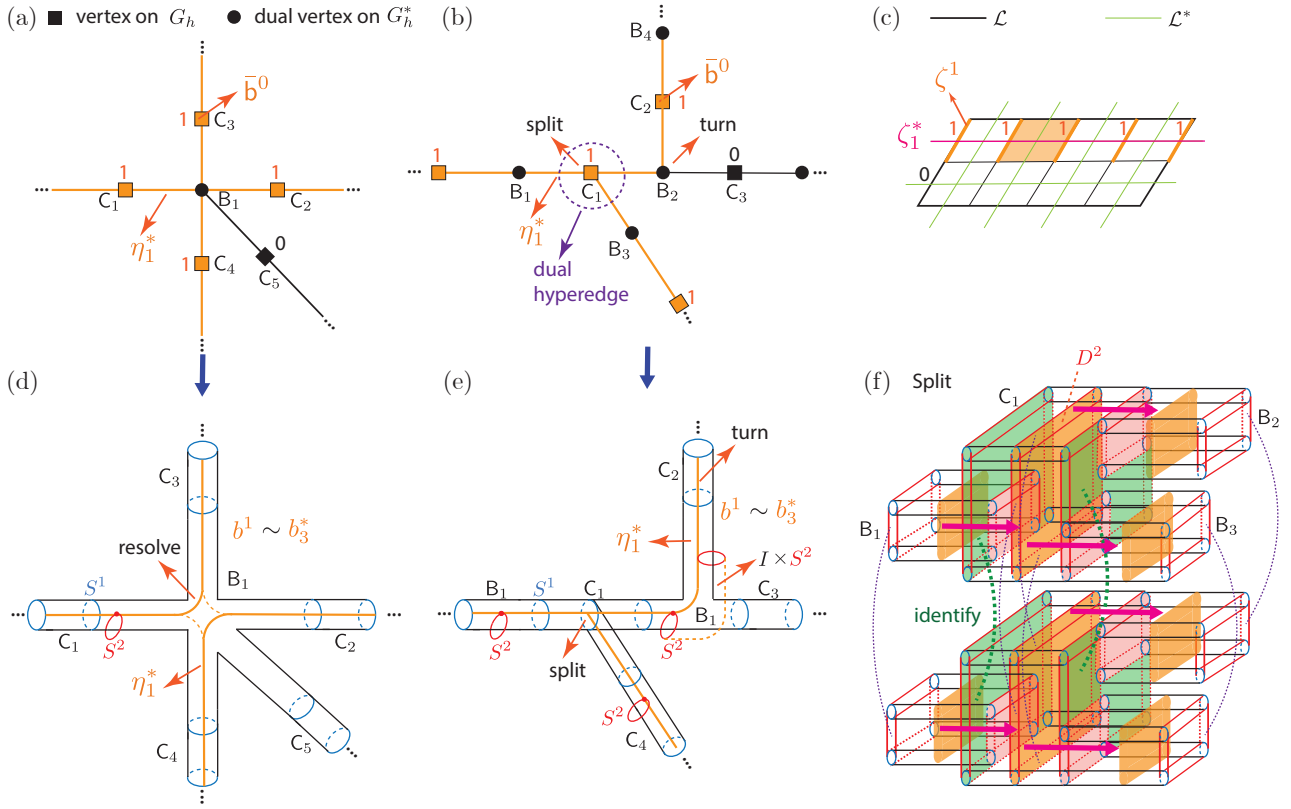


Figure 8. (a) Illustration of the 0-cocycle  $\bar{b}^0$  in the skeleton hypergraph  $G_h$  occupying vertices (square) and its dual 1-cycle  $\eta_1^*$  occupying the hyperedges in the dual hypergraph  $G_h^*$ . (b) The 0-cocycle can turn at a hyperedge (bit) and has to split into all branches at a vertex (check). (c) Illustration of a cocycle and its Poincaré dual cycle on a 2D square complex. (d) In the 4-manifold, the thickened 1-cocycle and its dual 3-cycle locally look like  $I \times S^2$  in a tubular segment, and can be resolved using the equivalence relation of cocycles when going into more than two legs in a  $B_i$ -“handle”. (e) The turning of the 1-cocycle in a  $B_i$ -“handle” and splitting of the 1-cocycle in the junction region of the  $C_j$ -“handle”. (f) Understanding the geometry of the splitting of 1-cocycle in the 3D projection. The 1-cocycle and its dual 3-cycle can be viewed as the worldsheet (trajectory) of a pair of vertical 2-disks  $D^2$  glued along their common  $S^1$  boundary. When moving across the boundary of the  $C_1$ -“handle”, a pair of 2-disks can be created or annihilated at the “wormhole” regions (highlighted in green) where the boundaries of the two copies are identified. During this moving process, a smaller vertical 2-disk hence first becomes a larger 2-disk and then splits into two smaller 2-disks.

Same as its skeleton  $\eta_1^*$ , the 1-cocycle  $b^1$  and the dual 3-cycle  $b_3^*$  can turn at the  $B_i$ -“handle” since locally (in a small tubular segment  $\tau$ ) they are just a 1-cycle thickened along the 2-sphere  $S^2$ , namely  $\eta_1^*|_{\tau} \times S^2$ . They also have to split into all branches at the  $C_j$ -“handle” with a junction, as illustrated in Fig. 8(e). The splitting of 1-cocycle  $b^1$  and the dual 3-cycle  $b_3^*$  is illustrated with the doubled picture and 3D projection in Fig. 8(f). The dual 3-cycle  $b_3^*$  can be interpreted as the world-volume (moving trajectory) of the two sphere  $S^2$ , which is allowed to split. In the doubled picture, two disks  $D^2$  (orange) are identified along their common  $S^1$  boundary to form the 2-sphere  $S^2$ . We can see that when we move the two glued disks across the attaching regions (red) of the  $B_1$ -“handle”, it becomes two larger glued disks. This is because on the two identified boundaries (green) of the 2-

handlebody  $H$  which behave like wormholes, a pair of glued disks (in the green regions) can be created together which compensates the difference between the smaller disks on the left and larger disks on the right. When we further move these two large glued disks towards the right and across the attaching region (red) of the  $B_2$ - and  $B_3$ -“handles”, we see that the membrane in the green regions get annihilated due to the identification, and the larger glued disks split into two pairs of smaller glued disks in the  $B_2$ - and  $B_3$ -“handles” respectively. The 1-cocycle and its dual 3-cycle  $b_3^*$  hence splits at the junction.

### 3. 1-cycles:

We now investigate the 0-cycle  $\bar{b}_0$  in the classical code  $\bar{\mathcal{C}}$  which is mapped to the 1-cycle  $b_1$  in the thickened code, as illustrated in Fig. 9. In contrast to  $\bar{a}_1$  and  $\bar{a}^0$  which are codeword of  $\bar{\mathcal{C}} = \text{Ker}(H^T H)$  and hence have minimum size

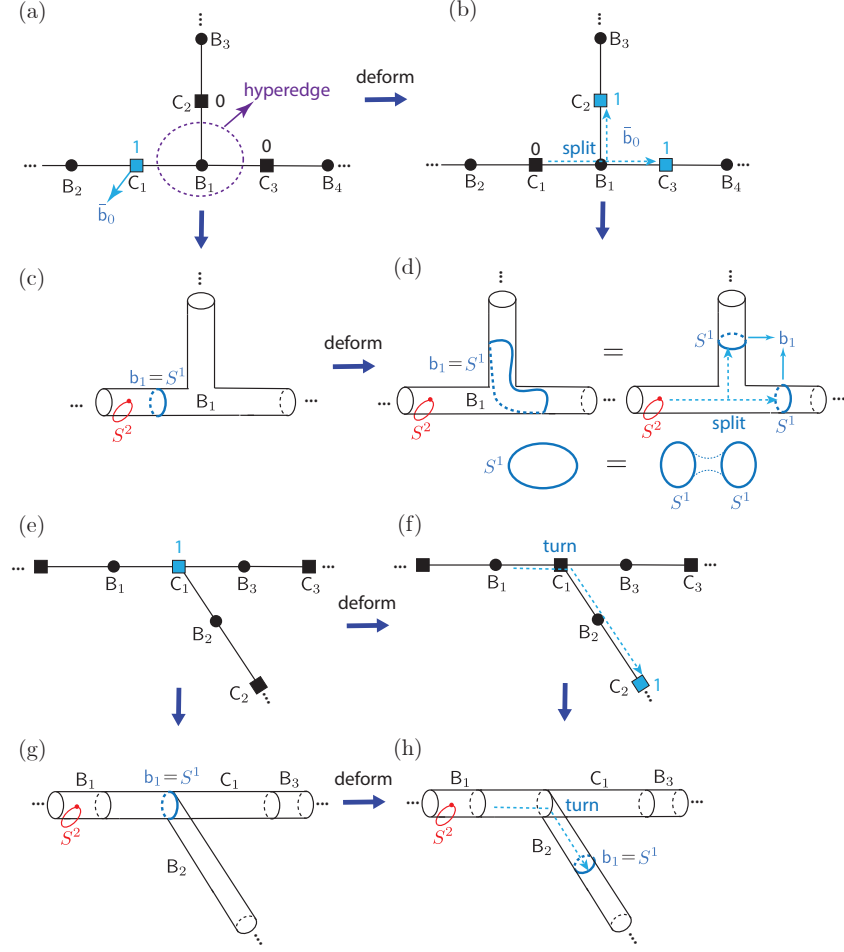


Figure 9. (a, b) A 0-cycle occupying a single vertex (check) in the skeleton hypergraph can be deformed into a representative occupying the rest of vertices connected to the same hyperedge  $B_1$ . (c,d) In the corresponding manifold, the thickened 1-cycle  $S^1$  can be deformed and split into two  $S^1$  when going through a  $B_i$  handles with more than two legs according to the homology relation shown below. (e,f) The 0-cycle representative can turn at the check location (square vertex). (g,h) The thickened 1-cycle can also turn at the junction region, with geometric interpretation essentially illustrated in Fig. 7(d).

$\Omega(n)$ ,  $\bar{b}_0$  can have only  $O(1)$  size. The corresponding 1-cycle  $b_1$  can hence also just have  $O(1)$  minimum size. Since  $\bar{b}_0 \in H_0(G_h) = \text{Ker}(\partial_0)/\text{Img}(\partial_1)$  and  $\partial_0$  maps all 0-chain to 0, any single vertex  $v \in G_h$  is a valid 0-cycle. Due to the isomorphism  $H_0(G_h; \mathbb{Z}_2) \cong H^0(G_h; \mathbb{Z}_2)$  from the universal coefficient theorem, we have the 0<sup>th</sup> Betti number equaling the linear dimension of the transposed code  $\bar{C}^T$ , i.e.,

$$\dim(H_0(G_h; \mathbb{Z}_2)) = \dim(H^0(G_h; \mathbb{Z}_2)) = \bar{k}^T = \bar{k} = \Theta(n). \quad (80)$$

Therefore, there are  $\Theta(n)$  equivalence classes of  $\bar{b}_0$ . Since  $\bar{b}_0$  is mapped to  $b_1$ , there are also  $\Theta(n)$  equivalence classes of  $b_1$ .

Distinct from the case of  $\bar{a}_1$  and  $\bar{a}^0$  which only has a unique representative, in each equivalence class of  $\bar{b}_0$ , there are equivalent representatives differing

by a 1-boundary, i.e.,

$$\bar{b}_0 = \bar{b}_0 + \partial_1 \chi_1 \quad (81)$$

( $\chi_1$  is any 1-chain), due to the definition of  $\bar{H}_0(G_h)$  above which mods out  $\text{Img}(\partial_1)$ . As illustrated in Fig. 9(a,b) a 0-cycle  $\bar{b}_0$  (blue) on the check  $C_1$  (vertex) is deformed to an equivalent representative occupying two vertices  $C_2$  and  $C_3$  by adding a 1-boundary  $\bar{\partial}_1 e_{h,1} = v_1 + v_2 + v_3$ , where  $e_{h,1}$  represents the hyperedge associated with bit  $B_1$ , and  $v_j$  the vertex corresponds to check  $C_j$ . The deformation trajectory needs to split to the complementary branches at a bit  $B_i$  (hyperedge). When mapped to the manifold  $\mathcal{M}^4$ , the corresponding thickened 1-cycle has the following equivalence relation up to adding a 2-boundary:

$$b_1 = b_1 + \partial_2 \chi_2 \quad (82)$$

( $\chi_2$  is any 2-chain). Therefore, the 1-cycle  $b_1 = S^1$

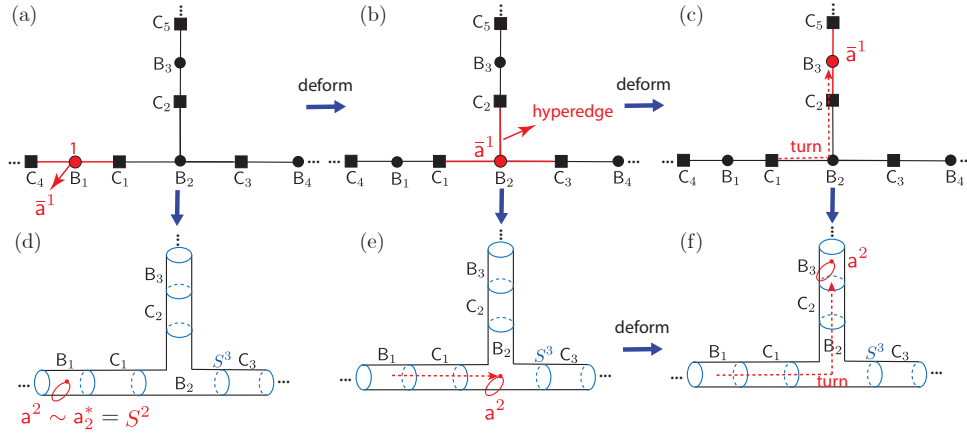


Figure 10. (a,b,c) A 1-cocycle representative occupying a single hyperedge in the skeleton hypergraph can turn at a hyperedge (bit). (d,e,f) In the corresponding manifold, the thickened 2-cocycle  $S^2$  can also turn in a  $B_i$ -“handle” when there are more than two legs.

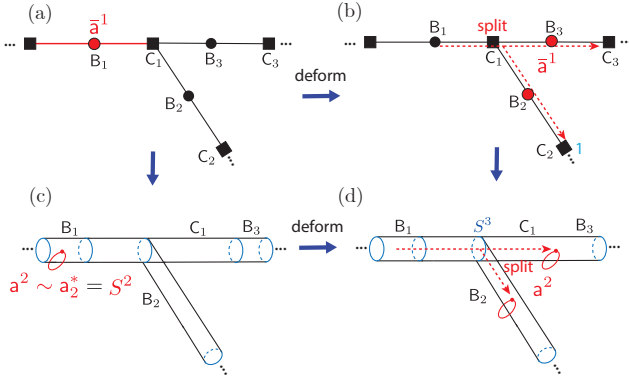


Figure 11. (a,b) When deforming a 1-cycle representative on a single hyperedge across the check (square vertex), it has two splits and occupying the rest of the bits (hyperedges) connected to the check. (c, d) In the corresponding manifold, the thickened 2-cocycle also has to split at the junction region. The geometric interpretation has essentially been illustrated in Fig. 8(f).

can be deformed to a larger  $b_1 = S^1$  going into all the remaining legs when the  $B_1$  bifurcate, and then being split into two  $S^3$ , as shown in Fig. 9(c,d). This splitting is due to the recoupling relation in homology, which has been illustrated in the lower panel of (d). Since the 2-cycle  $a_2$  discussed above can be considered as the worldsheet (moving trajectory) of the 1-cycle  $b_1 = S^1$  here, the above splitting picture of  $b_1$  is consistent with the splitting of  $a_2$  into all legs in the  $B_1$ -“handle” as illustrated in Fig. 7(b).

Moreover, at the check  $C_1$ , the 0-cycle  $\bar{b}_0$  can be deformed and turn to any branch as shown in Fig. 9(e,f). In the illustrated example, the deformation is achieved by adding a 1-boundary  $\partial_1 e_2 =$

$v_1 + v_2$ , where  $e_2$  is the edge corresponding to bit  $B_2$ , and  $v_1$  and  $v_2$  are the vertices associated with checks  $C_1$  and  $C_2$ . The 0-cycle  $\bar{b}_0$  hence turns to the lower branch. Similarly, the 0-cycle can also be deformed to the right branch. When mapped to the manifold  $\mathcal{M}^4$ , the 1-cycle  $b_1 = S^1$  can be deformed and turn at the junction of the  $C_j$ -“handle” to any branch, as illustrated in Fig. 9(g,h). Since the 2-cycle  $a_2 = S^1$  can be considered as the worldsheet (moving trajectory) of the 1-cycle  $b_1$  as mentioned above, we can understand this turning with the more concrete 3D projection picture in Fig. 7(d), where the worldsheet of  $S^1$  turns at the junction.

#### 4. 2-cocycles:

We now consider the 1-cocycle  $\bar{a}^1$  in the classical code  $\bar{C}$  which is mapped to the 2-cocycle  $a^2$  in the thickened code defined on  $\mathcal{M}^4$ , as illustrated in Fig. 10 and 11. Similar to the case of 0-cycle  $\bar{b}_0$  and the corresponding 1-cycle  $b_1$ , the 1-cocycle  $\bar{a}^1$  and the corresponding 2-cocycle  $a^2$  also have  $O(1)$  minimum size and  $\Theta(n)$  equivalence classes.

Note that since  $\bar{a}^1 = H^1(G_h; \mathbb{Z}_2) = \text{Ker}(d^1) / \text{Im}(d^0)$  and  $\bar{d}^1$  acts trivially, any single hyperedge in  $G_h$  is a valid 1-cocycle  $\bar{a}^1 = \bar{e}_{h,i}$  ( $\bar{e}_{h,i}$  is the indicator 1-cochain at hyperedge  $e_{h,i}$ ), as shown in Fig. 10(a). There are equivalent representatives differing by the 0-coboundary:

$$\bar{a}^1 = \bar{a}^1 + d^0 \chi^0, \quad (83)$$

where  $\chi^0$  is any 0-cocycle. As illustrated in Fig. 10(a,b), a representative of  $\bar{a}^1$  occupying the bit  $B_1$  (edge  $e_1$ ) can be moved to the neighboring bit  $B_2$  (hyperedge  $e_{h,2}$ ) by adding a 0-coboundary of the indicator cochain  $\bar{v}_1$  at  $C_1$  (vertex):  $d^0 \bar{v}_1 = \bar{e}_1 + \bar{e}_{h,2}$ . Furthermore,  $\bar{a}^1$  can turn at  $B_2$  to the upper branch and moves to  $B_3$  by adding a 0-coboundary of the indicator cochain at  $\bar{v}_2$  at  $C_2$ :

$d^0\bar{v}_2 = \bar{e}_{h,2} + \bar{e}_3$ , as illustrated in Fig. 10(c). When mapped to the 4-manifold  $\mathcal{M}^4$ , the corresponding 2-cocycle and its dual 2-cycle  $\mathbf{a}^2 \sim \mathbf{a}_2^* = S^2$  can also turn at the  $B_2$ -“handle” since it can be freely deformed to any point on the  $B_2$ -“handle”, as illustrated in Fig. 10(d-f). Since the 1-cocycle  $\mathbf{b}^1$  and its dual 3-cycle  $\mathbf{b}_3^*$  discussed previously can be considered as the worldsheet (moving trajectory) of the 2-cocycle and its dual 2-cycle  $\mathbf{a}^2 \sim \mathbf{a}_2^* = S^2$ , this turning is consistent with the turning of the 1-cocycle  $\mathbf{b}^1 \sim \mathbf{b}_3^*$  illustrated in Fig. 8(e).

Moreover, when moving through a check  $C_1$ , the 1-cocycle  $\bar{\mathbf{a}}^1$  needs to be split into all the remaining branches by adding a 0-coboundary of an indicator 0-cochain at  $C_1$  (vertex), i.e.,  $d^0\bar{v}_1$ , as illustrated in Fig. 11(a,b). The corresponding 2-cocycle and its dual 2-cycle  $\mathbf{a}^2 \sim \mathbf{a}_2^* = S^2$  also splits at the junction in the  $C_1$ -“handle” into all remaining branches, as shown in Fig. 11(c,d). As mentioned above, the worldsheet of 2-cocycle and its dual 2-cycle  $\mathbf{a}^2 \sim \mathbf{a}_2^* = S^2$  corresponds to the 1-cocycle and its dual 3-cycle  $\mathbf{b}^1 \sim \mathbf{b}_3^*$  discussed before. Hence the splitting of  $S^2$  has already been illustrated concretely in the 3D projection picture in Fig. 8(f).

#### 5. 0-cocycles, 4-cycles and 0-cycles:

Besides the doubling of existing cycles and cocycles in the skeleton classical code due to the introduction of Poincaré duality, the construction of the 4-manifold  $\mathcal{M}^4$  out of the skeleton classical code also introduces new emergent cycles and cocycles which were not present in the classical code. One of them is the 0-cocycle  $\mathbf{c}^0$  and its Poincaré dual 4-cycle  $\mathbf{c}_4^*$  which are supported on the entire manifold  $\mathcal{M}^4$ : the 0-cocycle  $\mathbf{c}^0$  occupies all the vertices in  $\mathcal{M}^4$ , while the 4-cycle  $\mathbf{c}_4^*$  occupies all the 4-simplexes in  $\mathcal{M}^4$ .

The 0-cocycle  $\mathbf{c}^0$  has a conjugate 0-cycle  $\mathbf{c}_0$ . Any 0-cycle occupying a single vertex  $v$  in  $\mathcal{M}^4$  is a valid representative of  $\mathbf{c}_0$ . According to Eq. (73), the conjugate pair overlap at a single vertex  $v$  as:

$$\int_{\mathbf{c}_0} \mathbf{c}^0 = |\mathbf{c}_0 \cap \mathbf{c}^0| = 1, \quad (84)$$

which also leads to the following non-trivial cup product between  $\mathbf{c}^0$  and the Poincaré dual of  $\mathbf{c}_0$ , i.e.,  $\mathbf{c}^{*4}$ :

$$\int_{\mathcal{M}^4} \mathbf{c}^0 \cup \mathbf{c}^{*4} = |\mathbf{c}_4^* \cap \mathbf{c}_0| = 1, \quad (85)$$

where the first equality shows its equivalence to the  $\mathbb{Z}_2$  intersection between the Poincaré dual cycles.

#### 6. Spurious cycles and cocycles:

There also exist spurious cycles in the manifold which were not present in the skeleton classical

code. For each class of 1-cycle  $\mathbf{b}_1 = S^1 \in H_1(\mathcal{L}; \mathbb{Z}_2)$ , one can thicken it along the  $S^2$  direction and get  $\mathbf{f}_3 = \mathbf{b}_1 \times S^2 = S^1 \times S^2$  which also has  $O(1)$  size. This means there also exist  $\Theta(n)$  equivalence classes in the 3-cycle basis  $\{\mathbf{f}_3\}$ .

Due to the isomorphism in Eq. (72), we also have the dual 1-cycle  $\mathbf{f}_1^* \in H_1(\mathcal{L}; \mathbb{Z}_2)$  which intersects with the 3-cycle  $\mathbf{f}_3$  at a single point, i.e.,  $|\mathbf{f}_3 \cap \mathbf{f}_1^*| = 1$ . The size of  $\mathbf{f}_3$  is unclear. Nevertheless, since it is a 1-cycle on a 4D simplicial complex, it may have an upper bound of  $O(\log n)$  size obtained from the case of random simplicial complex.

Beside these pairs of dual cycles, there are also their Poincaré dual cocycles  $\mathbf{f}^{*1}$  and  $\mathbf{f}^3$ , which have the same size and number of equivalence classes.

### C. Thickened 3D hypergraph-product code and its code parameter scaling

When taking a homological product of three identical copies of classical codes defined on the triangulation of the 4-manifolds constructed above, we get a thickened 3D hypergraph product defined on the product simplicial complex  $\tilde{\mathcal{L}} = \mathcal{L} \otimes \mathcal{L}' \otimes \mathcal{L}''$  which forms the triangulation of the product manifold  $\tilde{\mathcal{M}}^{12} = \mathcal{M}^4 \times \mathcal{M}^{4'} \times \mathcal{M}^{4''}$ . Here,  $\mathcal{L}$ ,  $\mathcal{L}'$  and  $\mathcal{L}''$  represent the simplicial complex (triangulation) associated with the three constituent 4-manifolds  $\mathcal{M}^4$ ,  $\mathcal{M}^{4'}$  and  $\mathcal{M}^{4''}$ . In particular, we place the qubits on the 4-simplexes of the triangulation  $\tilde{\mathcal{L}}$ . Therefore, the logical- $Z$  operators are hence associated with the 4-cycles, while the logical- $X$  operator are associated with the 4-cocycles or equivalently their Poincaré dual 8-cycles in the dual triangulation  $\tilde{\mathcal{L}}^*$ .

Due to the presence of spurious cycles/cocycles as discussed in the last section, the 4-systole and 4-cosystole can end up being small, which can give rise to  $O(1)$  code distance. However, instead of using the conventional subspace code to encode the logical information into the manifold  $\tilde{\mathcal{M}}^{12}$ , one can use the more flexible subsystem code idea to encode logical information only into a subset of homology/cohomology classes.

One can get more intuition from the following example illustrated in Fig. 12. We start with a torus  $T^2$  having 1-systole of size  $L$ , i.e.,  $\min(|\alpha_1|) = \min(|\beta_1|) = L$ , where  $\alpha_1$  and  $\beta_1$  represent the longitudinal and meridian 1-cycles. We then remove two small disks on  $T^2$  and glue a small handle on that to form a genus-2 surface  $\Sigma_2$ , which introduces two additional cycles  $\alpha'_1$  and  $\beta'_1$  both with  $O(1)$  size. We can choose the following homology basis for this surface:  $\{\alpha_1, \beta_1, \alpha'_1, \beta'_1\}$ . This gives rise to four pairs of conjugate logical operators encoding four logical qubits as illustrated in Fig. 12, where the logical- $X$  and logical- $Z$  operators of the same logical qubit are defined on a pair of dual basis cycles intersecting with each other, such as  $\bar{X}_{\alpha_1}$  and  $\bar{Z}_{\beta_1}$  where  $|\alpha_1 \cap \beta_1| = 1$ . Since the shortest 1-cycle has only  $O(1)$  size, the 1-systole

is hence  $O(1)$ . If one defines a conventional subspace code with the code space being  $\mathcal{C} = 2^{|\mathcal{H}_1(\Sigma_2; \mathbb{Z}_2)|}$ , the code distance is only  $d = O(1)$ . However, we can treat the logical qubits associated with short cycles as gauge qubits (which do not store any information), and choose only a subset of basis cycles to encode the information, e.g.,  $\{\alpha_1, \beta_1\}$  composed of only the long cycles and encoding two logical qubits corresponding to the dual pair of logical operators:  $\bar{X}_{\alpha_1}$  and  $\bar{Z}_{\beta_1}$ ,  $\bar{Z}_{\alpha_1}$  and  $\bar{X}_{\beta_1}$ . Note that any  $Z$  or  $X$  errors along the two short cycles  $\alpha'_1$  and  $\beta'_1$  does not intersect with the long cycles  $\alpha_1$  and  $\beta_1$  and hence cannot induce a logical error in the subsystem code. Therefore, the distance of the subsystem code is still determined by the shortest length of the large cycles, i.e.,  $d = L$ .

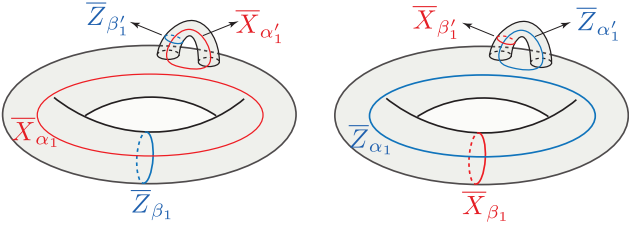


Figure 12. Illustration of the subsystem encoding of the homological code defined on a manifold. With a chosen homology basis, two logical qubits are encoded into a dual pair of mutually intersecting cycles  $\alpha_1$  and  $\beta_1$  with minimum size  $O(L)$ , while the other two logical qubits are encoded into a dual pair of  $\alpha'_1$  and  $\beta'_1$  cycles with minimum size  $O(1)$ . One can then set the logical qubits supported on the short cycles as gauge qubits and hence do not store quantum information in them. For the rest of the two logical qubits, there subsystem code distance is still large, i.e.,  $O(L)$ , despite the systole in this manifold is only  $O(1)$  due to the presence of short cycles.

For general situations, we have the following lemma:

**Lemma 3.** *For a homological quantum code defined on the triangulation of a  $k$ -manifold  $\mathcal{M}^k$ , one can define a subsystem code by associating the logical- $Z$  operators with a subset of an  $i^{\text{th}}$  homology basis  $\{\alpha_i\}$  and the conjugate logical- $X$  operators on the dual subset of  $(k-i)^{\text{th}}$  homology basis  $\{\beta_{k-i}^*\}$  satisfying the intersection relation  $|\alpha_i \cap \beta_{k-i}^*| = \delta_{\alpha, \beta}$ . The distance of the subsystem code is hence  $d = \min(\min\{|\alpha_i|\}, \min\{|\beta_{k-i}^*|\})$ .*

*Proof.* Due to the intersection relation  $|\alpha_i \cap \beta_{k-i}^*| = \delta_{\alpha, \beta}$ , any logical- $Z$  operator supported on the basis cycle  $\alpha_i$  only anticommutes with the logical- $X$  operator supported on the dual cycle  $\alpha_{k-i}^*$ , namely

$$\bar{Z}_{\alpha_i} \bar{X}_{\alpha_{k-i}^*} = -\bar{X}_{\alpha_{k-i}^*} \bar{Z}_{\alpha_i}. \quad (86)$$

Therefore, only the  $X$ -errors wrapped around the dual cycle  $\alpha_{k-i}^*$  can flip the eigenvalue of the logical operator  $\bar{Z}_{\alpha_i}$ . Similarly, on the  $Z$ -errors wrapped around the cycle  $\alpha_i$  can flip the eigenvalue of the logical operator  $\bar{X}_{\alpha_{k-i}^*}$ .

Therefore, the  $Z$ -distance of this subsystem code is the smallest size of all basis  $i$ -cycles in the subset  $\{\alpha_i\}$ , i.e.,  $d_Z = \min\{|\alpha_i|\}$  (which takes the minimum size among all representatives of the basis  $i$ -cycles in the subset  $\{\alpha_i\}$ ), while the  $X$ -distance is the smallest size of all basis  $(k-i)$ -cycles in the subset  $\{\beta_{k-i}^*\}$ , i.e.,  $d_X = \min\{|\beta_{k-i}^*|\}$ . We hence obtain the overall code distance as

$$d = \min(d_X, d_Z) = \min(\min\{|\alpha_i|\}, \min\{|\beta_{k-i}^*|\}). \quad (87)$$

□

Based on the above lemma and Lemma 2, we can reach the following theorem:

**Theorem 1.** *Given a skeleton classical code  $\bar{\mathcal{C}} = \text{Ker}(\mathbf{H}^T \mathbf{H})$ , where  $\mathbf{H}$  is a full-rank parity check matrix of a good classical LDPC code with parameters  $[n, \Theta(n), \Omega(n)]$ , the homological product of three identical copies of 4-manifolds  $\mathcal{M}^4$  obtained from the handle construction with the input of  $\bar{\mathcal{C}}$  gives rise to an  $[[N, \Theta(N), \Omega(N^{1/3})]]$  qLDPC code with constant stabilizer weight  $\omega = O(1)$ .*

*Proof.* According to the Künneth theorem, the homology/cohomology groups of the triple product manifold  $\underline{\mathcal{M}}^{12} = \mathcal{M}^4 \times \mathcal{M}^4 \times \mathcal{M}^4$  can be decomposed as a direct sum of the homology/cohomology groups of the constituent manifold:

$$\begin{aligned} \tilde{H}_4 &= (H_2 \otimes H'_1 \otimes H''_1) \oplus (H_2 \otimes H'_2 \otimes H''_0) \\ &\quad \oplus (H_3 \otimes H'_1 \otimes H''_0) \oplus \text{perm.} \\ \tilde{H}^4 &= (H^2 \otimes H'^1 \otimes H''^1) \oplus (H^2 \otimes H'^2 \otimes H''^0) \\ &\quad \oplus (H^3 \otimes H'^1 \otimes H''^0) \oplus \text{perm.}, \end{aligned} \quad (88)$$

where “perm.” stands for permutations. From Poincaré duality, the 4th cohomology group is isomorphic to the 8th homology group, i.e.,

$$\begin{aligned} \tilde{H}^4 \cong \tilde{H}_8 &= (H_2 \otimes H'_3 \otimes H''_3) \oplus (H_2 \otimes H'_2 \otimes H''_4) \\ &\quad \oplus (H_1 \otimes H'_3 \otimes H''_4) \oplus \text{perm.}, \end{aligned} \quad (89)$$

From the above expression, we see that the contributions to the homology/cohomology can be divided into three groups (2, 1, 1), (2, 2, 0) and (3, 1, 0) (and their permutations). Since the 1-cycle and 0-cycle of the skeleton classical code  $\bar{\mathcal{C}}$  (corresponding to chain complex  $X$ ) is mapped to 2-cycle and 1-cycle in  $\mathcal{M}^4$ , we have the  $\mathbb{Z}_2$  Betti number:

$$\begin{aligned} \tilde{b}_2 &= \dim(H_2(\mathcal{M}^4; \mathbb{Z}_2)) = b_1 = \dim(H_1(X; \mathbb{Z}_2)) = \Theta(n), \\ \tilde{b}_1 &= \dim(H_1(\mathcal{M}^4; \mathbb{Z}_2)) = b_0 = \dim(H_0(X; \mathbb{Z}_2)) = \Theta(n), \end{aligned} \quad (90)$$

where we have used  $b_1 = b_0 = \bar{k} = \Theta(n)$  from Lemma 1. We then apply the Künneth theorem to the Betti number and obtain the total number of logical qubits  $K$ :

$$\begin{aligned} K &= \tilde{b}_4 = b_2 \cdot b'_1 \cdot b''_1 + b_2 \cdot b'_2 \cdot b''_0 + b_3 \cdot b'_1 \cdot b''_0 + \text{perm.} \\ &= \Theta(n) \cdot \Theta(n) \cdot \Theta(n) + \Theta(n) \cdot \Theta(n) \cdot 1 + \Theta(n) \cdot \Theta(n) \cdot 1 \\ &= \Theta(n^3) = \Theta(N). \end{aligned} \quad (91)$$

Here,  $N = \Theta(n) \cdot \Theta(n) \cdot \Theta(n) = \Theta(n^3)$  are the total number of qubits (4-simplices) in the qLDPC codes defined on the triangulation of  $\tilde{M}^{12}$ , which is given by condition 2 in Lemma 2.

Following Lemma 3, now we select a subset of 4-cycle basis and its dual 8-cycle basis to form a subsystem code. In particular, we compose these basis cycles in  $\mathcal{M}^{12}$  with all the basis cycles of  $\mathcal{M}^4$  introduced in Sec. IV B 2 except those spurious cycles/cocycles. According to the Künneth formula in Eq. (88) the basis 4-cycles in the chosen subset can be divided into three groups:

$$\begin{aligned} \mathbf{A}_4 &= \mathbf{a}_2 \otimes \mathbf{b}'_1 \otimes \mathbf{b}''_1 \quad (\text{and perm.}) \\ \mathbf{B}_4 &= \mathbf{a}_2 \otimes \mathbf{a}'_2 \otimes \mathbf{c}''_0 \quad (\text{and perm.}) \\ \mathbf{C}_4 &= \mathbf{b}_3^* \otimes \mathbf{b}'_1 \otimes \mathbf{c}''_0 \quad (\text{and perm.}) \end{aligned} \quad (92)$$

Their conjugate 4-cocycles are

$$\begin{aligned} \mathbf{A}^4 &= \mathbf{a}^2 \otimes \mathbf{b}'^1 \otimes \mathbf{b}''^1 \quad (\text{and perm.}) \\ \mathbf{B}^4 &= \mathbf{a}^2 \otimes \mathbf{a}'^2 \otimes \mathbf{c}''^0 \quad (\text{and perm.}) \\ \mathbf{C}^4 &= \mathbf{b}^{*3} \otimes \mathbf{b}'^1 \otimes \mathbf{c}''^0 \quad (\text{and perm.}) \end{aligned} \quad (93)$$

The corresponding dual basis 8-cycles are given by Poincaré duality as

$$\begin{aligned} \mathbf{A}_8^* &= \mathbf{a}_2^* \otimes \mathbf{b}_3^* \otimes \mathbf{b}_3^{*''} \quad (\text{and perm.}) \\ \mathbf{B}_8^* &= \mathbf{a}_2^* \otimes \mathbf{a}_2^{*'} \otimes \mathbf{c}_4^{*''} \quad (\text{and perm.}) \\ \mathbf{C}_8^* &= \mathbf{b}_1 \otimes \mathbf{b}_3^{*'} \otimes \mathbf{c}_4^{*''} \quad (\text{and perm.}) \end{aligned} \quad (94)$$

For any basis cycle in the first group  $\{\mathbf{A}_4\}$ , we have

$$\begin{aligned} \min(|\mathbf{A}_4|) &= \min(|\mathbf{a}_2|) \cdot \min(|\mathbf{b}'_1|) \cdot \min(|\mathbf{b}''_1|) \\ &\geq \min(|\bar{\mathbf{a}}_1|) \cdot \min(|\bar{\mathbf{b}}'_0|) \cdot \min(|\bar{\mathbf{b}}''_0|) \\ &= \Omega(n) \cdot \Omega(1) \cdot \Omega(1) \\ &= \Omega(n) = \Omega(N^{\frac{1}{3}}). \end{aligned} \quad (95)$$

Here we have used the fact that the 2-cycle  $\mathbf{a}_2$  is a thickened version of the 1-cycle skeleton  $\bar{\mathbf{a}}_1 = \xi_1$  in the classical code  $\bar{\mathcal{C}}$  (see Sec. IV B 2), which has a lower bound in size  $\min|\mathbf{a}_2| \geq \min|\bar{\mathbf{a}}_1| = \Omega(n)$ . Moreover, the 1-cycle  $\mathbf{b}_1$  is a thickened version of the 0-cycle  $\bar{\mathbf{b}}_0$  in the skeleton classical code, and has size  $O(1)$ . For any basis cycle in the second group, we have

$$\begin{aligned} \min(|\mathbf{B}_4|) &= \min(|\mathbf{a}_2|) \cdot \min(|\mathbf{a}'_2|) \cdot \min(|\mathbf{c}''_0|) \\ &\geq \min(|\bar{\mathbf{a}}_1|) \cdot \min(|\bar{\mathbf{a}}'_1|) \cdot 1 \\ &= \Omega(n) \cdot \Omega(n) \\ &= \Omega(n^2) = \Omega(N^{\frac{2}{3}}), \end{aligned} \quad (96)$$

where we have used the fact that  $\mathbf{c}''_0$  is only a single vertex in the triangulation of 4-manifold  $\mathcal{M}^{4''}$  and hence  $|\mathbf{c}''_0|=1$ .

For any basis cycle in the third group, we have

$$\begin{aligned} \min(|\mathbf{C}_4|) &= \min(|\mathbf{b}_3^*|) \cdot \min(|\mathbf{b}'_1|) \cdot \min(|\mathbf{c}''_0|) \\ &= \min(|\mathbf{b}^1|) \cdot \min(|\mathbf{b}'_1|) \cdot 1 \\ &\geq \min(|\bar{\mathbf{b}}^0|) \cdot \min(|\bar{\mathbf{b}}'_0|) \\ &= \Omega(n) \cdot \Omega(1) \\ &= \Omega(n) = \Omega(N^{\frac{1}{3}}), \end{aligned} \quad (97)$$

where we have used the fact that  $\mathbf{b}_3^*$  is the Poincaré dual of  $\mathbf{b}^1$  and hence has the same size  $\min(|\mathbf{b}_3^*|) = \min(|\mathbf{b}^1|)$ . Now combining the results from the above three groups, we obtain the logical- $Z$  distance according to Lemma 3:

$$d_Z = \min(\{\mathbf{A}_4\}, \{\mathbf{B}_4\}, \{\mathbf{C}_4\}) = \Omega(N^{\frac{1}{3}}). \quad (98)$$

We then consider the size of the dual basis 8-cycles in Eq. (94), or equivalently that of the conjugate 4-cocycles in Eq. (93). For any basis cocycle in the first group, we have

$$\begin{aligned} \min(|\mathbf{A}_8^*|) &= \min(|\mathbf{A}^4|) = \min(|\mathbf{a}^2|) \cdot \min(|\mathbf{b}'^1|) \cdot \min(|\mathbf{b}''^1|) \\ &\geq \min(|\bar{\mathbf{a}}^1|) \cdot \min(|\bar{\mathbf{b}}'^0|) \cdot \min(|\bar{\mathbf{b}}''^0|) \\ &= \Omega(1) \cdot \Omega(n) \cdot \Omega(n) \\ &= \Omega(n^2) = \Omega(N^{\frac{2}{3}}), \end{aligned} \quad (99)$$

where we have used fact that  $\mathbf{a}^2$  and  $\mathbf{b}^1$  are thickened versions of the  $O(1)$  size skeleton 1-cocycle  $\bar{\mathbf{a}}^1$  and the  $\Omega(n)$ -size skeleton 0-cocycle  $\bar{\mathbf{b}}^0$  in the classical code  $\bar{\mathcal{C}}$  respectively. For any basis cocycle in the second group, we have

$$\begin{aligned} \min(|\mathbf{B}_8^*|) &= \min(|\mathbf{B}^4|) = \min(|\mathbf{a}^2|) \cdot \min(|\mathbf{a}'^2|) \cdot \min(|\mathbf{c}''^0|) \\ &\geq \min(|\bar{\mathbf{a}}^1|) \cdot \min(|\bar{\mathbf{a}}'^1|) \cdot \min(|\mathbf{c}''^0|) \\ &= \Omega(1) \cdot \Omega(1) \cdot \Omega(n) \\ &= \Omega(n) = \Omega(N^{\frac{1}{3}}), \end{aligned} \quad (100)$$

where we have used the fact that  $\mathbf{c}''^0 \sim \mathbf{c}^{*''}_4$  is supported on the entire 4-manifold  $\mathcal{M}^4$  and hence has the size  $|\mathbf{c}''^0| = |\mathbf{c}^{*''}_4| = \Omega(n)$ . For any basis cocycle in the third group, we have

$$\begin{aligned} \min(|\mathbf{C}_8^*|) &= \min(|\mathbf{C}^4|) = \min(|\mathbf{b}^{*3}|) \cdot \min(|\mathbf{b}'^1|) \cdot \min(|\mathbf{c}''^0|) \\ &= \min(|\mathbf{b}_1|) \cdot \min(|\mathbf{b}'^1|) \cdot \min(|\mathbf{c}''^0|) \\ &\geq \min(|\bar{\mathbf{b}}_0|) \cdot \min(|\bar{\mathbf{b}}'^0|) \cdot \min(|\mathbf{c}''^0|) \\ &= \Omega(1) \cdot \Omega(n) \cdot \Omega(n) \\ &= \Omega(n^2) = \Omega(N^{\frac{2}{3}}), \end{aligned} \quad (101)$$

where we have used the fact that the 3-cocycle and its dual 1-cycle  $\mathbf{b}^{*3} \sim \mathbf{b}_1$  is a thickened version of the  $O(1)$ -size skeleton 0-cycle  $\bar{\mathbf{b}}_0$  in the classical code  $\bar{\mathcal{C}}$ . Combining



the results from the above three groups, we obtain the logical- $X$  distance according to Lemma 3:

$$d_X = \min(\{A_8^*\}, \{B_8^*\}, \{C_8^*\}) = \Omega(N^{\frac{1}{3}}). \quad (102)$$

We then get the overall distance of the code as

$$d = \min(d_X, d_Z) = \Omega(N^{\frac{1}{3}}). \quad (103)$$

Finally the constant stabilizer weight  $\omega = O(1)$  is equivalent to the bounded local geometry of the product manifold  $\tilde{\mathcal{M}}^{12} = \mathcal{M}^4 \times \mathcal{M}^{4'} \times \mathcal{M}^{4''}$ , which is in turn given by the bounded local geometry of the constituent manifolds  $\mathcal{M}^4$ ,  $\mathcal{M}^{4'}$  and  $\mathcal{M}^{4''}$  according to Lemma 2.  $\square$

#### D. Triple cup product and logical non-Clifford gates on the thickened 3D hypergraph product codes

We can now evaluate cup products in three copies of identical codes defined on manifold  $\tilde{\mathcal{M}}^{12}$  and obtain the following theorem:

**Theorem 2.** *There exist a family of thickened 3D hypergraph product codes  $\tilde{\mathcal{C}}$  defined on the triangulation of a 12-manifold  $\tilde{\mathcal{M}}^{12}$  with rate  $K = \Theta(N)$ , subsystem-code distance  $D = \Omega(N^{1/3})$  and constant stabilizer weight  $w = O(1)$ , such that a constant-depth circuit implementing the cohomology operation of a triple cup product on three identical copies of  $\tilde{\mathcal{C}}$  give rise to a non-Clifford logical gate.*

*Proof.* We consider the case of the logical CCZ gate, where a triple cup product of operator-valued 4-cochains from three copies of thickened 3D hypergraph product codes are summed over the product simplicial complex  $\tilde{\mathcal{L}} = \mathcal{L} \otimes \mathcal{L}' \otimes \mathcal{L}''$  forming the triangulation of the product manifold  $\tilde{\mathcal{M}}^{12} = \mathcal{M}^4 \times \mathcal{M}^{4'} \times \mathcal{M}^{4''}$ . According to Eq. (39), we have the following unitary implementing the logical gate:

$$\begin{aligned} U &= (-1)^{\int_{\tilde{\mathcal{M}}^{12}} a_{(1)}^4 \cup a_{(2)}^4 \cup a_{(3)}^4} \\ &= \prod_{\alpha^4, \beta^4, \gamma^4} \overline{\text{CCZ}}[(\alpha^4; 1), (\beta^4; 2), (\gamma^4; 3)]^{\int_{\tilde{\mathcal{M}}^{12}} \alpha^4 \cup \beta^4 \cup \gamma^4}, \end{aligned} \quad (104)$$

where  $a_{(i)}^4$  represents an operator-valued 4-cocycles in the  $i^{\text{th}}$  copy of thickened 3D hypergraph product code, and  $\alpha^4, \beta^4, \gamma^4$  are 4-cocycles from a cohomology basis  $\{\alpha^4\}$ ,  $\{\beta^4\}$  and  $\{\gamma^4\}$  for copy 1, 2 and 3 respectively.

Now it is clear that  $U$  is a logical gate since it maps the code back to itself, as proven in Sec. II. Nevertheless, for the logical gate to be non-trivial, i.e., not a logical identity, we need to make sure the triple cup product sum  $\int_{\tilde{\mathcal{M}}^{12}} \alpha^4 \cup \beta^4 \cup \gamma^4$  in the exponent of Eq. (104) evaluates non-trivially. There are two types of choices of triplets of cocycles satisfy this condition.

We first consider the following cohomology classes using the Künneth theorem:

$$\begin{aligned} \alpha^4 &= \mathbf{a}^2 \otimes \mathbf{c}'^0 \otimes \mathbf{a}^{*''2} \\ \beta^4 &= \mathbf{a}^{*2} \otimes \mathbf{a}'^2 \otimes \mathbf{c}''^0 \\ \gamma^4 &= \mathbf{c}^0 \otimes \mathbf{a}^{*'}^2 \otimes \mathbf{a}''^2. \end{aligned} \quad (105)$$

Here,  $\mathbf{a}^2$ ,  $\mathbf{a}'^2$  and  $\mathbf{a}''^2$  are three arbitrary 2-cocycles from the 2nd cohomology basis  $\{\mathbf{a}^2\}$ ,  $\{\mathbf{a}'^2\}$  and  $\{\mathbf{a}''^2\}$  in the constituent 4-manifolds  $\mathcal{M}^4$ ,  $\mathcal{M}^{4'}$  and  $\mathcal{M}^{4''}$ . Due to Poincaré duality, the basis 2-cocycle  $\mathbf{a}^2$  has a unique dual basis 2-cocycle denoted by  $\mathbf{a}^{*2}$ , satisfying the intersection condition:

$$\int_{\mathcal{M}^4} \mathbf{a}^2 \cup \mathbf{a}^{*2} \equiv \int_{\mathcal{L}} \mathbf{a}^2 \cup \mathbf{a}^{*2} = |\mathbf{a}_2^* \cap \mathbf{a}_2| = 1, \quad (106)$$

where the sum over the 4-manifold  $\mathcal{M}^4$  corresponds to the sum over its triangulation  $\mathcal{L}$  in the discrete description. Similarly,  $\mathbf{a}^{*'}^2$  and  $\mathbf{a}^{*''2}$  are the unique dual basis 2-cocycles of  $\mathbf{a}'^2$  and  $\mathbf{a}''^2$  respectively. In addition, we have used the unique 0-cocycle class  $\mathbf{c}^0$ ,  $\mathbf{c}'^0$  and  $\mathbf{c}''^0$  from each 4-manifold whose Poincaré dual  $\mathbf{c}_4^*$ ,  $\mathbf{c}_4^{*'}$  and  $\mathbf{c}_4^{*''}$  are the cocycles enclosing the entire 4-manifolds  $\mathcal{M}^4$ ,  $\mathcal{M}^{4'}$  and  $\mathcal{M}^{4''}$ .

Within the constituent 4-manifold  $\mathcal{M}^4$ , there is a non-trivial triple cup product and the triple intersection structure:

$$\begin{aligned} \int_{\mathcal{M}^4} \mathbf{a}^2 \cup \mathbf{a}^{*2} \cup \mathbf{c}^0 &\equiv \int_{\mathcal{L}} \mathbf{a}^2 \cup \mathbf{a}^{*2} \cup \mathbf{c}^0 \\ &= |\mathbf{a}_2^* \cap \mathbf{a}_2 \cap \mathbf{c}_4^*| = 1. \end{aligned} \quad (107)$$

The interpretation of the triple intersection is that the Poincaré dual pair  $\mathbf{a}_2^*$  and  $\mathbf{a}_2$  intersect at a single point which in term intersects with the 4-cycle  $\mathbf{c}_4^*$  wrapping around the entire 4-manifold  $\mathcal{M}^4$  at a single point. Similar triple cup product structure also occurs in the second and third constituent manifold  $\mathcal{M}^{4'}$  and  $\mathcal{M}^{4''}$ .

Using the Künneth theorem, we can re-express this triple cup product sum in the exponent of Eq. (104) as:

$$\begin{aligned} &\int_{\tilde{\mathcal{M}}^{12}} \alpha^4 \cup \beta^4 \cup \gamma^4 \\ &= \int_{\tilde{\mathcal{M}}^{12}} (\mathbf{a}^2 \otimes \mathbf{c}'^0 \otimes \mathbf{a}^{*''2}) \cup (\mathbf{a}^{*2} \otimes \mathbf{a}'^2 \otimes \mathbf{c}''^0) \\ &\quad \cup (\mathbf{c}^0 \otimes \mathbf{a}^{*'}^2 \otimes \mathbf{a}''^2) \\ &= \int_{\mathcal{M}^4} (\mathbf{a}^2 \cup \mathbf{a}^{*2} \cup \mathbf{c}^0) \cdot \int_{\mathcal{M}^{4'}} (\mathbf{c}'^0 \cup \mathbf{a}'^2 \cup \mathbf{a}^{*'}^2) \\ &\quad \cdot \int_{\mathcal{M}^{4''}} (\mathbf{a}^{*''2} \cup \mathbf{c}''^0 \cup \mathbf{a}''^2) \\ &= 1 \cdot 1 \cdot 1 = 1, \end{aligned} \quad (108)$$

where in the third equality we have used Eq. (107) and its analogy for the other two constituent manifolds to give the non-trivial triple cup product within each constituent manifold  $\mathcal{M}^4$ ,  $\mathcal{M}^{4'}$  and  $\mathcal{M}^{4''}$ .

There exist another set of cohomology classes which have non-trivial cup products:

$$\begin{aligned}\tilde{\alpha}^4 &= \mathbf{b}^1 \otimes \mathbf{c}^0 \otimes \mathbf{b}^{* \prime 3} \\ \tilde{\beta}^4 &= \mathbf{b}^{* 3} \otimes \mathbf{b}^{\prime 1} \otimes \mathbf{c}^{\prime 0} \\ \tilde{\gamma}^4 &= \mathbf{c}^0 \otimes \mathbf{b}^{* \prime 3} \otimes \mathbf{b}^{\prime 1},\end{aligned}\quad (109)$$

where  $\mathbf{b}^1$  and  $\mathbf{b}^{* 3}$  are a pair of dual basis cocycles of the manifold in  $\mathcal{M}^4$  satisfying the intersection condition:

$$\int_{\mathcal{M}^4} \mathbf{b}^1 \cup \mathbf{b}^{* 3} = |\mathbf{b}_3^* \cap \mathbf{b}_1| = 1. \quad (110)$$

Similarly, there exist the other two pairs of dual basis cocycles  $(\mathbf{b}^{\prime 1}, \mathbf{b}^{* \prime 3})$  and  $(\mathbf{b}^{\prime \prime 1}, \mathbf{b}^{* \prime \prime 3})$  in  $\mathcal{M}^4$  and  $\mathcal{M}^{\prime 4}$  respectively. We hence have the following non-trivial triple cup product sum using the Künneth theorem:

$$\begin{aligned}& \int_{\tilde{\mathcal{M}}^{12}} \tilde{\alpha}^4 \cup \tilde{\beta}^4 \cup \tilde{\gamma}^4 \\ &= \int_{\mathcal{M}^4} (\mathbf{b}^1 \cup \mathbf{b}^{* 3} \cup \mathbf{c}^0) \cdot \int_{\mathcal{M}^{\prime 4}} (\mathbf{c}^{\prime 0} \cup \mathbf{b}^{\prime 1} \cup \mathbf{b}^{* \prime 3}) \\ & \quad \cdot \int_{\mathcal{M}^{\prime \prime 4}} (\mathbf{b}^{* \prime \prime 3} \cup \mathbf{c}^{\prime \prime 0} \cup \mathbf{b}^{\prime \prime 1}) \\ &= 1.\end{aligned}\quad (111)$$

Based on the above two types of non-trivial triple cup product sum, the logical gate  $U$  in Eq. (104) implements non-trivial collective logical CCZ gates.  $\square$

### E. Magic rate and logical gate structure: counting the number of logical CCZ's from the number of triple intersection points

As has been shown in Ref. [22] and also above, the logical gate structure is completely determined by the triple intersection (cup product) structure in the underlying manifold  $\tilde{\mathcal{M}}^{12}$ . In particular, the number of logical CCZs is determined by the number of  $\mathbb{Z}_2$  triple intersection points in  $\tilde{\mathcal{M}}^{12}$ .

Now we have two types of contributions to the  $\mathbb{Z}_2$  triple intersection points given by Eq. (105) and Eq. (109) respectively. For the first type [Eq. (105)] and the basis 4-cocycle  $\alpha^4 = \mathbf{a}^2 \otimes \mathbf{c}^0 \otimes \mathbf{a}^{* \prime 2}$ , we recall that the number of basis cocycle classes in the set  $\{\mathbf{a}^2\}$  and  $\{\mathbf{a}^{* \prime 2}\}$  are both  $\Theta(n)$ , while there is only a unique class of  $\mathbf{c}^0$ . Therefore, the number of basis cocycle classes in the subset  $\{\alpha^4\}$  is  $\Theta(n^2) = \Theta(N^{\frac{2}{3}})$ . Similarly, there are  $\Theta(N^{\frac{2}{3}})$  basis cocycle classes in the subset  $\{\beta^4\}$  and  $\{\gamma^4\}$ . For the second type [Eq. (109)], there are also  $\Theta(N^{\frac{2}{3}})$  cocycle classes in the subsets  $\{\tilde{\alpha}^4\}$ ,  $\{\tilde{\beta}^4\}$ , and  $\{\tilde{\gamma}^4\}$  from similar reasoning. In sum, the logical non-Clifford gate  $U$  addresses  $\Theta(N^{\frac{2}{3}})$  logical qubits in the qLDPC code, with the addressing rate being  $r_A = \Theta(N^{\frac{2}{3}})/N = \Theta(1/N^{\frac{1}{3}})$ .

Now we further investigate the logical gate connectivity and total number of logical CCZ's. For the first type

[Eq. (105)] and a given basis cocycle  $\alpha^4$ , i.e., with fixed choice of  $\mathbf{a}^2$  and  $\mathbf{a}^{* \prime 2}$  ( $\Theta^{N^{2/3}}$  possible choices), there are  $\Theta(n) = \Theta(N^{\frac{1}{3}})$  possible choices of basis cocycles  $\beta^4$  since  $\mathbf{a}^{* 2}$  is fixed by the dual of  $\mathbf{a}^2$  due to Poincaré duality while there are  $\Theta(n)$  possible choices of  $\mathbf{a}^{\prime 2}$ . Now for a given pair of  $\alpha^4$  and  $\beta^4$ , there is a unique choice of basis cocycle  $\gamma^4$  since both  $\mathbf{a}^{* \prime 2}$  and  $\mathbf{a}^{\prime 2}$  are fixed to be the dual cocycles of  $\mathbf{a}^{\prime 2}$  and  $\mathbf{a}^{* \prime 2}$ . In other words, each  $\alpha^4$  is coupled to  $\Theta(n) = \Theta(N^{\frac{1}{3}})$  pairs of  $\beta^4$  and  $\gamma^4$  via logical CCZ's. By symmetry, each  $\beta^4$  is also coupled to  $\Theta(N^{\frac{1}{3}})$  pairs of  $\gamma^4$  and  $\alpha^4$ , while each  $\gamma^4$  is also coupled to  $\Theta(N^{\frac{1}{3}})$  pairs of  $\alpha^4$  and  $\beta^4$ . For the second type [Eq. (109)] involving cocycle classes  $\tilde{\alpha}^4$ ,  $\tilde{\beta}^4$ , and  $\tilde{\gamma}^4$ , the logical gate structure is completely the same as those for  $\alpha^4$ ,  $\beta^4$  and  $\gamma^4$  in the first type based on similar reasoning. Now the total number of logical CCZ's implemented by  $U$  is hence  $n_{\text{CCZ}} = \Theta(N^{\frac{2}{3}}) \cdot \Theta(N^{\frac{1}{3}}) = \Theta(N)$ , which gives rise to the magic rate  $r_M = n_{\text{CCZ}}/N = O(1)$ .

We see that one drawback of the current scheme is that it only addresses a fraction of the logical qubits, i.e.,  $\Theta(N^{\frac{2}{3}})$ . This issue will be cured in the alternative scheme in the Sec. V which takes a homological product of a good quantum LDPC code and a good classical LDPC code.

## V. PARALLELIZABLE NON-CLIFFORD LOGICAL GATES AND MAGIC STATE FOUNTAIN ON CONSTANT-RATE 3D HOMOLOGICAL PRODUCT CODES WITH $\Omega(\sqrt{N})$ -DISTANCE

### A. Constructing the thickened 3D homological product codes and logical non-Clifford gates

We first consider a 3D homological product code that is the homological product [46] of a good classical LDPC code  $\bar{\mathcal{C}}$  with  $n$  bits and a good quantum LDPC code  $\bar{\mathcal{C}}'$  by Panteleev and Kalachev [6] with  $m = \Theta(n)$  qubits. Here, 3D just means the underlying chain complex is a 3D (4-term) chain complex. We also note that in this construction we can use any good classical code, either from random bipartite expander graphs or the Sipser-Spielman construction [50], and there is no need to pick a symmetric parity-check matrix  $\mathbf{H}^T \mathbf{H}$ . We then construct thickened homological product codes by mapping the good classical LDPC code  $\bar{\mathcal{C}}$  into a 4-manifold  $\mathcal{M}^4$  (as discussed in Sec. IV B) and the good qLDPC code  $\bar{\mathcal{C}}'$  into an 11-manifold  $\mathcal{M}^{\prime 11}$  using the Freedman-Hastings mapping [48]. The thickened homological product codes are then defined on the triangulation of the 15D product manifold  $\mathcal{M}^{15} = \mathcal{M}^4 \times \mathcal{M}^{\prime 11}$ .

The details of the Freedman-Hastings mapping from the quantum code to an 11-manifold can be found in Ref. [48]. Besides the procedure introduced in Sec. IV A about attaching “4-handles” to the “3-handles” according to the boundary map obtained from the  $X$ -checks, one needs to further attach “5-handles” to the “4-

handles” according to the boundary map obtained from the  $Z$ -checks. One then obtains a 5-handlebody  $H$ , and taking the double of two identical copies of  $H$  will produce the 11-manifold  $\mathcal{M}^{11} = \mathcal{D}H$ . The logical- $Z$  operators are supported on the 4-cycles, which has been visualized in Fig. 3(h) inside the handlebody with the replacement of  $D^6$  to  $D^7$ . The logical- $X$  operators are supported on the dual 7-cycles due to Poincaré duality, and can be visualized in the same way as the 4-cycles in Fig. 3(h) with the additional trick of using the dual handlebody, i.e., the other upsidedown copy of handlebody in the double construction built from handles with dual indices similar to the situation in Eq. (63).

We now introduce the following theorem essentially obtained from Ref. [48] (Theorem 1.2.1) with the additional input from Ref. [6], which has also been used to construct the 3D local code with optimal code parameters in Ref. [63] (restated as Theorem 5)<sup>5</sup>:

**Theorem 3.** (Freedman and Hastings [48]) *Given the good qLDPC code  $\tilde{\mathcal{C}}'$  from Ref. [6] with the parameters  $[[m, \Theta(m), \Theta(m)]]$  as an input, it can be mapped to a good homological qLDPC code with the parameters  $[[\Theta(m), \Theta(m), \Theta(m)]]$  defined on the triangulation of an 11-manifold  $\mathcal{M}^{11}$  with bounded local geometry and with its 4-systole and 7-systole corresponding to the logical- $Z$  and  $-X$  distance respectively and both having size  $\Theta(m)$ .*

We now consider the three following cohomology classes in the product manifold  $\tilde{\mathcal{M}}^{15} = \mathcal{M}^4 \times \mathcal{M}^{11}$ :

$$\begin{aligned}\alpha^6 &= \mathbf{a}^{*2} \otimes \mathbf{f}'^4, \\ \beta^2 &= \mathbf{a}^2 \otimes \mathbf{g}'^0, \\ \gamma^7 &= \mathbf{c}^0 \otimes \mathbf{f}^{*7},\end{aligned}\quad (112)$$

where  $\mathbf{a}^{*2} \sim \mathbf{a}_2$  and  $\mathbf{a}^2$  are a pair of dual cocycles with minimum size  $\Omega(n)$  and  $\Omega(1)$  respectively in  $\mathcal{M}^4$ ;  $\mathbf{f}'^4$  and  $\mathbf{f}^{*7} \sim \mathbf{f}'_4$  are a pair of dual cocycles in  $\mathcal{M}^{11}$  which corresponds to the logical- $Z$  and  $-X$  operators in the qLDPC code  $\tilde{\mathcal{C}}'$ . Their minimum size corresponds to the 4-systoles and 7-systoles and both having size  $\Omega(m) = \Omega(n)$ ;  $\mathbf{c}^0$  and  $\mathbf{g}'^0$  are the unique 0-cocycle class in  $\mathcal{M}^4$  and  $\mathcal{M}^{11}$  respectively and both have size  $\Omega(n)$ . We have the following non-trivial triple cup product using the Künneth theorem:

$$\begin{aligned}& \int_{\tilde{\mathcal{M}}^{15}} \alpha^6 \cup \beta^2 \cup \gamma^7 \\ &= \int_{\mathcal{M}^4} (\mathbf{a}^2 \cup \mathbf{a}^{*2} \cup \mathbf{c}^0) \cdot \int_{\mathcal{M}^{11}} (\mathbf{f}'^4 \cup \mathbf{g}'^0 \cup \mathbf{f}^{*7}) \\ &= 1\end{aligned}\quad (113)$$

<sup>5</sup>As has been clarified below Theorem 5 in Ref. [63], the original Theorem 1.2.1 in Ref. [48] has a *polylog*( $m$ ) reduction in the rate and distance due to the additional requirement that the underlying manifold is simply connected for the interest of systolic geometry. When dropping this additional requirement which is unnecessary for the present paper, the proof in Ref. [48] gives the optimal parameters without the *polylog*( $m$ ) reduction.

Based on the above triple intersection property we can construct three non-identical copies of qLDPC codes  $\mathcal{C}_{(1)}$ ,  $\mathcal{C}_{(2)}$ , and  $\mathcal{C}_{(3)}$  all defined on the same triangulation of 15-manifold  $\tilde{\mathcal{M}}^{15}$  with the qubits placed on 6-simplices, 3-simplices, and 7-simplices respectively. We also define a total code involving all the three copies of codes as  $\tilde{\mathcal{C}} = \mathcal{C}_{(1)} \otimes \mathcal{C}_{(2)} \otimes \mathcal{C}_{(3)}$ . Therefore, the basis cocycle classes  $\alpha^6$ ,  $\beta^2$  and  $\gamma^7$  correspond to the support of logical- $X$  operators in the three copies of codes respectively, while their conjugate basis cycle classes  $\alpha_6$ ,  $\beta_3$  and  $\gamma_7$  correspond to the support of the logical- $Z$  operators. Since there exist spurious cycles in both the manifold  $\mathcal{M}^4$  and  $\mathcal{M}^{11}$ <sup>6</sup> constructed from the classical and quantum codes respectively, we also choose the subsystem-code encoding, and only encode the logical- $X$  operators into the cohomology basis subset  $\{\alpha^6\}$ ,  $\{\beta^2\}$ , and  $\{\gamma^7\}$  in the three copies respectively, with their conjugate logical- $Z$  operators encoded into the conjugate homology basis subset  $\{\alpha_6\}$ ,  $\{\beta_3\}$ , and  $\{\gamma_7\}$  respectively, which are decomposed by the Künneth theorem as:

$$\begin{aligned}\alpha_6 &= \mathbf{a}_2^* \otimes \mathbf{f}'_4, \\ \beta_3 &= \mathbf{a}_2 \otimes \mathbf{g}'_0, \\ \gamma_7 &= \mathbf{c}_0 \otimes \mathbf{f}'_7.\end{aligned}\quad (114)$$

We hence introduce the following theorem:

**Theorem 4.** *There exist a family of thickened 3D homological product codes  $\tilde{\mathcal{C}}$  defined on the triangulation of a 15-manifold  $\tilde{\mathcal{M}}^{15}$  with encoding rate  $K = \Theta(N)$ , subsystem-code distance  $D = \Omega(\sqrt{N})$  and constant stabilizer weight  $w = O(1)$ , such that a constant-depth circuit implementing the cohomology operation of a triple cup product can give rise to non-Clifford logical gates on  $\tilde{\mathcal{C}}$ .*

*Proof.* We first estimate the total number of qubits in each code copy, which equals the total number of 6-simplices, 2-simplices and 7-simplices on  $\tilde{\mathcal{M}}^{15}$  respectively. Due to Lemma 2 and Theorem 3, the constituent manifold  $\mathcal{M}^4$  and  $\mathcal{M}^{11}$  both have bounded local geometry, i.e., each vertex in its triangulation is adjacent to  $O(1)$   $k$ -simplices, the product manifold  $\tilde{\mathcal{M}}^{15} = \mathcal{M}^4 \times \mathcal{M}^{11}$  also has bounded local geometry. Therefore, the number of  $k$ -simplices in these manifolds are all proportional to the number of vertices and the volume of the manifold. Using the fact that  $\tilde{\mathcal{M}}^{15}$  is the product of  $\mathcal{M}^4$  and  $\mathcal{M}^{11}$ , we know the number of  $k$ -simplices in  $\tilde{\mathcal{M}}^{15}$ , i.e., the dimension of the  $k$ -chain groups, all scale as

$$\dim(C_k) = \Theta(n) \cdot \Theta(m) \cdot \Theta(n^2) = \Theta(N), \quad (115)$$

where  $N$  is the total number of vertices in  $\tilde{\mathcal{M}}^{15}$ .

<sup>6</sup>For the quantum code defined on the 11-manifold  $\mathcal{M}^{11}$ , the spurious 1-cycles/cocycles and the dual 11-cycles/cocycles are separated from the 4-cycles and 7-cycles where logical  $Z$  and  $X$  are encoded respectively.

Now since both cocycles basis  $\{\mathbf{a}^2\}$  and  $\{\mathbf{f}'^4\}$  have dimension  $\Theta(n)$ , which come from the code dimension of the input classical code  $\bar{C}$  and quantum code  $\bar{C}'$ , the cocycle basis subset  $\{\alpha^6\}$  has dimension  $\Theta(n^2)$  according to the Künneth theorem. Therefore, the first copy of qLDPC code  $\mathcal{C}_{(1)}$  with qubits placed on 6-simplices has linear dimension  $K^{(1)} = \Theta(n^2) = \Theta(N)$ , i.e., constant encoding rate. For the second and third copies of qLDPC codes  $\mathcal{C}_{(2)}$  and  $\mathcal{C}_{(3)}$ , since both the cocycle basis  $\{\mathbf{a}^{*2}\}$  and  $\{\mathbf{f}^{*7}\}$  have dimension  $\Theta(n)$ , which again come from the code dimension of the classical and quantum codes, the code dimension is hence  $K^{(2)} = K^{(3)} = \Theta(n) = \Theta(\sqrt{N})$  for both the second and third copies. When summing up all the logical qubits in these three code blocks, the overall encoding rate of the total code  $\tilde{C} = \mathcal{C}_{(1)} \otimes \mathcal{C}_{(2)} \otimes \mathcal{C}_{(3)}$  is still constant, i.e.,

$$r_E = \frac{K}{\Theta(N)} = \frac{K^{(1)} + K^{(2)} + K^{(3)}}{\Theta(N)} = O(1). \quad (116)$$

We hence call the first qLDPC code copy the memory register which is used for information storage with a constant encoding rate, and the second and third qLDPC code copies the ancilla registers which are used to assist the memory register for doing logical non-Clifford gates.

We then bound the distance of the subsystem-code encoding using Lemma 3. For the first code copy  $\mathcal{C}_{(1)}$ , the logical- $Z$  distance is determined by the minimum size of any basis 6-cycle in the basis subset  $\{\alpha_6\}$  defined in Eq. (114), i.e.,

$$\begin{aligned} \min(|\alpha_6|) &= \min(|\mathbf{a}_2^*|) \cdot \min(|\mathbf{f}'_4|) \\ &= \Omega(1) \cdot \Omega(m) = \Omega(n) = \Omega(\sqrt{N}), \end{aligned} \quad (117)$$

where we have used the bound of the cycle/cocycle length  $|\mathbf{a}_2^*| = |\mathbf{a}^2| = \Omega(1)$  in the thickened good classical LDPC code as discussed in the proof of Theorem 1 and the  $Z$ -distance bound (4-systole) of the thickened good qLDPC code for  $|\mathbf{f}'_4| = \Omega(m)$  according to Theorem 3. We hence have

$$d_Z^{(1)} = \min(\{\alpha_6\}) = \Omega(\sqrt{N}). \quad (118)$$

Meanwhile, the  $X$ -distance is determined by the minimum size of any conjugate basis 6-cocycle in the basis subset  $\{\alpha^6\}$  defined in Eq. (112), or equivalently that of its Poincaré dual basis 9-cycle in the basis subset  $\{\alpha_9^*\}$ :

$$\begin{aligned} \min(|\alpha^6|) &= \min(|\alpha_9^*|) = \min(|\mathbf{a}^{*2}|) \cdot \min(|\mathbf{f}'^4|) \\ &= \min(|\mathbf{a}_2|) \cdot \min(|\mathbf{f}^{*7}|) = \Omega(n) \cdot \Omega(m) \\ &= \Omega(n^2) = \Omega(\sqrt{N}), \end{aligned} \quad (119)$$

where we have used the distance bound of the thickened classical code, i.e.,  $|\mathbf{a}_2| = |\mathbf{a}^{*2}| = \Omega(n)$ , as well as the  $X$ -distance bound (7-systole) of the thickened good qLDPC code for  $|\mathbf{f}'^4| = |\mathbf{f}^{*7}| = \Omega(m)$ . We hence have

$$d_X^{(1)} = \min(\{\alpha^6\}) = \min(\{\alpha_9^*\}) = \Omega(N), \quad (120)$$

and the overall code distance:

$$d^{(1)} = \min(d_X^{(1)}, d_Z^{(1)}) = \Omega(\sqrt{N}). \quad (121)$$

For the second code copy  $\mathcal{C}_{(2)}$ , the  $Z$ -distance is determined by the minimum size of any basis 2-cycle in the basis subset  $\{\beta_2\}$ :

$$\begin{aligned} \min(|\beta_2|) &= \min(|\mathbf{a}_2|) \cdot \min(|\mathbf{g}'_0|) \\ &= \Omega(n) \cdot 1 = \Omega(\sqrt{N}), \end{aligned} \quad (122)$$

where we have used the fact that  $\mathbf{g}'_0$  is a single vertex in the triangulation of the 11-manifold  $\mathcal{M}^{11}$ . We hence have

$$d_Z^{(2)} = \min(\{\beta_2\}) = \Omega(\sqrt{N}). \quad (123)$$

Meanwhile, the  $X$ -distance is determined by the minimum size of any conjugate basis 2-cocycle in the basis subset  $\{\beta^2\}$ , or equivalently that of its Poincaré dual basis 13-cycle in the basis subset  $\{\beta_{13}^*\}$

$$\begin{aligned} \min(|\beta^2|) &= \min(|\beta_{13}^*|) = \min(|\mathbf{a}^2|) \cdot \min(|\mathbf{g}^{*0}|) \\ &= \Omega(1) \cdot \Omega(m) = \Omega(n) = \Omega(\sqrt{N}), \end{aligned} \quad (124)$$

where we have used the fact that  $|\mathbf{a}^2| = \Omega(1)$  in the thickened classical code, and  $|\mathbf{g}^{*0}| = |\mathbf{g}_{11}^{*7}| = \Omega(m)$  occupies the entire 11-manifold  $\mathcal{M}^{11}$ . We hence have

$$d_X^{(2)} = \min(\{\beta^2\}) = \min(\{\alpha_{13}^*\}) = \Omega(\sqrt{N}), \quad (125)$$

and the overall distance is hence

$$d^{(2)} = \min(d_X^{(2)}, d_Z^{(2)}) = \Omega(\sqrt{N}). \quad (126)$$

For the third copy  $\mathcal{C}_{(3)}$ , the 0-cycle  $\mathbf{c}_0$  is a single vertex in the thickened classical code and hence has  $|\mathbf{c}_0| = 1$ ; its conjugate 0-cocycle (Poincaré dual to a 4-cycle)  $\mathbf{c}^0 \sim \mathbf{c}_4^*$  occupies the entire 4-manifold  $\mathcal{M}^4$  which leads to  $|\mathbf{c}^0| = |\mathbf{c}_4^*| = 1$ . Meanwhile,  $|\mathbf{f}_7^{*7}|$  and  $|\mathbf{f}^{*7}| = |\mathbf{f}'_4|$  correspond to the 7-systole and 4-systole of the 11-manifold  $\mathcal{M}^{11}$ . This similarly gives rise to

$$\begin{aligned} d_Z^{(3)} &= \min|\gamma_7| = \Omega(\sqrt{N}), \\ d_X^{(3)} &= \min|\gamma^7| = \min|\gamma_8^*| = \Omega(\sqrt{N}) \\ d^{(3)} &= \min(d_X^{(3)}, d_Z^{(3)}) = \Omega(\sqrt{N}). \end{aligned} \quad (127)$$

The overall distance of the total code  $\tilde{C} = \mathcal{C}_1 \otimes \mathcal{C}_2 \otimes \mathcal{C}_3$  is hence  $D = \min(d^{(1)}, d^{(2)}, d^{(3)}) = \Omega(\sqrt{N})$ .

Finally, we implement the following constant-depth circuits corresponding to the triple cup product of a higher gauge theory defined on the 15-manifold  $\tilde{\mathcal{M}}^{15}$  according to Eq. (39):

$$\begin{aligned} U &= (-1)^{\int_{\tilde{\mathcal{M}}^{15}} \alpha_{(1)}^6 \cup \alpha_{(2)}^2 \cup \alpha_{(3)}^7} \\ &= \prod_{\alpha^6, \beta^2, \gamma^7} \overline{\text{CCZ}}[(\alpha^6; 1), (\beta^2; 2), (\gamma^7; 3)]^{\int_{\tilde{\mathcal{M}}^{15}} \alpha^6 \cup \beta^2 \cup \gamma^7}. \end{aligned} \quad (128)$$

Since the triple cup product sum in the exponent is non-trivial, we obtain a non-Clifford logical gate.  $\square$

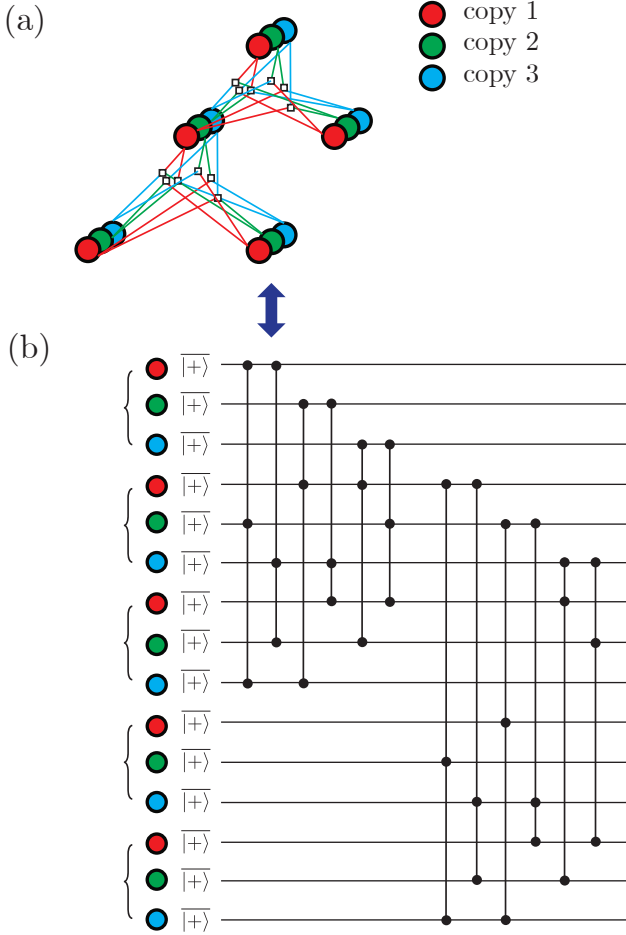


Figure 13. (a) Illustration of an interaction hypergraph involving three identical copies of codes, where each vertex represents a logical qubit and each hyperedge (3-way junction) represents a logical CCZ gate acting on the code. (b) When initializing all the logical qubits into the logical state  $|+\rangle$ , the application of the logical gate  $U$  effectively applies the logical CCZ's illustrated in the circuit and hence injects a hypergraph magic state.

## B. Magic state fountain and logical gate structure

As has been first introduced in Ref. [22], the collective logical CCZ gate structure is encoded into an *interaction hypergraph*  $G_h = (V, E_h)$ . The vertex  $v \in V$  represents a logical qubit labeled by the cocycle label and copy number, such as  $(\alpha^6; 1)$ ,  $(\beta^2; 2)$  or  $(\gamma^7; 3)$ , while a hyperedge  $e_h \in E_h$  coupling logical qubits corresponds to a triple intersection point or equivalently a non-trivial cup product such as  $\int_{\widetilde{\mathcal{M}}^{15}} \alpha^6 \cup \beta^2 \cup \gamma^7 = 1$  in the current code. An example of the interaction hypergraph is given by Fig. 13(a) where the three copies of codes are identical, as in the case of the thickened 3D hypergraph code in Sec. IV.

As has been pointed out in Ref. [22], the interaction hypergraph has a one-to-one correspondence with the

*quantum hypergraph states* [64–66] as the generalization of graph states. One can define a 3-uniform hypergraph state on a hypergraph  $G_h = (V, E_h)$  as follows: one assigns to each vertex a qubit initialized in the  $|+\rangle$  state; for each hyperedge, one perform a CCZ gate between the three connected qubits (vertices) labeled by  $v_1, v_2, v_3$ . We then obtain the following 3-uniform hypergraph state:

$$|g_3\rangle = \prod_{\{v_1, v_2, v_3\} \in E_h} \text{CCZ}(v_1, v_2, v_3) |+\rangle^{\otimes m}, \quad (129)$$

where  $m = |V|$  represents the total number of qubits (vertices). We also call this state a hypergraph magic state, since it is beyond the stabilizer description [22, 65]. When considering our collective logical CCZ gate  $U$  and its corresponding interaction hypergraph, we can first initialize all the logical qubits in the logical state  $|+\rangle$ , and then apply the collective logical CCZ gate  $U$  which hence produces the hypergraph magic state, as illustrated in Fig. 13(b). We call this type of scheme *magic state fountain*, which directly injects high-fidelity magic states into an qLDPC code block instead of doing a state distillation with multiple rounds. This idea has already appeared in Ref. [22].

We now investigate the logical gate structure from the  $\mathbb{Z}_2$  triple intersection structure in Eq. (112) and Eq. (113), and then connect it to the magic state fountain scheme.

As has been discussed above, there are  $\Theta(N)$  inequivalent choices of  $\alpha^6 = \mathbf{a}^{*2} \otimes \mathbf{f}^{/4}$  coming from the  $\Theta(\sqrt{N})$  choices for both  $\mathbf{a}^{*2}$  and  $\mathbf{f}^{/4}$ . For each choice of  $\alpha^6$ , there is a unique pair of  $\beta^2$  and  $\gamma^7$  (involving the dual components  $\mathbf{a}_2$  and  $\mathbf{f}^{*/7}$ ) that has non-trivial triple cup product (intersection) with  $\alpha^6$  due to Poincaré duality, although the different pairs can still share the same  $\beta^2$  or  $\gamma^7$ . The total number of logical CCZ's implemented by the constant-depth circuit  $U$  is hence  $n_{\text{CCZ}} = \Theta(N)$  corresponding to a constant magic rate  $r_M = n_{\text{CCZ}}/\Theta(N) = O(1)$ . This magic rate also quantifies the complexity of the corresponding hypergraph magic state injected to the code when applying  $U$  to the logical state  $|+\rangle^{\otimes K}$ , which grows linearly with the number of qubits  $N$ . All logical qubits in the total code  $\widetilde{\mathcal{C}} = \mathcal{C}_{(1)} \otimes \mathcal{C}_{(2)} \otimes \mathcal{C}_{(3)}$  participate in the logical gate  $U$ , therefore the addressing rate is  $r_A = \Theta(N)/\Theta(N) = O(1)$ .

We then delve more deeply into the logical gate structure by looking at the interaction hypergraph as shown in Fig. 14(a). Since  $\alpha^6 = \mathbf{a}^{*2} \otimes \mathbf{f}^{/4}$ , we can divide the logical qubits in copy 1 labeled by  $\alpha^6$  (red circles) into  $\Theta(\sqrt{N})$  groups (dashed ellipse) with different  $\mathbf{a}^{*2}$  label, while in each group we choose all possible  $\mathbf{f}^{/4}$  labels and hence have  $\Theta(\sqrt{N})$  logical qubits. These  $\Theta(N)$  logical qubits labeled by  $\alpha^6$  in copy 1 are then coupled to  $\Theta(\sqrt{N})$  logical qubits labeled by  $\beta^2$  in copy 2 and  $\gamma^7$  in copy 3 respectively via logical CCZ. Note that since  $\beta^2 = \mathbf{a}^2 \otimes \mathbf{g}^{/0}$  and  $\gamma^7 = \mathbf{c}^0 \otimes \mathbf{f}^{*/7}$ , and  $\mathbf{g}^{/0}$  as well as  $\mathbf{f}^{*/7}$  are unique choices, we can just use label  $\mathbf{a}^2$  and  $\mathbf{f}^{*/7}$  to label the qubits in copy 2 and 3 respectively. In particular, each

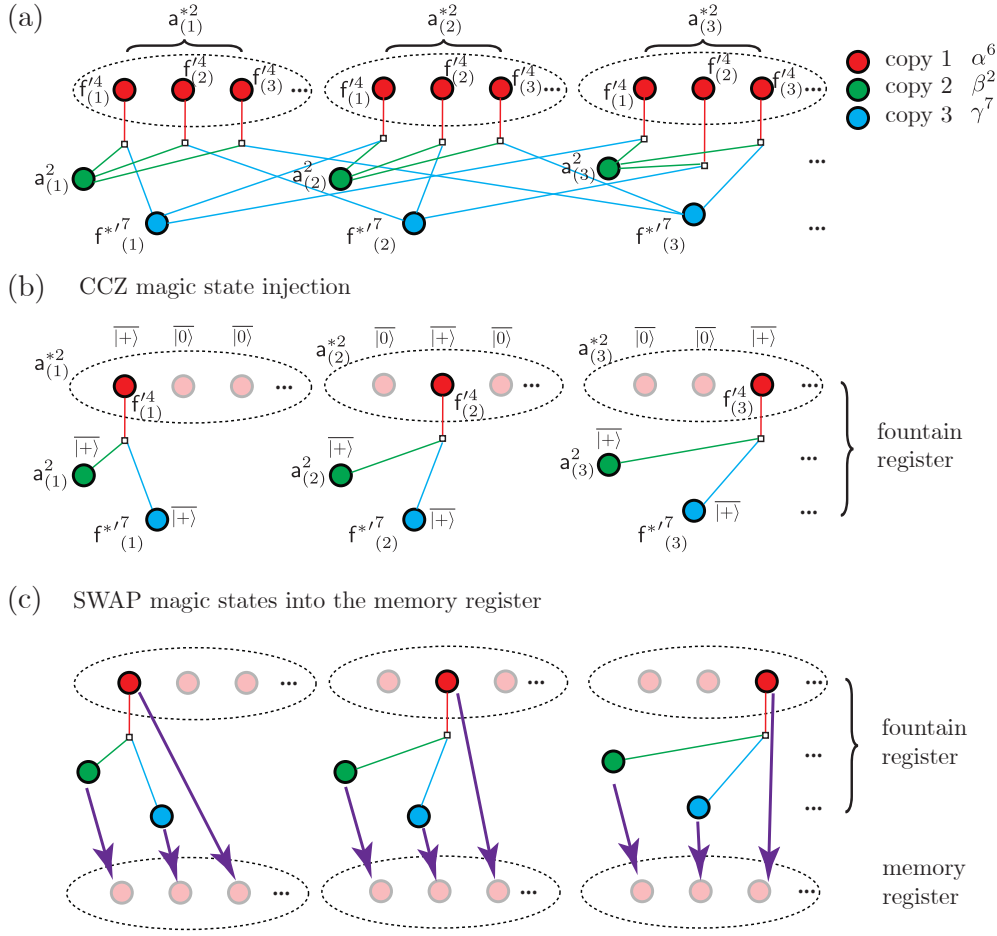


Figure 14. Illustration of the logical gate structure and magic state fountain in the homological product code. (a) The interaction hypergraph involving three non-identical copies of codes. The logical qubits in copy 1 has two cocycle labels  $a_{(i)}^{*2}$  and  $f_{(j)}'^4$ , while those in copy 2 and copy 3 has one cocycle label. (b) Illustration of the injection of non-overlapping CCZ magic states into the fountain register. One deliberately sets a fraction of logical qubits in copy 1 at  $|0\rangle$  state which effectively turns off all the hyperedges (CCZ's) connected two these logical qubits. The remaining  $\Theta(\sqrt{N})$  CCZ magic states are hence non-overlapping. (c) After injecting the magic states into the fountain register, one further SWAPs these resource states into the memory register via logical Clifford gates and then use gate teleportation to turn them into parallelizable logical CCZ gates.

logical qubit in copy 1 with cocycle label  $a^{*2}$  couples to a unique logical qubit in copy 2 with the dual cocycle label  $a^2$  according to Poincaré duality. Similarly, each logical qubit in copy 1 with cocycle label  $f'^4$  couples to a unique logical qubit in copy 2 with the dual cocycle label  $f^{*7}$ . This completes the description of the structure of the collective logical CCZ gate and the corresponding hypergraph magic state, as illustrated in Fig. 14(a).

As pointed out before, the complexity of the hypergraph magic state here grows linearly with the system size  $\Theta(N)$ , and is expected to be hard for a classical computer to simulate. So such a high-complexity state may be useful for demonstrate quantum advantage with a constant-depth circuit. On the other hand, for the purpose of universal quantum computation with the magic state fountain scheme, we may want to reduce the complexity of this hypergraph magic state.

We consider a *fountain register* composed of all three different copies of qLDPC codes, as shown in Fig. 14(b). We first initialize all the logical qubits in copy 2 and 3 (green and blue) into  $|+\rangle$  states. We then initialize  $\Theta(\sqrt{N})$  logical qubits in copy 1 (red) with different labels for both  $a^{*2}$  and  $f'^4$  into the logical state  $|+\rangle$ , while “turning off” the rest of the logical qubits into state  $|0\rangle$ . All the hyperedges coupled to the turned-off logical qubits in state  $|0\rangle$  are effectively removed, so are the corresponding logical CCZ's. The hypergraph magic state hence becomes a tensor product of  $\Theta(\sqrt{N})$  non-overlapping CCZ magic states, i.e.,  $\bigotimes_{j=1}^{\Theta(\sqrt{N})} |\overline{\text{CCZ}}\rangle_j$ , as illustrated in Fig. 14(b).

We then SWAP the  $\Theta(\sqrt{N})$  CCZ magic states into the memory register via logical Clifford gates, either using the combination of targeted logical CZ via a constant-



ogy groups as  $\mathcal{C}_{(1)} = \mathbb{C}_2^{|H_6(\tilde{\mathcal{M}}^{15}; \mathbb{Z}_2)|}$ ,  $\mathcal{C}_{(2)} = \mathbb{C}_2^{|H_3(\tilde{\mathcal{M}}^{15}; \mathbb{Z}_2)|}$ ,  $\mathcal{C}_{(3)} = \mathbb{C}_2^{|H_7(\tilde{\mathcal{M}}^{15}; \mathbb{Z}_2)|}$ . The code distance will hence be determined by the 6-systole and the dual 9-systole for  $\mathcal{C}_{(1)}$ , the 2-systole and the dual 13-systole for  $\mathcal{C}_{(2)}$ , the 7-systole and the dual 8-systole for  $\mathcal{C}_{(3)}$ . The rest of the analysis remains similar as done previously. We hence reach the following modified theorem:

**Theorem 5.** *There exist a family of thickened 3D homological product codes  $\tilde{\mathcal{C}}$  (subspace codes) defined on the triangulation of a 15-manifold  $\tilde{\mathcal{M}}^{15}$  with encoding rate  $K = \Omega(N)/\text{polylog}(N)$ , distance  $D = \Omega(\sqrt{N}/\text{polylog}(N))$  and constant stabilizer weight  $w = O(1)$ , such that a constant-depth circuit can give rise to non-Clifford logical gates on  $\tilde{\mathcal{C}}$ .*

We note that the  $\text{polylog}(N)$  space overhead comes from the proof technique used in Ref. [48] which utilizes the “decongestion lemma”. However, this  $\text{polylog}(N)$  factor may not be necessary and could be in principle removed.

#### D. Conjecture on the constant-depth equivalence between the skeleton and thickened qLDPC codes

Throughout this work, we have been constructing thickened qLDPC codes from a skeleton qLDPC code with a constant qubit overhead and the same code parameter scaling. More concretely, the thickened qLDPC codes are constructed by taking the product of thickened classical or quantum codes defined on manifolds constructed from the skeleton classical or quantum codes. To be more precise, the thickened classical or quantum codes should actually be called ‘*doubled thickened codes*’: recall that we have taken a double process during the manifold construction utilizing Poincaré duality. Now we conjecture that the thickening operation  $\mathcal{T}$  and double operations  $\mathcal{D}$  actually commute, which implies the existence of a doubled skeleton classical or quantum code  $D(\mathcal{C})$  constructed via a similar procedure due to the double construction of a manifold. We hence have following commutation relation:  $\mathcal{D}\mathcal{T}(\mathcal{C}) = \mathcal{T}\mathcal{D}(\mathcal{C})$ , i.e., the doubled thickened code is equivalent to the thickened doubled code. The skeleton qLDPC code mentioned above should be equivalent to the product of these doubled classical or quantum codes.

Since the thickened and skeleton qLDPC codes ( $\mathcal{C}$  and  $\tilde{\mathcal{C}}$ ) differ only by a constant qubit overhead, it is reasonable to conjecture that one can prepare the thickened qLDPC codes  $\mathcal{C}$  from the skeleton qLDPC codes  $\tilde{\mathcal{C}}$  with a constant factor of additional ancilla qubits initialized in a trivial product state  $|0\rangle^{\otimes m}$  via a single step of entanglement renormalization, which can be implemented by a constant-depth circuit  $V$ . We hence reach the following conjecture:

**Conjecture 1.** *A thickened qLDPC code  $\mathcal{C}$  is equivalent to a skeleton qLDPC code with a constant factor of*

*ancilla qubits  $\tilde{\mathcal{C}} \otimes |0\rangle^{\otimes m}$  up to a constant-depth circuit  $V$ . The non-Clifford logical gate via constant-depth circuit  $U$  acting on the thickened code  $\mathcal{C}$  can hence be turned into a constant-depth circuit  $V^\dagger UV$  acting directly on the skeleton code along with the ancillae, i.e.,  $\tilde{\mathcal{C}} \otimes |0\rangle^{\otimes m}$ .*

If the above conjecture holds, then instead of applying the constant-depth circuit  $U$  on the thickened qLDPC code  $\mathcal{C}$  with a constant qubit overhead, one can directly apply the conjugated circuit  $V^\dagger UV$  on the skeleton qLDPC code along with a constant factor of ancilla qubits, i.e.,  $\tilde{\mathcal{C}} \otimes |0\rangle^{\otimes m}$ . After the application of the logical gate, one can still use the skeleton  $\tilde{\mathcal{C}}$  as a quantum memory and only measure the stabilizers on  $\tilde{\mathcal{C}}$ . This may simplify the stabilizer measurement and decoding on the qLDPC code. We leave the proof of this conjecture to future work.

## VI. DISCUSSION AND OUTLOOK

Although we have picked good classical and qLDPC codes as input of our construction to reach desirable asymptotic scaling, we emphasize that the construction we have introduced in this paper is quite general: one can use the Tanner graphs of any classical or quantum codes as input for the manifold and product constructions, and the formalism will give rise to the collective logical CCZ gates. The input codes can also be general CSS codes instead of qLDPC codes. The only difference in this case is that the constructed manifold may not have bounded local geometry. In particular, this method will also be suitable for the near-term realization of small- and intermediate-scale codes. Various computational topology packages, such as the CGAL library [68], can be used to numerically construct the triangulation of manifolds following the recipe of handle construction.

In this paper, we have been focusing on the homological product construction [46]. Nevertheless, the construction also straightforwardly applies to the more general balanced product construction [69]. More concretely, one can map the classical or quantum code in the balanced product construction into a manifold first, and then take a balanced product of the produced manifolds, which is essentially a fibre-bundle construction of manifolds [70, 71]. This may lead to constructions with even better distance parameters which can now go beyond the  $\sqrt{N}$ -distance barrier and eventually construct non-Clifford logical gates in an asymptotically good qLDPC code. We leave this for future exploration.

Another future direction is to optimize the parallelizability in the magic state fountain scheme by introducing a more separable intersection structure, and combine it with highly parallelizable logical Clifford gates [17] to achieve a fault-tolerant computing scheme with very low space-time overhead. Even more interestingly, the implementation of such logical non-Clifford gates on quantum locally testable codes may also shed light on the study



of quantum PCP conjecture, where the connection between polylog PCP and fault-tolerance has been recently pointed out in Ref. [72].

In a related work [43], we have systematically classified various types of cohomology operations that can be used to implement logical gates via constant-depth circuits beyond  $k$ -fold cup products (the so-called color code paradigm), including Steenrod squares and new combinations of higher cup products called higher Pontryagin powers. These new cohomology operations can lead to more exotic logical gates other than the  $C^{n-1}Z$  family such as fine single-qubit rotation including  $T$ -gate and  $R_k$ -gate, as well as controlled rotation  $CR_k$ -gates etc. It would be very interesting to further incorporate these new cohomology operations with the high-rate and large-distance qLDPC codes, which for example can provide

fast  $T$ -state injection to the magic state fountain. A systematic classification of logical gates in qLDPC codes via cohomology operations and emergent symmetries will also be an interesting potential direction.

*Acknowledgements* — We thank Elia Portnoy and Michael Freedman for insightful discussion and early collaboration on this project, including the contribution of various original ideas. We thank Louis Golowich for the discussion on the related topics. We also thank Andrew Cross, Shehryar Sikander, Ben Brown, Po-Shen Hsin, Ryohi Kobayashi, and Maissam Barkeshli for the previous collaboration on related projects. G.Z. is supported by the U.S. Department of Energy, Office of Science, National Quantum Information Science Research Centers, Co-design Center for Quantum Advantage (C2QA) under contract number DE-SC0012704.

- 
- [1] S. Bravyi, A. W. Cross, J. M. Gambetta, D. Maslov, P. Rall, and T. J. Yoder, High-threshold and low-overhead fault-tolerant quantum memory, *Nature* **627**, 778 (2024).
  - [2] M. Hastings, J. Haah, and R. O’Donnell, Fiber bundle codes: breaking the  $n^{1/2}\text{polylog}(n)$  barrier for quantum ldpc codes, in *Proc. ACM STOC (Association for Computing Machinery, New York, NY, USA, 2021)* pp. 1276–1288.
  - [3] P. Pantelev and G. Kalachev, Quantum ldpc codes with almost linear minimum distance, *IEEE Trans. Inf. Theo.* **68**, 213 (2022).
  - [4] N. P. Breuckmann and J. N. Eberhardt, Balanced product quantum codes, *IEEE Trans. Inf. Theo.* **67**, 6653 (2021).
  - [5] M. Hastings, On quantum weight reduction, *arXiv:2102.10030* (2021).
  - [6] P. Pantelev and G. Kalachev, Asymptotically good quantum and locally testable classical ldpc codes, in *Proc. ACM STOC (Association for Computing Machinery, New York, NY, USA, 2022)* pp. 375–388.
  - [7] A. Leverrier and G. Zemor, Quantum tanner codes, in *Proc. IEEE FOCS (IEEE Computer Society, Los Alamitos, CA, USA, 2022)* pp. 872–883.
  - [8] T. Lin and M. Hsieh, Good quantum ldpc codes with linear time decoder from lossless expanders, *arXiv:2203.03581* (2022).
  - [9] S. Gu, C. Pattison, and E. Tang, An efficient decoder for a linear distance quantum ldpc code, *arXiv:2206.06557* (2022).
  - [10] I. Dinur, M. Hsieh, T. Lin, and T. Vidick, Good quantum ldpc codes with linear time decoders, in *Proc. ACM STOC (Association for Computing Machinery, New York, NY, USA, 2023)* pp. 905–918.
  - [11] A. Leverrier and G. Zemor, Efficient decoding up to a constant fraction of the code length for asymptotically good quantum codes, in *Proc. ACM SODA (2023)* pp. 1216–1244.
  - [12] S. Gu, E. Tang, L. Caha, S. Choe, Z. He, and A. Kubica, Single-shot decoding of good quantum ldpc codes, *arXiv:2306.12470* (2023).
  - [13] D. Gottesman, Fault-tolerant quantum computation with constant overhead, *QIC* **14**, 1338 (2014).
  - [14] Q. T. Nguyen and C. A. Pattison, Quantum fault tolerance with constant-space and logarithmic-time overheads, *arXiv preprint arXiv:2411.03632* (2024).
  - [15] L. Cohen, I. Kim, S. Bartlett, and B. Brown, Low-overhead fault-tolerant quantum computing using long-range connectivity, *Sci. Adv.* **8** (2022).
  - [16] S. Huang, T. Jochym-O’Connor, and T. J. Yoder, Homomorphic logical measurements, *PRX Quantum* **4**, 030301 (2023).
  - [17] Q. Xu, H. Zhou, G. Zheng, D. Bluvstein, J. Ataiades, M. D. Lukin, and L. Jiang, Fast and parallelizable logical computation with homological product codes, *arXiv preprint arXiv:2407.18490* (2024).
  - [18] A. Cross, Z. He, P. Rall, and T. Yoder, Improved qldpc surgery: Logical measurements and bridging codes, *arXiv preprint arXiv:2407.18393* (2024).
  - [19] D. J. Williamson and T. J. Yoder, Low-overhead fault-tolerant quantum computation by gauging logical operators, *arXiv preprint arXiv:2410.02213* (2024).
  - [20] E. Swaroop, T. Jochym-O’Connor, and T. J. Yoder, Universal adapters between quantum ldpc codes, *arXiv preprint arXiv:2410.03628* (2024).
  - [21] S. Bravyi and J. Haah, Magic-state distillation with low overhead, *Physical Review A—Atomic, Molecular, and Optical Physics* **86**, 052329 (2012).
  - [22] G. Zhu, S. Sikander, E. Portnoy, A. W. Cross, and B. J. Brown, Non-clifford and parallelizable fault-tolerant logical gates on constant and almost-constant rate homological quantum ldpc codes via higher symmetries, *arXiv preprint arXiv:2310.16982* (2023).
  - [23] H. Bombin and M. A. Martin-Delgado, Topological Computation without Braiding, *Phys. Rev. Lett.* **98**, 160502 (2007).
  - [24] H. Bombin, Gauge color codes: optimal transversal gates and gauge fixing in topological stabilizer codes, *New Journal of Physics* **17**, 083002 (2015).
  - [25] A. Kubica and M. E. Beverland, Universal transversal gates with color codes: A simplified approach, *Phys. Rev. A* **91**, 032330 (2015).
  - [26] A. Kubica, B. Yoshida, and F. Pastawski, Unfolding the color code, *New Journal of Physics* **17**, 083026 (2015).

- [27] H. Bombin, Transversal gates and error propagation in 3d topological codes, arXiv preprint arXiv:1810.09575 (2018).
- [28] H. Bombin, 2d quantum computation with 3d topological codes, arXiv preprint arXiv:1810.09571 (2018).
- [29] M. Vasmer and D. E. Browne, Three-dimensional surface codes: Transversal gates and fault-tolerant architectures, *Phys. Rev. A* **100**, 012312 (2019).
- [30] M. E. Beverland, A. Kubica, and K. M. Svore, Cost of universality: A comparative study of the overhead of state distillation and code switching with color codes, *PRX Quantum* **2**, 020341 (2021).
- [31] S. Bravyi and R. König, Classification of Topologically Protected Gates for Local Stabilizer Codes, *Phys. Rev. Lett.* **110**, 170503 (2013).
- [32] T. R. Scruby, A. Pesah, and M. Webster, Quantum rainbow codes, arXiv preprint arXiv:2408.13130 (2024).
- [33] D. Gaiotto, A. Kapustin, N. Seiberg, and B. Willett, Generalized global symmetries, (2014), arXiv:1412.5148.
- [34] F. Benini, C. Córdova, and P.-S. Hsin, On 2-group global symmetries and their anomalies, *Journal of High Energy Physics* **2019**, 118 (2019), arXiv:1803.09336.
- [35] C. Cordova, T. T. Dumitrescu, K. Intriligator, and S.-H. Shao, Snowmass white paper: Generalized symmetries in quantum field theory and beyond 10.48550/ARXIV.2205.09545 (2022).
- [36] J. McGreevy, Generalized symmetries in condensed matter 10.48550/ARXIV.2204.03045 (2022).
- [37] M. Barkeshli, Y.-A. Chen, S.-J. Huang, R. Kobayashi, N. Tantivasadakarn, and G. Zhu, Codimension-2 defects and higher symmetries in  $(3+1)$  d topological phases, *SciPost Physics* **14**, 065 (2023).
- [38] M. Barkeshli, Y.-A. Chen, P.-S. Hsin, and R. Kobayashi, Higher-group symmetry in finite gauge theory and stabilizer codes, arXiv preprint arXiv:2211.11764 (2022).
- [39] B. Yoshida, Topological color code and symmetry-protected topological phases, *Phys. Rev. B* **91**, 245131 (2015).
- [40] B. Yoshida, Topological phases with generalized global symmetries, *Phys. Rev. B* **93**, 155131 (2016).
- [41] B. Yoshida, Gapped boundaries, group cohomology and fault-tolerant logical gates, *Annals of Physics* **377**, 387 (2017).
- [42] P. Webster and S. D. Bartlett, Locality-preserving logical operators in topological stabilizer codes, *Phys. Rev. A* **97**, 012330 (2018).
- [43] P.-S. Hsin, R. Kobayashi, and G. Zhu, Classifying Logical Gates in Quantum Codes via Cohomology Operations and Symmetry, arXiv 10.48550/arxiv.2411.15848 (2024), 2411.15848.
- [44] A. Hatcher, *Algebraic Topology* (CUP, Cambridge; New York, 2001).
- [45] J.-P. Tillich and G. Zémor, Quantum ldpc codes with positive rate and minimum distance proportional to the square root of the blocklength, *IEEE Transactions on Information Theory* **60**, 1193 (2014).
- [46] S. Bravyi and M. B. Hastings, *Homological product codes*, the 46th Annual ACM Symposium (2014).
- [47] A. Lubotzky, High dimensional expanders, proceedings of the international congress of mathematicians: Rio de janeiro (World Scientific, 2018) pp. 705–730.
- [48] M. Freedman and M. B. Hastings, Building manifolds from quantum codes, arXiv:2012.02249 (2020).
- [49] R. Meshulam, Graph codes and local systems, arXiv 10.48550/arxiv.1803.05643 (2018), 1803.05643.
- [50] M. Sipser and D. Spielman, Expander codes, *Proceedings 35th Annual Symposium on Foundations of Computer Science*, 566 (1994).
- [51] J. McCullough and H. Newman, Asymptotically good homological error correcting codes, *Journal of Algebra Combinatorics Discrete Structures and Applications* **6**, 135 (2019).
- [52] D. Dotterer, L. Guth, and M. Kahle, 2-Complexes with Large 2-Girth, *Discrete & Computational Geometry* **59**, 383 (2018).
- [53] L. Aronshtam, N. Linial, T. Luczak, and R. Meshulam, Collapsibility and vanishing of top homology in random simplicial complexes, arXiv 10.48550/arxiv.1010.1400 (2010), 1010.1400.
- [54] N. Linial\* and R. Meshulam\*, Homological Connectivity Of Random 2-Complexes, *Combinatorica* **26**, 475 (2006).
- [55] R. Meshulam and N. Wallach, Homological connectivity of random k-dimensional complexes, arXiv 10.48550/arxiv.math/0609773 (2006), math/0609773.
- [56] A. O. Quintavalle, M. Vasmer, J. Roffe, and E. T. Campbell, Single-shot error correction of three-dimensional homological product codes, arXiv **quant-ph** (2020).
- [57] L. Golowich and T.-C. Lin, Quantum ldpc codes with transversal non-clifford gates via products of algebraic codes, arXiv preprint arXiv:2410.14662 (2024).
- [58] T.-C. Lin, Transversal non-clifford gates for quantum ldpc codes on sheaves, arXiv preprint arXiv:2410.14631 (2024).
- [59] N. P. Breuckmann, M. Davydova, J. N. Eberhardt, and N. Tantivasadakarn, Cups and gates i: Cohomology invariants and logical quantum operations, arXiv preprint arXiv:2410.16250 (2024).
- [60] A. Wills, M.-H. Hsieh, and H. Yamasaki, Constant-overhead magic state distillation, arXiv preprint arXiv:2408.07764 (2024).
- [61] Q. T. Nguyen, Good binary quantum codes with transversal ccz gate, arXiv preprint arXiv:2408.10140 (2024).
- [62] L. Golowich and V. Guruswami, Asymptotically good quantum codes with transversal non-clifford gates, arXiv preprint arXiv:2408.09254 (2024).
- [63] E. Portnoy, Local quantum codes from subdivided manifolds, arXiv preprint arXiv:2303.06755 (2023).
- [64] M. Rossi, M. Huber, D. Bruß, and C. Macchiavello, Quantum hypergraph states, *New Journal of Physics* **15**, 113022 (2013).
- [65] J. Chen, Y. Yan, and Y. Zhou, Magic of quantum hypergraph states, arXiv preprint arXiv:2308.01886 (2023).
- [66] Y. Takeuchi, T. Morimae, and M. Hayashi, Quantum computational universality of hypergraph states with pauli-x and z basis measurements, *Scientific Reports* **9**, 13585 (2019).
- [67] M. Beverland, E. Campbell, M. Howard, and V. Kliuchnikov, Lower bounds on the non-clifford resources for quantum computations, *Quantum Science and Technology* **5**, 035009 (2020).
- [68] The CGAL Project, *CGAL User and Reference Manual*, 6.0.1 ed. (CGAL Editorial Board, 2024).
- [69] N. P. Breuckmann and J. N. Eberhardt, Balanced Product Quantum Codes, arXiv:2012.09271 (2020).
- [70] M. H. Freedman, D. A. Meyer, and F. Luo,  $Z_2$ -systolic freedom and quantum codes, in

- Mathematics of quantum computation (Chapman and Hall/CRC, 2002) pp. 303–338.
- [71] M. B. Hastings, J. Haah, and R. O’Donnell, Fiber Bundle Codes: Breaking the  $N^{1/2} \text{polylog}(N)$  Barrier for Quantum LDPC Codes, arXiv:2009.03921 (2020).
- [72] A. Anshu, N. P. Breuckmann, and Q. T. Nguyen, Circuit-to-hamiltonian from tensor networks and fault tolerance, proceedings of the 56th annual acm symposium on theory of computing (2024) pp. 585–595.